Universidade de São Paulo
Instituto de Física

Estudando o sistema $KD\bar{D}^*$ com teorias de campos efetivas

Brenda Bertotto Malabarba

Orientador: Prof. Dr. Alberto Martínez Torres

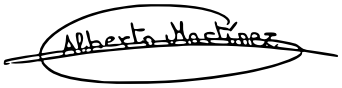

Dissertação de mestrado apresentada ao Instituto de Física da Universidade de São Paulo, como requisito parcial para a obtenção do título de Mestre em Ciências.

Banca Examinadora:

Prof. Dr. Alberto Martínez Torres - IF-USP

Prof. Dr. Alberto Correa dos Reis - CBPF

Prof. Dr. Diogo Rodrigues Boito - IFSC

São Paulo

2020

FICHA CATALOGRÁFICA
Preparada pelo Serviço de Biblioteca e Informação
do Instituto de Física da Universidade de São Paulo

Malabarba, Brenda Bertotto

Estudando o Sistema $KD\bar{D}^*$ com Teorias de Campos Efetivas / Studying the $KD\bar{D}^*$ System with Effective Field Theories . São Paulo, 2020.

Dissertação (Mestrado) – Universidade de São Paulo. Instituto de Física. Depto. de Física Nuclear.

Orientador: Prof. Dr. Alberto Martínez Torres.
Área de Concentração: Física Hadrônica.

Unitermos: 1. Hádrons; 2. Física de partículas; 3. Física Teórica.

USP/IF/SBI-036/2020

University of São Paulo
Physics Institute

Studying the $KD\bar{D}^*$ system with effective field theories

Brenda Bertotto Malabarba

Supervisor: Prof. Dr. Alberto Martínez Torres

Dissertation submitted to the Physics Institute of the University of São Paulo in partial fulfillment of the requirements for the degree of Master of Science.

Examining Committee:
Prof. Dr. Alberto Martínez Torres - IF-USP
Prof. Dr. Alberto Correa dos Reis - CBPF
Prof. Dr. Diogo Rodrigues Boito - IFSC

São Paulo
2020

Acknowledgements/Agradecimentos

Gostaria de agradecer primeiramente ao meu orientador Alberto Martínez Torres com quem tive a sorte de cruzar meu caminho e ainda mais sorte de ter sido aceita como orientanda sem que este tivesse nenhum conhecimento prévio sobre mim como aluna e física. Gostaria de agradecer a ele e também a sua esposa Kanchan por todo conhecimento que estes me passaram e mais que tudo pelo apoio incondicional que sempre ofereceram na física e na vida.

Por mais corrido que tenha sido o mestrado algumas pessoas fizeram que esse tempo passasse de forma mais tranquila e divertida, por isso gostaria de agradecer aos amigos que fiz aqui, em especial ao Ari, Samuel, Taís, Ana Camila e ao Giulio Halisson por todos os chafés da tarde/manhã/noite e todo conhecimento absolutamente inútil compartilhado nestes; À Lígia Trad e ao Ricardo Rizzo por serem a melhor familía da dança que eu poderia querer.

Aos meus companheiros de república Didi, Naimzin, Luluzin, Xuxu e Rafa pelas discussões totalmente relevantes sobre reptilianos, pelas jantas (com ou sem jaca envolvida) e principalmente pelas noites em claro bebendo (pelas manhãs e tardes também).

Também preciso agradecer aos meus amigos que por mais distantes físicamente que estejam sempre estiveram ao meu lado, à minha irmã de alma Cynthia Bortolotto por me apoiar em absolutamente tudo, sempre e ao Miguel Ratis por ser, possivelmente, a melhor pessoa que conheço.

Certamente sou grata a minha família por me apoiarem e confiarem nas minhas escolhas sempre, mesmo sem entenderem meus motivos.

O presente trabalho foi realizado com apoio do Conselho Nacional de Desenvolvimento Científico e Tecnológico (CNPq)

Resumo

Entender a natureza dos estados hadronicos é um dos problemas mais desafiadores na fronteira da física hadronica. Nos últimos anos, esforços experimentais e teóricos vem focando especialmente em estados hadronicos não-tradicionais, que não podem ser explicados como estados do tipo $q\bar{q}$ ou qqq. A despeito de todo esforço empregado, ainda existe uma vasta região de energia inexplorada e sistemas cujos estados com conteúdo de quarks não convencional podem ser encontrados, especialmente a energias de 4$\sim$ 5 GeV. Esta é precisamente a região de energias onde dados vem sendo obtidos em experimentos ao redor do mundo e também é a região em que diversos novos laboratórios estão previstos para trabalhar num futuro próximo.

Esta dissertação tem como propósito explorar as propriedades de hâdrons exóticos com massas na região de energia mecionada acima. Particularmente, estados hadronicos que apresentem uma natureza de três corpos com estranheza diferente de zero e com charme escondido (hidden charm). Como será visto nesta dissertação, um estado com $I(J^P) = 1/2(1^-)$ K^* com massa em torno de 4300 MeV, e largura de 18 MeV, é obtido da dinâmica do sistema $KD\bar{D}^*$ onde a interação do subsistema $D\bar{D}^*$ gera o estado $X(3872)$ em isospin zero e $Z_C(3900)$ em issopin 1.

Experimentalmente, a observação de tal estado K^* é possível nos experimentos atuais e constituiria um excitante novidade para o espectro do kaon. *Palavras-Chave: Hádrons exóticos; Sistema de poucos corpos; Simetria de Quark Pesado; Simetria $SU(4)$.*

Abstract

Understanding the nature of hadronic states is one of the most challenging issues in the frontiers of hadron physics. In recent years, experimental and theoretical efforts are especially being focussed on the nontraditional hadronic states, which cannot be explained either as $q\bar{q}$ or qqq states. Regardless of all the efforts made, there is still a vast unexplored energy region and systems in which states of non-conventional quark content could be found, especially at energies of 4$\sim$5 GeV. This is precisely the energy region in which data is being obtained by some experimental facilities around the world and in which even several new laboratories are being planned to work in the near future.

It is the purpose of this dissertation to explore the properties of exotic hadrons with masses in the above mentioned energy region. Particularly, hadron states with a three-body nature with nonzero strangeness and hidden charm. As shown in this dissertation, an $I(J^P) = 1/2(1^-)$ K^* state with mass around 4300 MeV, and width around 18 MeV, arises from the dynamics involved in the $KD\bar{D}^*$ system when the interaction of the $D\bar{D}^*$ subsystem generates the $X(3872)$ in the isospin 0 and the $Z_c(3900)$ in the isospin 1.

Experimentally, observation of such K^* state should be possible in the current facilities and it would constitute an exciting novelty in the Kaonic spectroscopy.

Keywords: Exotic hadrons; Few body systems; Heavy quark symmetry; $SU(4)$ symmetry.

List of Figures

2.1 Chiral versus non-chiral 6
2.2 Parity operation 6
2.3 Right/left-handed particles 8
2.4 Helicity as a function of the reference frame 9
2.5 $SU(4)$ multiplets 29
2.6 Nuclear interaction: two different visions 30
2.7 Hidden local symmetry versus Chiral symmetry 34

3.1 Scattering on a hard sphere. 37
3.2 Collision between two hard spheres. 37
3.3 Projectile approaching a target 38
3.4 A target assembly 39
3.5 Structure function of the proton for $\lambda >> r_p$ 40
3.6 Structure function of the proton for $\lambda \approx r_p$ 41
3.7 Structure function of the proton for $\lambda \approx r_p$ by considering the Heisenberg principle 41
3.8 Structure function of the proton for $\lambda << r_p$ 42
3.9 Diagrams for the calculation of the amplitude for the reaction $D\phi \to D\phi$. . . 45
3.10 Diagram related to $T^{(2)}$. A virtual $D\phi$ state is produced. 45
3.11 One loop contribution to the T-matrix 49
3.12 s-channel exchange of the resonance formed from the $D\phi$ interaction. . . . 51
3.13 $\phi D \to \phi D$ with formation of a state with mass M and width Γ. 54

3.14 Process $D^0K^+ \to D^0K^+$ in the center of the mass frame 58
3.15 Real and imaginary part of G_{DK} 61
3.16 T-matrices obtained within the heavy quark model. 63
3.17 T-matrix in the complex energy plane for the heavy quark model 66
3.18 T-matrices found within the $SU(4)$ model (real axis) 68
3.19 T-matrices found within the $SU(4)$ model (complex plane) 69

4.1 Simplest contribution to the three-body scattering 71
4.2 Bethe-Salpeter equation 71
4.3 Interaction between three particles 71
4.4 Interaction between a particle and a cluster 73
4.5 Propagation of a particle in the cluster 74
4.6 Other contributions to the scattering of a particle and a cluster 75
4.7 Other series of diagrams contributing to the scattering of a particle and a cluster 76
4.8 $|T_{XX}|^2$ (isospin $1/2$, single channel, $\Gamma_Z = 0$ MeV) 81
4.9 $|T_{ZZ}|^2$ (isospin $1/2$, single channel, $\Gamma_Z = 0$ MeV) 81
4.10 $|T_{ZZ}|^2$ (isospin $1/2$, single channel, $\Gamma_Z = 28$ MeV) 82
4.11 $|T_{XX}|^2$ and $|T_{ZZ}|^2$ (isospin $1/2$, coupled channels, $\Gamma_Z = 28$ MeV) 82
4.12 $|T_{ZZ}|^2$ (isospin $3/2$, $\Gamma_Z = 28$ MeV) 83

5.1 Two-body decay channels for K_R^* 85
5.2 Decay mechanism of $K_R^* \to J/\psi K^*$ 85
5.3 Decay mechanism of $X \to J/\psi\rho$ 86
5.4 Decay process of $K_R^* \to \bar{D}^* D_s$ 86
5.5 Decay mechanism of $K_R^{*0} \to J/\psi K^{*0}$ 86
5.6 Momenta and mass assignment in the decay process of the K_R^* state. . . . 87
5.7 Decay mechanism of $K_R^{*0} \to D^- D_s^{*+}$ with a D^* exchange 93
5.8 Decay mechanism of $K_R^{*0} \to D^{*-} D_s^{*+}$ with a D exchange 94
5.9 Decay mechanism of $K_R^{*0} \to D^{*-} D_s^{*+}$ with a D^* exchange 95

List of Tables

3.1 Coefficients α_{ij} for charm +1 in the charge basis 60
3.2 Coefficients α_{ij} for charm +1 in the isospin basis 61
3.3 Coefficients α_{ij} for charm -1 in the isospin basis 61

4.1 Linear combinations of two-body t-matrices appearing in t_{31} and t_{32} 80

Contents

Acknowledgements **6**

Resumo **i**

Abstract **ii**

List of Figures **iii**

List of Tables **v**

1 Introduction **1**

2 Symmetry and Symmetry Breaking **5**

2.1 Chiral symmetry 5

2.2 Quantum chromodynamics and chiral symmetry 11

2.2.1 Noether's theorem 14

2.2.2 Chiral symmetry breaking and the Goldstone theorem 18

2.2.3 Goldstone's theorem for the mexican hat potential 24

2.3 Heavy quark symmetry 27

2.4 $SU(4)$ flavor symmetry 28

2.5 An effective theory 29

2.5.1 Effective Lagrangian based on the heavy quark symmetry 31

2.5.2 Effective Lagrangian based on $SU(4)$ 33

3 Two-Body Interactions **36**

3.1 Scattering: a classical view 36
3.2 Scattering: a quantum mechanical view 40
3.3 Scattering matrix 43
3.4 Determination of the T-matrix 44
3.4.1 The isospin base 54
3.4.2 T-matrices obtained with the HQ Lagrangian 57
3.4.3 T-matrices obtained with the $SU(4)$ Lagrangian 67

4 Three-body Interactions and the $KD\bar{D}^*$ System 70
4.1 The Faddeev equations 70
4.2 Fixed center approximation to the Faddeev equations 72
4.3 Determination of the $\tilde{t}_{31}$ and $\tilde{t}_{32}$ two-body T-matrices 78
4.4 Results 80

5 On the two-body decay widths of $K^*(4307)$ 84
5.1 Theoretical framework 84
5.1.1 Determination of the vertices 86
5.1.2 Triangular loops 90
5.2 Results and discussions 96

6 Conclusions 99

A Kernels V: isospin vs. charge 101
A.1 $C = +1$ and $I = 0,\ 1$ 101
A.2 $C = -1$ and $I = 0,\ 1$ 102

B Amplitudes V within the $SU(4)$ Lagrangian 104

C Determination of the a^i_j coefficients 107

Bibliography 112

CHAPTER 1

Introduction

The existence of exotic mesons and baryons, whose masses, widths and/or quantum numbers can not be explained within the constituent quark model of Gell-Mann and Zweig, is one of the peculiar characteristics of Quantum Chromodynamics which has been, and still is being, intensively explored in experiments and in theoretical models. Typical examples are: the scalar nonet in the meson sector, which includes the $f_0(500)$, $\kappa(800)$, $f_0(980)$, $a_0(980)$ states [1–6], and the $\Lambda(1405)$ in the baryon sector [7–11]. With the increase of the accessible energy range by the experimental facilities, claims for the observation of such states, especially in the heavy quark sector, with a hidden charm content, started appearing in the last decade, as the so called X, Y and Z families (see, e.g., Refs. [12–20] for reviews on the topic). In case of the Z family, consisting of charged particles with masses in the charmonium mass range, $3.9-4.2$ GeV, at least two quarks and two antiquarks are necessarily required, with a $c\bar{c}$ pair being responsible for their heavier masses. The isoscalar partners, belonging to the X and Y families, are also categorized as exotic, not due to the fact that to obtain their quantum numbers we need to invoke a different structure to that of $q\bar{q}$, but because their masses and widths cannot be explained within the traditional constituent quark model [17, 19].

All these heavy exotic mesons found experimentally in the recent years share a common feature: they are mesons with null strangeness. A glance at the summary of the Particle Data Group (PDG) [21] shows a low activity in the strange pseudoscalar and vector meson sectors since the last 30 years: in the Kaon sector, the last state reported corresponds to $K(1830)$. Its existence was claimed in 1983 from a partial wave analyses of the $K^-\phi$ system produced in the reaction $K^-p \to K^+K^-K^-p$ [22], and, recently, the

LHCb collaboration took it into account in the amplitude analysis of the $B^+ \to J/\psi\phi K^+$ decay [23]. Similarly, in the vector meson sector, the latest $I(J^P) = 1/2(1^-)$ K^* state listed in Ref. [21] is the $K^*(1680)$, whose existence dates to experiments and partial wave analysis performed during 1978-1988 [24–27]. As in the case of $K(1830)$, the LHCb collaboration has also recently considered its existence in the analysis of the amplitude for the decay process $B^+ \to J/\psi\phi K^+$ [23]. And, overall, the final excited state in the meson sector, with nonzero strangeness quantum number, reported by the PDG corresponds to $K(3100)$, whose quantum numbers are unknown, and which was observed in several $\Lambda\bar{p}(\bar{\Lambda}p)$+pions reactions during the years 1986-1993 [23].

In view of such a panorama, it is worth exploring whether or not there could be another family member to be added to the already known X, Y, Z families whose members will also have masses in the charmonium mass range, i.e., $\sim 3-4$ GeV, but nonzero strangeness. Such states are manifestly exotic, since within a quark description, we will need at least a $c\bar{c}$ pair as well as a s quark and a light antiquark ($\bar{u}$, $\bar{d}$) to account for their masses and quantum numbers. Surprisingly, although this energy region is currently accessible, the existence of such states has not been yet explored experimentally. But formation of such states has been claimed theoretically very recently using different models: in Ref. [28], the DD^*K system was studied by solving the Schrödinger equation and considering a pion exchange potential model to describe the interactions between the pairs forming the three-body system. As a result, a bound state with mass $4317.92^{+3.66}_{-4.32}$ MeV was obtained. Considering G-parity arguments, the authors of Ref. [28] claim also the existence of a $D\bar{D}^*K$ bound state with basically the same mass.

As we will discuss in this thesis, we recently studied the $KD\bar{D}^*$ system [29] by solving the Faddeev equations under the fixed center approximation [30–37]. In this case, the interaction between the particles in the two-body subsystems are obtained by solving the Bethe-Salpeter equation within a coupled channel approach with kernels determined from an effective field theory implementing symmetries like the chiral symmetry [38, 39] and/or the heavy quark symmetry [40–42]. Within such an approach, the states $D^*_{s0}(2317)$, $X(3872)$ and $Z_c(3900)$ are generated from the coupled channel dynamics and are mainly DK bound states in isospin 0, $D\bar{D}^*$ states in isospin 0 and 1, respectively [43–46]. As a consequence of the dynamics involved, an evidence for an

$I(J^P) = 1/2(1^-)$ K^* state with a mass of $M - i\frac{\Gamma}{2} = (4307 \pm 2) - i(9 \pm 2)$ MeV is obtained when the $D\bar{D}^*$ system clusters as $X(3872)$ or $Z_c(3900)$.

Theoretically, the attraction in the DK and $D\bar{D}^*$ subsystems, which leads to the generation of the $D_{s0}^*(2317)$, $X(3872)$ and $Z_c(3900)$ states, constitutes a compelling argument in favor of the existence of such exotic K^* state with a mass around 4.3 GeV and hidden charm. Experimentally, observation of such K^* state should be possible in the current facilities and it would constitute an exciting novelty in the Kaonic spectroscopy and in that of the exotic mesons.

In order to provide more reliable information for a possible experimental analysis of such state, we continue investigating further properties of the $K^*(4307)$ state found and calculate the decay widths to several open two-body channels [47]. Particularly, we consider the channels $J/\psi K^*(892)$, $\bar{D}D_s^*$, $\bar{D}^*D_s^*$ and $\bar{D}D_s$, which are the most relevant ones, based on the nature of $K^*(4307)$.

This thesis is organized as follows

- In chapter 2 we give a brief introduction on symmetries relevant to the hadron system at hand and which are needed to determine the amplitudes describing the two body-interactions, which in our case are the chiral, heavy quark and SU(4) symmetries. We also introduce the concept of explicit and spontaneous symmetry breaking for the chiral symmetry and its consequences. After this is done, we give a brief idea on the meaning of an effective theory and how the above symmetries can be used to obtain effective Lagrangians describing the interactions between mesons.

- In chapter 3 we give a brief introduction to the scattering and the resolution of the Bethe-Salpeter equation in a coupled channel approach, which is needed to determine the scattering matrix for the two-body subsystems involved in the $KD\bar{D}^*$ system. This scattering matrix, as we will show, will be used as input for solving the Faddeev equations.

- The chapter 4 is dedicated to the study of the three-body system $KD\bar{D}^*$. Here we introduce the Faddeev equations and the fixed center approximation to solve them. By solving these equations, we obtain the T-matrix for the three-body system and we show the results found for the different isospin configurations. An

isospin $1/2$ state with strangeness $+1$ and hidden charm is generated with a mass around 4307 MeV.

- In chapter 5 we continue investigating the nature and properties of the $K^*(4307)$ obtained in chapter 4. To be more concrete, we have investigated relevant two-body decay processes for $K^*(4307)$ and determine the corresponding widths.

CHAPTER 2

Symmetry and Symmetry Breaking

One of the most relevant concepts in physics is that of a symmetry: the fact that certain properties or laws of a given system remain unaltered when something changes. Particularly, symmetry in physics is directly related to the notion of invariance: when some properties of a system do not change if a particular transformation is performed we say that there is an invariance under such transformation.

In this chapter we revise some of the basic properties related to the symmetries used to construct the effective Lagrangians describing the interactions between mesons.

2.1 Chiral symmetry

Chirality is directly related to the mirror image of the object under consideration. The mirror image of any object or system can be thought of as the space inversion of it and this inversion is related to the parity operation.

Chirality

The term *chirality* is derived from the ancient greek word for hand *(kheir)*.
In the macroscopic world we can think of chirality as the structural characteristic of a finite system that makes impossible to overlap it on its mirror image (see Figure 2.1).

The application of the parity operator, P, over any system will reflect its coordinates to the inverse direction, for instance

$$P : \vec{x} \rightarrow \vec{x}' = -\vec{x}. \tag{2.1}$$

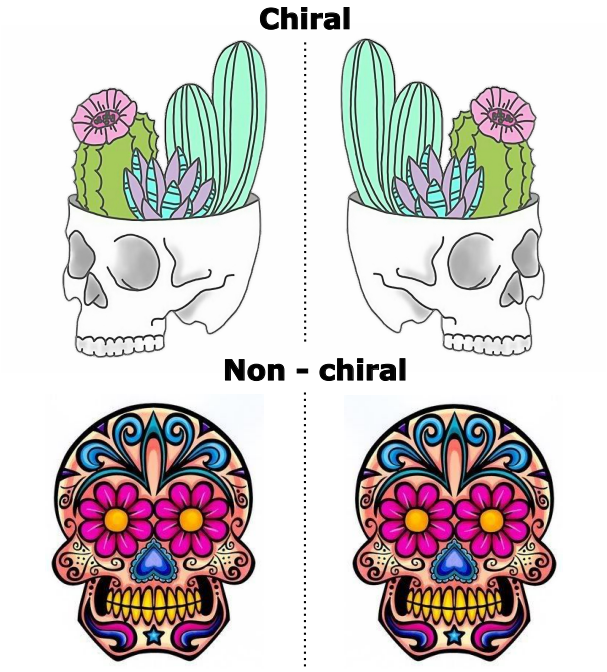

Figure 2.1: Two different skulls. The upper one is a chiral skull, while the lower one is a non-chiral skull.

that is, P projects the axes x, y and z to the inverted coordinate system x', y', z', as shown in Fig. 2.2.

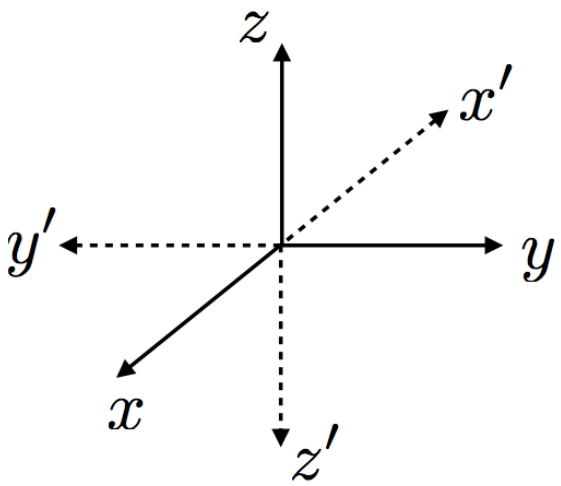

Figure 2.2: Space inversion or parity operation.

If we consider, for example, the reflection with respect to the xy plane, we have then

$$x \to x' = x, \qquad y \to y' = y, \qquad z \to z' = -z, \tag{2.2}$$

and if we apply now a continuous rotation of π around the z axis

$$x' \to -x, \qquad y' \to -y, \qquad z' \to -z. \tag{2.3}$$

Thus, we obtain the same result as if we had applied the parity operator over the system. In this way, the space inverted state can be obtained by a continuous transformation from the mirror reflected image.

In the example above, it is also interesting to notice that the parity operation transforms a system which is right-handed, (x,y,z), into a left handed one, (x',y',z'). In this form, the invariance of a system under space inversion implies the impossibility of distinguishing the right from the left.

With this description, the chirality seems to be a trivial concept for macroscopic objects, since we are able to see the object. But how can the concept be used in the microscopic world, particularly, at the quark level?

Quarks are particles with spin 1/2, thus, fermions. If we consider a particle with spin 1/2 and linear momentum $\vec{p}$, we can define a quantity which corresponds to the projection of its spin in the direction of its linear momentum. Such an operator is called as helicity and is, mathematically, given by

$$h = \frac{\vec{\sigma}\cdot\vec{p}}{|\vec{p}|} = \vec{\sigma}\cdot\hat{p}, \tag{2.4}$$

where $\hat{p}$ is a unit vector along the direction of the linear momentum of the particle, that is $\hat{p} \equiv \frac{\vec{p}}{|\vec{p}|}$, and $\vec{\sigma}$ are the Pauli matrices, $\vec{\sigma} = (\sigma_x, \sigma_y, \sigma_z)$. In this way, we can have two possible eigenvalues for h, $+1$ or -1. The value "+1" means that the spin and the momentum are aligned, while the value "-1" means that the spin and the momentum have opposite directions.

In this context, it's quite common to use the nomenclature of *right-handed* and *left-handed* particles, respectively. To define the "handedness" of a particle, let us consider the classical (although misleading) picture of a particle spinning on its axis and interpret the spin of the particle as the angular momentum associated with this rotation. The fingers of the right-hand are used to indicate the sense of the spin of the particle with the thumb pointing in the direction of the defined angular momentum. The linear momentum of the particle is used to define a preferred direction in space, and if one curls the fingers of one's right hand to indicate the sense of the "spinning" of a particle, and the thumb of the same hand points in the direction of the linear momentum, then we say that we have a right-handed particle [see Fig. 2.3 (left)]. If to get the thumb pointing in the direction of the linear momentum one has to use the fingers of one's left hand, then we have a left-handed particle [see Fig. 2.3 (right)].

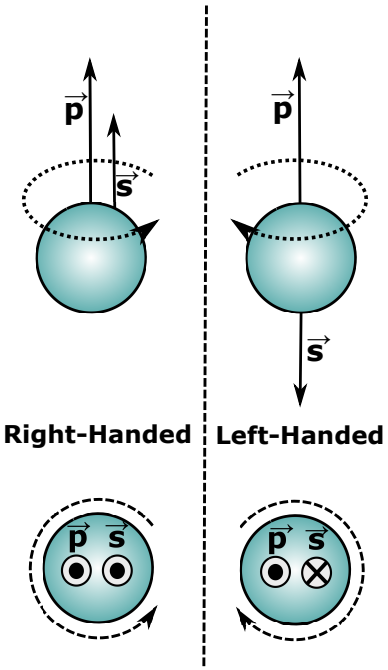

Figure 2.3: Classical interpretation of a right-handed particle (left side) and a left-handed particle (right side).

A problem with this concept is that the helicity, in general, is not Lorentz invariant. Consider, for instance, a particle with spin 1/2 and mass m which is a right-handed particle in a particular reference frame. In this frame, the particle moves with velocity, say, $\vec{v} = v\,\hat{i}$ in the positive direction of the x-axis. For an observer in an inertial reference frame moving parallel to the particle with a velocity $\vec{u} = u\,\hat{i}$, such that $u > v$, the particle would be actually traveling in the opposite direction in this frame with velocity $\vec{w} = w\,\hat{i}$, with $w = v - u$ (we are considering a non-relativistic particle). Thus, for this new observer, the particle will be a left-handed particle (see Fig. 2.4). Therefore, helicity is not Lorentz invariant [48]. The only situation where the helicity is Lorentz invariant is in the case where the particle is massless. That's because if the particle is massless it travels with speed c (the speed of light), irrespective of the inertial reference frame considered. In such a case, it is impossible to reverse the direction of motion as in the previous example.

The "handedness" of a particle is an important property in particle physics and it is important to define an operator similar to the helicity, which is Lorentz invariant. This can be achieved by using the γ^5 Dirac matrix. In the Weyl representation of the γ^μ

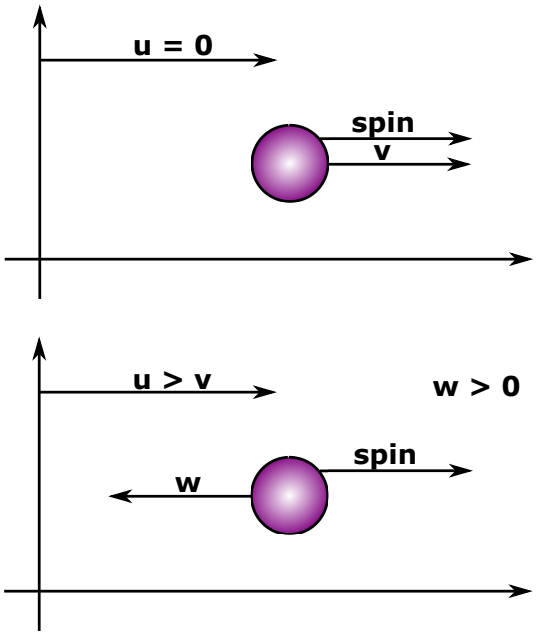

Figure 2.4: The helicity of a particle depends on the reference frame. A right-handed particle for an observer in an inertial reference frame (top) becomes a left-handed particle (bottom) for an observer in another inertial reference frame.

matrices, we have

$$\gamma^5 = i\gamma^0\gamma^1\gamma^2\gamma^3 = \begin{pmatrix} -I_{2\times 2} & 0 \\ 0 & I_{2\times 2} \end{pmatrix}. \tag{2.5}$$

As in the case of the helicity, γ^5 has also eigenvalues $+1$ and -1. If we call Ψ_R and Ψ_L the eigenvectors of γ^5, we have

$$\begin{aligned} \gamma^5\Psi_R &= \Psi_R, && \text{Positive Chirality,} \\ \gamma^5\Psi_L &= -\Psi_L, && \text{Negative Chirality,} \end{aligned}$$

and Ψ_R (Ψ_L) has eigenvalue $+1$ (-1) or positive (negative) chirality.

The main difference between the γ^5 operator, which is called the chirality operator, and the helicity is that γ^5 commutes with the generators of the Lorentz transformations, i.e., boosts and rotations. The chirality can be interpreted then as a Lorentz extended version of the helicity. Note that the left (L) and right (R) labels on the eigenvectors do not indicate real handedness: they just give information about the eigenvalues of γ^5 ($-1 = L$; $+1 = R$). Probably the origin of such a notation is the fact that in the limit of ultrarelativistic particles or massless particles, chirality coincides with the helicity, which is related to the classical idea of handedness via the right hand rule. Effectively, if we consider the Dirac equation for a free particle of mass m described by the field Ψ, we

have

$$(i\gamma^\mu \partial_\mu - m)\Psi = 0. \tag{2.6}$$

The field describing such a state, Ψ, is not necessarily a chiral field, but we can rewrite it in terms of its chiral components by using the chiral projectors, which are defined as $P_L = \frac{1}{2}(1-\gamma_5)$ and $P_R = \frac{1}{2}(1+\gamma_5)$, such that

$$\Psi_L(x) = P_L\Psi(x), \qquad \Psi_R(x) = P_R\Psi(x). \tag{2.7}$$

Note that P_L and P_R have the properties $P_L^2 = P_L$, $P_R^2 = P_R$ and $P_L P_R = P_R P_L = 0$, i.e., they are projectors (see Ref. [49]).

In this way, the field Ψ can be written in terms of the fields Ψ_L and Ψ_R as

$$\Psi = \Psi_R + \Psi_L = \begin{pmatrix} \psi_1 \\ \psi_2 \end{pmatrix}. \tag{2.8}$$

Note that in Eq. (2.8) ψ_i, with $i = 1,2$, is a spinor (thus a 2×1 matrix), while Ψ, Ψ_L and Ψ_R are bispinors (thus 4×1 matrices).

In the Weyl representation we have the γ matrices given by

$$\gamma^5 = \begin{pmatrix} -I_{2\times 2} & 0 \\ 0 & I_{2\times 2} \end{pmatrix}, \qquad \gamma^\mu = \begin{pmatrix} 0 & \sigma^\mu \\ \bar{\sigma}^\mu & 0 \end{pmatrix}, \tag{2.9}$$

where $\sigma^\mu = \left(\sigma^0, \sigma^i\right)$ and $\bar{\sigma}^\mu = (\sigma^0, -\sigma^i)$ with $\sigma^0 = I_{2\times 2}$. In this way, from Eq. (2.7)

$$\begin{aligned} \Psi_R = P_R\Psi &= \begin{pmatrix} 0 & 0 \\ 0 & I_{2\times 2} \end{pmatrix}\begin{pmatrix} \psi_1 \\ \psi_2 \end{pmatrix} = \begin{pmatrix} 0 \\ \psi_2 \end{pmatrix} \equiv \begin{pmatrix} 0 \\ \psi_R \end{pmatrix}, \\ \Psi_L = P_L\Psi &= \begin{pmatrix} I_{2\times 2} & 0 \\ 0 & 0 \end{pmatrix}\begin{pmatrix} \psi_1 \\ \psi_2 \end{pmatrix} = \begin{pmatrix} \psi_1 \\ 0 \end{pmatrix} \equiv \begin{pmatrix} \psi_L \\ 0 \end{pmatrix}, \end{aligned}$$

such that

$$\Psi = \Psi_R + \Psi_L = \begin{pmatrix} \psi_L \\ \psi_R \end{pmatrix}. \tag{2.10}$$

Then, in the Weyl representation, the upper component of Ψ corresponds to a left-handed spinor, ψ_L, and the lower component to a right-handed spinor, ψ_R.

Using Eqs. (2.9) and (2.10), we can write Eq. (2.6) as

$$\begin{pmatrix} -m & i\sigma^\mu\partial_\mu \\ i\bar{\sigma}^\mu\partial_\mu & -m \end{pmatrix}\begin{pmatrix} \psi_L \\ \psi_R \end{pmatrix} = \begin{pmatrix} 0 \\ 0 \end{pmatrix},$$

which results in two coupled equations

$$i\sigma^\mu \partial_\mu \psi_R - m\psi_L = 0,$$
$$i\bar{\sigma}^\mu \partial_\mu \psi_L - m\psi_R = 0.$$

But, if the particle is massless, the equations become decoupled

$$i\sigma^\mu \partial_\mu \psi_R = 0, \tag{2.11}$$
$$i\bar{\sigma}^\mu \partial_\mu \psi_L = 0. \tag{2.12}$$

By identifying $i\partial_\mu$ with p_μ, the above equations can be written as

$$\begin{aligned} &\sigma^\mu p_\mu \psi_R = 0, && \bar{\sigma}^\mu p_\mu \psi_L = 0, \\ &\Rightarrow \left(p^0 - \vec{\sigma}\cdot\vec{p}\right)\psi_R = 0, && \Rightarrow (p^0 + \vec{\sigma}\cdot\vec{p})\psi_L = 0, \\ &\Rightarrow \frac{\vec{\sigma}\cdot\vec{p}}{p^0}\psi_R = \psi_R, && \Rightarrow \frac{\vec{\sigma}\cdot\vec{p}}{p^0}\psi_L = -\psi_L. \end{aligned} \tag{2.13}$$

If we consider the positive energy solution, $p^0 = \sqrt{\vec{p}^2 + m^2}$, for a massless particle (or in the ultrarelativistic limit) we get $p^0 = \sqrt{\vec{p}^2} \equiv |\vec{p}|$. Then we can write Eq. (2.13) as

$$\frac{\vec{\sigma}\cdot\vec{p}}{|\vec{p}|}\psi_R = \vec{\sigma}\cdot\hat{p}\psi_R = h\psi_R = \psi_R, \qquad \frac{\vec{\sigma}\cdot\vec{p}}{|\vec{p}|}\psi_L = \vec{\sigma}\cdot\hat{p}\psi_L = h\psi_L = -\psi_L. \tag{2.14}$$

So, in such a limit, the Dirac equation reduces to a set of the helicity eigenstate equations. Note that under a parity transformation

$$P : \Psi_R(t,\vec{x}) \to \gamma^0 P_R \Psi(t,-\vec{x}) = P_L \gamma^0 \Psi(t,-\vec{x}) = P_L \Psi'(t,\vec{x}') \equiv \Psi'_L(t,\vec{x}'), \tag{2.15}$$

thus, the field does not transform into itself. In fact, it transforms into a field with the opposite chirality: they are then chiral fields.

The concept of chirality appears in different contexts, but we are particularly interested in its relevance for the Quantum Chromodynamics (QCD).

2.2 Quantum chromodynamics and chiral symmetry

Within the current understanding of nature, the theory explaining the interaction between hadrons is the so called Quantum Chromodynamics (QCD) [50, 51]. The former is a quantum field theory invariant under the local $SU_C(3)$ gauge transformations, where

C refers to the color quantum number, and where the degrees of freedom are the quarks and gluons.

The QCD Lagrangian describing the interactions between quarks and gluons is given by

$$\mathscr{L}_{QCD} = \bar{q}_{\alpha,f,k}(i\gamma^{\mu}D_{\mu} - m_f)q_{\alpha,f,k} - \frac{1}{2}\mathrm{Tr}\{\mathscr{G}_{\mu\nu}\mathscr{G}^{\mu\nu}\}, \tag{2.16}$$

where f represents the flavor index [$f = 1,2,\ldots,6$ or u (up), d (down), s (strange), c (charm), b (bottom), t (top)], α stands for the spinor index $(\alpha = 1,2,3,4)$, k is the color index ($k = 1,2,3$) and an implicit summation is understood whenever repeated indices appear. The trace in Eq. (2.16) is taken over the color space. The D_{μ} in Eq. (2.16) represents the covariant derivative, given by

$$D_{\mu} \equiv \partial_{\mu} - i\frac{\lambda_a}{2}G^a_{\mu} \equiv \partial_{\mu} - igG_{\mu}, \tag{2.17}$$

with

$$G_{\mu} \equiv \frac{\lambda_a}{2}G^a_{\mu}, \tag{2.18}$$

In Eq. (2.17), g is the coupling constant between quarks and gluons, λ_a are the Gell-Mann matrices and G^a_{μ} are the gluon fields $(a = 1,2,\ldots,8)$. The $\mathscr{G}_{\mu\nu}$ in Eq. (2.16) is the so called field strength tensor, which is written in terms of G_{μ} as

$$\mathscr{G}_{\mu\nu} = \partial_{\mu}G_{\nu} - \partial_{\nu}G_{\mu} - ig\big[G_{\mu}, G_{\nu}\big]. \tag{2.19}$$

At the energy scale of 1 GeV, the heavy quark degrees of freedom are not relevant and can be ignored, while the mass associated with the light quarks, u, d, s (between 2 and 12 MeV for u and d quarks and about 160 MeV for the s quark) is much smaller than the energy scale considered. It is therefore interesting to investigate the limit where the masses of the quarks u, d and s are exactly zero, i.e., m_u, m_d, $m_s \to 0$. In this limit, the Lagrangian given in Eq. (2.16) becomes

$$\mathscr{L}^0_{\mathrm{QCD}} = \bar{q}i\not{D}q - \frac{1}{2}\mathrm{Tr}\{\mathscr{G}_{\mu\nu}\mathscr{G}^{\mu\nu}\}, \tag{2.20}$$

where from now onwards, to simplify the notation, we introduce the array q

$$q = \begin{pmatrix} u \\ d \\ s \end{pmatrix}, \tag{2.21}$$

and omit the spinor and color indices of the quark fields.

As done in section 2.1, we can decompose q into its right-handed (q_R) and left-handed (q_L) components, i.e., $q = q_R + q_L$. In terms of q_R and q_L, Eq. (2.20) can be written as

$$\mathscr{L}^0_{\text{QCD}} = \left[\bar{q}_L i\not{\partial} q_L + \bar{q}_R i\not{\partial} q_R\right] - \frac{1}{2}\,\text{Tr}\{\mathscr{G}_{\mu\nu}\mathscr{G}^{\mu\nu}\}. \tag{2.22}$$

As can be seen from Eq. (2.22), the contributions to the Lagrangian from the left-handed fields are decoupled to the one from the right-handed fields. This fact makes that the Lagrangian in Eq. (2.22) remains invariant under independent global $SU(3)$ rotations of the fields, i.e.,

$$q_L(x) \to q_L(x), \qquad q_R(x) \to U_R\, q_R(x) = \exp\left\{-i\theta_{Ra}\frac{\lambda_a}{2}\right\} q_R(x), \tag{2.23}$$

or

$$q_R(x) \to q_R(x), \qquad q_L(x) \to U_L\, q_L(x) = \exp\left\{-i\theta_{La}\frac{\lambda_a}{2}\right\} q_L(x), \tag{2.24}$$

with θ_{Ra} and θ_{La} being arbitrary real parameters ($a = 1,2,\ldots,8$). We have then that the Lagrangian in Eq. (2.22) has an $SU_R(3)\otimes SU_L(3)$ symmetry, which is called chiral symmetry [38, 39]. This is the microscopic version of the chiral symmetry described in section 2.1.

The $SU(N)$ Group

The Special Unitary Group [$SU(N)$] is the Lie group formed by all $n\times n$ unitary matrices with determinant equal to one. Thus, there are n^2-1 parameters in the group. An element of the group can be written in terms of the generators of the group, T_a, as

$$U = e^{-i\theta_a T_a},$$

where θ_a are real parameters ($a = 1,2,\ldots,n^2-1$).

Since $\det U = 1$, we can write

$$e^{\ln[\det U]} = 1.$$

If we consider now a base where U is diagonal, we have

$$\begin{aligned}\exp\left[\ln(\det U)\right] &= \exp\left(\ln\prod_{i=1}^{n} U_{ii}\right) = \exp\left(\sum_{i=1}^{n}\ln U_{ii}\right)\\ &= \exp\left(\mathrm{Tr}\{\ln U\}\right) = \exp\{\mathrm{Tr}\{\ln[\exp(-i\theta_a T_a)]\}\}\\ &= \exp[\mathrm{Tr}(-i\theta_a T_a)] = 1 \Rightarrow \mathrm{Tr}(\theta_a T_a) = 0.\end{aligned}$$

Since θ_a are arbitrary parameters we have that

$$\mathrm{Tr}[T_a] = 0.$$

Thus the generators, T_a, are traceless.

In case of $SU(3)$, it is quite common to use as generators the Gell-Mann matrices, λ_a. In this way, we can write $U_R \equiv \exp\left\{-i\theta_{Ra}\frac{\lambda_a}{2}\right\}$ and $U_L \equiv \exp\left\{-i\theta_{La}\frac{\lambda_a}{2}\right\}$, where θ_{Ra} and θ_{La} are parameters.

Besides this symmetry, the Lagrangian in Eq. (2.22) has also a global $U(1)$ symmetry associated with independent phase transformation of the fields. That is, the Lagrangian is invariant under the following transformations

$$q_L(x) \to q_L(x), \qquad q_R(x) \to u_R\, q_R(x) = \exp\{-i\theta_R\} q_R(x), \tag{2.25}$$

or

$$q_R(x) \to q_R(x), \qquad q_L(x) \to u_L\, q_L(x) = \exp\{-i\theta_L\} q_L(x), \tag{2.26}$$

where θ_L and θ_R are arbitrary real parameters. Thus, the Lagrangian in Eq. (2.22) is also $U_R(1)\otimes U_L(1)$ invariant. In this way, the symmetry group for this theory, in the limit where the quarks are massless, is $SU_R(3)\otimes SU_L(3)\otimes U_R(1)\otimes U_L(1)$.

For a better understanding of the consequences of this symmetry we can use the Noether's Theorem [52].

2.2.1 Noether's theorem

The theorem stated by Emmy Noether permits the relation between a continuous symmetry of a Lagrangian and certain conserved quantities. Particularly, we are interested

in studying the invariance of the Lagrangian in Eq. (2.22) under the transformations given by Eqs. (2.23)-(2.26).

Noether's Theorem

For every continuous symmetry of the Lagrangian there is a conserved current and the associated charge is independent of time.

Let us consider a Lagrangian which depends on the fields ϕ_i and $\partial_\mu \phi_i$. An infinitesimal transformation on the fields ϕ_i, changes $\phi_i(x)$ into $\phi_i'(x)$ such that

$$\phi_i(x) \to \phi_i'(x) = \phi_i(x) + \delta\phi_i(x) = \phi_i(x) - i\varepsilon_a F_{ai}[\phi(x)], \tag{2.27}$$

$$\Rightarrow \delta\phi_i(x) = -i\varepsilon_a F_{ai}[\phi(x)], \tag{2.28}$$

where ε_a represents arbitrary infinitesimal real constants and $F_{ai}[\phi(x)]$ is a function of the fields. Such transformations on the fields lead to a change of the Lagrangian of the form

$$\mathscr{L} \to \mathscr{L}' = \mathscr{L} + \delta\mathscr{L}, \tag{2.29}$$

where, given the dependence of $\mathscr{L}$ on the fields,

$$\delta\mathscr{L} = \frac{\partial\mathscr{L}}{\partial\phi_i}\delta\phi_i + \frac{\partial\mathscr{L}}{\partial\left(\partial_\mu\phi\right)}\delta\left(\partial_\mu\phi\right). \tag{2.30}$$

Using Eq. (2.28), we can write Eq. (2.30) as

$$\delta\mathscr{L} = \varepsilon_a\left(-i\frac{\partial\mathscr{L}}{\partial\phi_i}F_{ai} - i\frac{\partial\mathscr{L}}{\partial\partial_\mu\phi_i}\partial_\mu F_{ai}\right). \tag{2.31}$$

If we impose now that $\mathscr{L}$ satisfies the Euler-Lagrange equations, we have that

$$\frac{\partial\mathscr{L}}{\partial\phi_i} = \partial_\mu\left(\frac{\partial\mathscr{L}}{\partial\left(\partial_\mu\phi_i\right)}\right), \tag{2.32}$$

then, Eq. (2.31) becomes

$$\begin{aligned}\delta\mathscr{L} &= \varepsilon_a\left(-i\partial_\mu\left(\frac{\partial\mathscr{L}}{\partial\left(\partial_\mu\phi_i\right)}\right)F_{ai} - i\frac{\partial\mathscr{L}}{\partial\left(\partial_\mu\phi_i\right)}\partial_\mu F_{ai}\right),\\ &= \varepsilon_a\partial_\mu\left(-i\frac{\partial\mathscr{L}}{\partial\left(\partial_\mu\phi_i\right)}F_{ai}\right).\end{aligned} \tag{2.33}$$

Defining

$$J_a^\mu \equiv -i\frac{\partial\mathscr{L}}{\partial\left(\partial_\mu\phi_i\right)}F_{ai}, \tag{2.34}$$

we get

$$\delta\mathscr{L} = \varepsilon_a \partial_\mu J_a^\mu . \tag{2.35}$$

If the Lagrangian is invariant under the transformation given in Eq. (2.28), $\mathscr{L}' = \mathscr{L}$, so, $\delta\mathscr{L} = 0$. This, according to Eq. (2.35), implies that $\partial_\mu J_a^\mu = 0$, since the parameters ε_a are arbitrary. We have precisely reached to the Noether's theorem: for each infinitesimal transformation of the fields which leaves the Lagrangian invariant there is a conserved current J_a^μ, i.e.,

$$\partial_\mu J_a^\mu = 0 \Rightarrow \frac{\partial J_a^0}{\partial t} + \vec{\nabla}\cdot\vec{J}_a = 0, \tag{2.36}$$

which is a continuity equation, where J_a^0 is the charge density and $\vec{J}_a$ corresponds to the current density. The total charge, Q_a, will be the integral over the volume of the charge density

$$Q_a \equiv \int d^3x\, J_a^0(t,\vec{x}), \tag{2.37}$$

such that, from Eq. (2.36)

$$\frac{dQ_a}{dt} = \int d^3x\, \frac{\partial J_a^0}{\partial t} = -\int d^3x\, \vec{\nabla}\cdot\vec{J}_a = -\oint_S d\vec{S}\cdot\vec{J}_a = 0 \tag{2.38}$$

where we have used as boundary condition that the fields vanish at infinity, i.e., when $|\vec{x}| \to \infty$.

Let us now determine the conserved currents and the charges associated with the symmetry transformations of Eqs. (2.23)-(2.26). For infinitesimal θ_{Ra} and θ_{La}, Eqs. (2.23) and (2.24) can be written as

$$q_R(x) \to \left(1 - i\theta_{Ra}\frac{\lambda_a}{2}\right) q_R(x), \qquad q_L(x) \to q_L(x), \tag{2.39}$$

$$q_L(x) \to \left(1 - i\theta_{La}\frac{\lambda_a}{2}\right) q_L(x), \qquad q_R(x) \to q_R(x). \tag{2.40}$$

By using Eqs. (2.27) and (2.34) together with Eq. (2.22) we find the corresponding conserved currents, which are

$$J_{Ra}^\mu = \bar{q}_R \gamma^\mu \frac{\lambda_a}{2} q_R, \qquad J_{La}^\mu = \bar{q}_L \gamma^\mu \frac{\lambda_a}{2} q_L, \tag{2.41}$$

with $\partial_\mu J_{Ra}^\mu = \partial_\mu J_{La}^\mu = 0$.

Similarly, from Eqs (2.25) and (2.26) considering infinitesimal θ_R and θ_L, we have

$$q_R(x) \to (1 - i\theta_R) q_R(x), \qquad q_L(x) \to q_L(x),$$

$$q_L(x) \to (1 - i\theta_L) q_L(x), \qquad q_R(x) \to q_R(x),$$

and by means of Eq. (2.27), (2.34) and (2.22) we find the corresponding conserved currents to be

$$J_R^\mu = \bar{q}_R \gamma^\mu q_R, \qquad J_L^\mu = \bar{q}_L \gamma^\mu q_L. \tag{2.42}$$

For a deeper understanding of the currents found, it is useful to construct a linear combination of them. Particularly, we define

$$\begin{aligned} V_a^\mu &= J_{Ra}^\mu + J_{La}^\mu, \qquad & A_a^\mu &= J_{Ra}^\mu - J_{La}^\mu, \\ V^\mu &= J_R^\mu + J_L^\mu, \qquad & A^\mu &= J_R^\mu - J_L^\mu. \end{aligned} \tag{2.43}$$

Using Eqs. (2.42) and (2.41), and working out the expressions, we have [53]

$$\begin{aligned} V_a^\mu &= \bar{q}\gamma^\mu \frac{\lambda_a}{2} q, \qquad & A_a^\mu &= \bar{q}\gamma^\mu\gamma^5 \frac{\lambda_a}{2} q, \\ V^\mu &= \bar{q}\gamma^\mu q, \qquad & A^\mu &= \bar{q}\gamma^\mu\gamma^5 q. \end{aligned} \tag{2.44}$$

Interestingly, the currents given in Eqs. (2.44) have a well defined transformation under parity. For instance

$$\begin{aligned} P : V_a^\mu(t;\vec{x}) \xrightarrow[\vec{x}\to-\vec{x}]{q\to\gamma^0 q} (q\gamma^0)^\dagger \gamma^0\gamma^\mu \frac{\lambda_a}{2}\gamma^0 q &= q^\dagger \gamma^\mu \gamma^0 \frac{\lambda_a}{2} q \\ &= \left(q^\dagger \gamma^0\gamma^0 \frac{\lambda_a}{2} q;\, q^\dagger \gamma^i \gamma^0 \frac{\lambda_a}{2} q \right) = \left(\bar{q}\gamma^0 \frac{\lambda_a}{2} q;\, -\bar{q}\gamma^i \frac{\lambda_a}{2} q \right), \\ &\to V_{a\mu}(t;\, -\vec{x}), \end{aligned} \tag{2.45}$$

and

$$\begin{aligned} P : A_a^\mu(t;\vec{x}) \xrightarrow[\vec{x}\to-\vec{x}]{q\to\gamma^0 q} (q\gamma^0)^\dagger \gamma^0\gamma^\mu\gamma^5 \frac{\lambda_a}{2}\gamma^0 q &= q^\dagger \gamma^\mu\gamma^5 \gamma^0 \frac{\lambda_a}{2} q \\ &= \left(-q^\dagger \gamma^0\gamma^0\gamma^5 \frac{\lambda_a}{2} q;\, -q^\dagger \gamma^i \gamma^0\gamma^5 \frac{\lambda_a}{2} q \right) = \left(-\bar{q}\gamma^0\gamma^5 \frac{\lambda_a}{2} q;\, \bar{q}\gamma^i\gamma^5 \frac{\lambda_a}{2} q \right), \\ &\to -A_{a\mu}(t;\, -\vec{x}). \end{aligned} \tag{2.46}$$

Thus, V_a^μ transforms under parity as a vector current, while A_a^μ transforms as an axial current. Similarly, $V^\mu(t,\vec{x})[A^\mu(t,\vec{x})]$ transforms under parity as a vector (axial) current, i.e.,

$$P : V^\mu(t;\vec{x}) \xrightarrow[\vec{x}\to-\vec{x}]{q\to\gamma^0 q} V_\mu(t;-\vec{x}), \qquad P : A^\mu(t;\vec{x}) \xrightarrow[\vec{x}\to-\vec{x}]{q\to\gamma^0 q} -A_\mu(t;-\vec{x}). \tag{2.47}$$

From these currents we can obtain the charge operators by using Eq. (2.37), and they are given by

$$Q_{Va} = \int d^3x\, q^\dagger \frac{\lambda_a}{2} q, \qquad Q_{Aa} = \int d^3x\, q^\dagger \gamma^5 \frac{\lambda_a}{2} q, \tag{2.48}$$

$$Q_V = \int d^3x\, q^\dagger q, \qquad Q_A = \int d^3x\, q^\dagger \gamma^5 q. \tag{2.49}$$

As in case of the currents, the charge operators also transform under parity as axial and vector quantities

$$P : \begin{cases} Q_{Va} \to Q_{Va}, & Q_{Aa} \to -Q_{Aa} \\ Q_V \to Q_V, & Q_A \to -Q_A. \end{cases} \tag{2.50}$$

So, in total, we have found 18 currents with the corresponding charges, which are conserved quantities. These currents are associated with the invariance of the QCD Lagrangian in the limit of massless quarks under $SU_L(3) \otimes SU_R(3) \otimes U_V(1) \otimes U_A(1)$ transformations of the quark fields. However, the consideration of quantum corrections (related to quantum fluctuations of the quarks fields in the gluon background) produces an anomaly in the results, breaking the conservation of the axial current A^μ even if the masses of the quarks are set to zero (a phenomenon known as the $U_A(1)$ anomaly) such that [52]

$$\partial_\mu A^\mu = \frac{3g^2}{32\pi^2} \varepsilon_{\mu\nu\rho\sigma} \mathcal{G}_a^{\mu\nu} \mathcal{G}_a^{\rho\sigma} \neq 0. \tag{2.51}$$

Thus, we end up having 17 conserved currents and their respective charges. In particular, the $U_V(1)$ symmetry results in the conservation of the baryon number B (which is related to the charge Q_V) and provides a classification of hadrons into mesons ($q\bar{q}$ pairs, thus $B = 0$) and baryons (qqq system, thus $B = 1$).

2.2.2 Chiral symmetry breaking and the Goldstone theorem

In the previous subsection we have seen that in the limit of massless quarks the QCD Lagrangian exhibits a symmetry, the chiral symmetry. In nature, however, the quark masses are not zero, though are small. If the explicit value of the quark masses are taken into account, the QCD Lagrangian develops a term which mixes right-handed and left-handed fields in such a way that it is not anymore invariant under the transformations given by Eqs. (2.39) and (2.40). This means that the QCD Lagrangian has terms which

explicitly break the chiral symmetry. For instance, from Eq. (2.16)

$$\begin{aligned}\mathscr{L} &= (\bar{q}_R + \bar{q}_L)\left(i\gamma^\mu D_\mu - m_f\right)(q_R + q_L) - \frac{1}{2}\mathrm{Tr}\{\mathscr{G}_{\mu\nu}\mathscr{G}^{\mu\nu}\}, \\ &= \bar{q}_R(i\gamma^\mu D_\mu)q_R + \bar{q}_L(i\gamma^\mu D_\mu)q_L - (\bar{q}_R + \bar{q}_L)m_f(q_R + q_L) - \frac{1}{2}\mathrm{Tr}\{\mathscr{G}^{\mu\nu}\mathscr{G}_{\mu\nu}\},\end{aligned}$$

and we get terms which couple right-handed and left-handed fields.

Besides the explicit symmetry breaking, we can also have the so called *spontaneous symmetry breaking*, which corresponds to a situation in which the Lagrangian preserves the symmetry, but the vacuum (state of minimum energy) doesn't. For a better understanding of the consequences of having a symmetry which is spontaneously broken we can use the Goldstone theorem [54–56].

Goldstone Theorem

Consider any field theory in which the Hamiltonian H is invariant under some Lie group G. Then, if we denote by T_a the generators of the group we have

$$[T_a, H] = 0. \tag{2.52}$$

A symmetry is called spontaneously broken if the ground state (or vacuum) of the theory, denoted by $|0\rangle$, is not invariant under G. In other words, that is, if for some generators of the group we have

$$T_a|0\rangle \neq 0. \tag{2.53}$$

The theorem establishes that for each generator that doesn't annihilate the ground state, there is a Goldstone Boson with zero mass and quantum numbers of T_a.

According to the Goldstone theorem, to get an insight regarding the spontaneous breaking of the symmetry, we need to find if there are generators related to the symmetry of the theory which do not annihilate the vacuum of the theory. To do this, it is actually more convenient to work directly with the charges found in Eqs. (2.49) and (2.48), which satisfy the same algebra as the generator of the group and therefore can also be considered generators of the transformations in Eqs. (2.40) and (2.39).

Charges vs. Generators

The Lie algebra of $SU_R(3) \otimes SU_L(3) \otimes U(1)_V$ implies some commutation relations for the generators of the group. Let T_{Ra} be the generators of the group associated with the $SU_R(3)$ symmetry (a = 1, ..., 8), T_{La} are the generators related with the $SU_L(3)$ group and T_V corresponds to the generator associated with the $U_V(1)$ group.

By working out the commutators between them, it is possible to show that [52]

$$\begin{aligned} [T_{Ra}, T_{Lb}] &= 0, & [T_{Ra}, T_{Rb}] &= i f_{abc} T_{Rc}, \\ [T_{La}, T_{Lb}] &= i f_{abc} T_{Lc}, & [T_{Ra}, T_V] &= [T_{La}, T_V] = 0, \end{aligned}$$

where f_{abc} are the structure constants of the group.

By using Eqs. (2.41) and (2.43), the corresponding charges are given by

$$\begin{aligned} Q_{La}(t) &= \int d^3x\, q_L^\dagger(t,\vec{x}) \frac{\lambda_a}{2} q_L(t,\vec{x}) = \int d^3x\, q^\dagger(t,\vec{x}) P_L \frac{\lambda_a}{2} q(t,\vec{x}), \\ Q_{Ra}(t) &= \int d^3x\, q_R^\dagger(t,\vec{x}) \frac{\lambda_a}{2} q_R(t,\vec{x}) = \int d^3x\, q^\dagger(t,\vec{x}) P_R \frac{\lambda_a}{2} q(t,\vec{x}), \\ Q_V(t) &= \int d^3x \left[q_L^\dagger(t,\vec{x}) q_L(t,\vec{x}) + q_R^\dagger(t,\vec{x}) q_R(t,\vec{x}) \right] = \int d^3x\, q^\dagger(t,\vec{x}) q(t,\vec{x}). \end{aligned}$$

By expressing the commutators of the charges in terms of equal-time anti-commutation relations of the quark fields, it can be found that [52]

$$\begin{aligned} [Q_{Ra}, Q_{Lb}] &= 0, & [Q_{Ra}, Q_{Rb}] &= i f_{abc} Q_{Rc}, \\ [Q_{La}, Q_{Lb}] &= i f_{abc} Q_{Lc}, & [Q_{Ra}, Q_V] &= [Q_{La}, Q_V] = 0, \end{aligned}$$

which reflects the underlying Lie algebra of $SU_L(3) \otimes SU_R(3) \otimes U_V(1)$. We conclude then that the charges are actually the generators of the infinitesimal transformations of the Hilbert space associated with the Lagrangian of Eq. (2.16) whose symmetry group is $SU_R(3) \otimes SU_L(3) \otimes U_V(1)$.

Since the charges are conserved quantities, i.e., their values do not change with time, they commute with the Halmiltonian H of the theory by means of

$$[H, Q] = i \frac{dQ}{dt} = 0, \tag{2.54}$$

for a given charge Q. Thus, for the charges Q_{Va} and Q_{Aa} we have that

$$[H, Q_{Aa}] = [H, Q_{Va}] = 0. \tag{2.55}$$

But as we have seen in Sec. 2.2.1, Q_{Aa} and Q_{Va} are operators with opposite parity. This means that for each state with positive parity we should expect the existence of another state with same energy as the previous one but negative parity. Indeed, if we call a state with energy E_α and positive parity as $|\alpha,+\rangle$, such that, $H^0_{QCD}|\alpha,+\rangle = E_\alpha|\alpha,+\rangle$ (the superscript 0 indicates that we work in the chiral limit of the QCD Hamiltonian) and define the states $|\phi_{\alpha,Va}\rangle$ and $\left|\phi_{\alpha,Aa}\right\rangle$ as

$$|\phi_{\alpha,Va}\rangle \equiv Q_{Va}|\alpha,+\rangle\,, \qquad \left|\phi_{\alpha,Aa}\right\rangle \equiv Q_{Aa}|\alpha,+\rangle\,, \tag{2.56}$$

we have

$$\begin{aligned} H^0_{\text{QCD}}\left|\phi_{\alpha,Aa}\right\rangle &= H^0_{\text{QCD}}Q_{Aa}|\alpha,+\rangle = Q_{Aa}H^0_{\text{QCD}}|\alpha,+\rangle = E_\alpha\left|\phi_{\alpha,Aa}\right\rangle, \\ H^0_{\text{QCD}}|\phi_{\alpha,Va}\rangle &= H^0_{\text{QCD}}Q_{Va}|\alpha,+\rangle = Q_{Va}H^0_{\text{QCD}}|\alpha,+\rangle = E_\alpha|\phi_{\alpha,Va}\rangle\,, \end{aligned}$$

so $\left|\phi_{\alpha,Aa}\right\rangle$ and $|\phi_{\alpha,Va}\rangle$ are degenerate states. By using Eq. (2.50) we can obtain the parity associated with these states

$$\begin{aligned} P\left|\phi_{\alpha,Aa}\right\rangle &= PQ_{Aa}|\alpha,+\rangle = PQ_{Aa}P^{-1}P|\alpha,+\rangle = -Q_{Aa}(+|\alpha,+\rangle) = -\left|\phi_{\alpha,Aa}\right\rangle, \\ P|\phi_{\alpha,Va}\rangle &= PQ_{Va}|\alpha,+\rangle = PQ_{Va}P^{-1}P|\alpha,+\rangle = +Q_{Va}(+|\alpha,+\rangle) = +|\phi_{\alpha,Va}\rangle\,. \end{aligned}$$

Thus, $\left|\phi_{\alpha,Aa}\right\rangle$ and $|\phi_{\alpha,Va}\rangle$ are degenerate states with opposite parities. However, the hadron spectrum at low energies does not show the existence of such a parity doubling. For instance, the low-energy spectrum of baryons is formed by a $\frac{1}{2}^+$ octet to which p and n belong, but there is not a $\frac{1}{2}^-$ octet of baryons with the same mass. The natural question which raises at this stage is: what are we missing? To answer this question it is important to notice that in the former discussions it is implicitly assumed that the charges Q_{Aa} annihilate the vacuum. Let us see the consequences of such an assumption.

If we consider that we have multiplets formed by states with positive parity, which are represented by the kets $|\alpha,+\rangle$, and a degenerate multiplet formed by states with negative parity, which are represented by the states $|\beta,-\rangle$, we can write

$$\left|\phi_{\alpha,Aa}\right\rangle = Q_{Aa}|\alpha,+\rangle = |\beta,-\rangle\langle\beta,-|Q_{Aa}|\alpha,+\rangle\,, \tag{2.57}$$

where we have used the fact that the states $|\beta,-\rangle$ form a complete set (and there is an implicit summation on the index β). If we define $t_{Aa,\beta\alpha} \equiv \langle\beta,-|\,Q_{Aa}\,|\alpha,+\rangle$ we obtain

$$\left|\phi_{\alpha,Aa}\right\rangle = Q_{Aa}\,|\alpha,+\rangle = t_{Aa,\beta\alpha}\,|\beta,-\rangle\,. \tag{2.58}$$

At the same time, if we denote by $c^{\dagger}_{\alpha,+}$ the creation operator which when acting on the vacuum produces the state $|\alpha,+\rangle$, we can also write

$$\left|\phi_{\alpha,Aa}\right\rangle = Q_{Aa}c^{\dagger}_{\alpha,+}\,|0\rangle\,. \tag{2.59}$$

If we now use the fact that

$$Q_{Aa}c^{\dagger}_{\alpha,+} = \left[Q_{Aa},c^{\dagger}_{\alpha,+}\right] + c^{\dagger}_{\alpha,+}Q_{Aa}, \tag{2.60}$$

then, Eq. (2.59) can be expressed as

$$\left|\phi_{\alpha,Aa}\right\rangle = \left[Q_{Aa},c^{\dagger}_{\alpha,+}\right]|0\rangle + c^{\dagger}_{\alpha,+}Q_{Aa}\,|0\rangle\,. \tag{2.61}$$

Given the field $\phi_i(x)$ and an infinitesimal transformation which is linear in field, i.e., $\phi_i(x) \to \phi_i'(x) = \phi_i(x) - i\varepsilon_a t_{a,ij}\phi_j$, the commutator of a charge operator Q_a and a field ϕ_i, considering canonical commutation rules for the field ϕ_i and its conjugate momentum, can be written as [52]

$$[Q_a(t),\phi_i(t,\vec{y})] = t_{a,ji}\phi_j(t,\vec{y}). \tag{2.62}$$

In view of this result, if we denote now $c^{\dagger}_{\beta,-}$ as the operator which produces a state degenerate with $|\alpha,+\rangle$, but with opposite parity, it is possible to expand $\left[Q_{Aa},c^{\dagger}_{\alpha,+}\right]$ as a linear combination of states with negative parity, thus, as a linear combination of the operators $c^{\dagger}_{\beta,-}$ [52]

$$\left[Q_{Aa},c^{\dagger}_{\alpha,+}\right] = t_{Aa,\beta\alpha}c^{\dagger}_{\beta,-}.$$

In this way, Eq. (2.61) can be written as

$$\begin{aligned}\left|\phi_{\alpha,Aa}\right\rangle = Q_{Aa}\,|\alpha,+\rangle &= \left\{t_{Aa,\beta\alpha}c^{\dagger}_{\beta,-} + c^{\dagger}_{\alpha,+}Q_{Aa}\right\}|0\rangle \\ &= t_{Aa,\beta\alpha}\,|\beta,-\rangle + c^{\dagger}_{\alpha,+}Q_{Aa}\,|0\rangle\,.\end{aligned} \tag{2.63}$$

Comparing this equation with Eq. (2.58), we need to assume that

$$Q_{Aa}\,|0\rangle = 0.$$

But if $Q_{Aa}|0\rangle \neq 0$, then there would not be the parity doubling puzzle and the $SU_L(3) \otimes SU_R(3)$ symmetry would be broken to $SU(3)_V$. In particular, the $SU_L(3) \otimes SU_R(3)$ symmetry of the QCD Lagrangian is spontaneously broken to $SU_V(3)$, since the vacuum does not share the symmetry of the Lagrangian. According to the Coleman theorem [57] the symmetry of the observed spectrum is determined by the symmetry of the ground state. Since

$$Q_{Va}|0\rangle = 0, \qquad Q_V|0\rangle = 0, \tag{2.64}$$

we should expect the existence of $SU_V(3)$ multiplets which can be classified according to their baryon number. Since this fact is compatible with the approximate $SU(3)$ flavor symmetry observed for the low-lying hadron spectrum, it is assumed then that

$$Q_{Aa}|0\rangle \neq 0. \tag{2.65}$$

According to the Goldstone theorem there should be 8 bosons with negative parity and spin zero which are massless. Effectively, if we set, for convenience, the energy of the vacuum to be zero, i.e.,

$$H^0_{\mathrm{QCD}}|0\rangle = 0, \tag{2.66}$$

since $\left[Q_{Aa}, H^0_{\mathrm{QCD}}\right] = 0$, for the state $Q_{Aa}|0\rangle$, we have

$$H^0_{\mathrm{QCD}}[Q_{Aa}|0\rangle] = +Q_{Aa}H^0_{\mathrm{QCD}}|0\rangle = 0. \tag{2.67}$$

We should have then 8 massless pseudoscalar mesons. The hadron spectrum shows the existence of 8 pseudoscalar mesons $\pi^{\pm}$,π^0,$K^{\pm}$,K^0,$\bar{K}^0$ and η which are much lighter than the rest of hadrons. They are precisely the Goldstone bosons. The fact that they are not massless is a reflection of the explicit breaking of the $SU_L(3) \otimes SU_R(3)$ symmetry due to the small, although nonzero, value of the quark masses.

Classically, the Goldstone bosons can be viewed as massless excitations living in the quotient $SU_L(3) \otimes SU_R(3)/SU_V(3)$. Each Goldstone boson would have an associated independent field ϕ_i, which are functions on the Minkowski space, and, can be collected in a vector $\phi = (\phi_1, \phi_2, \phi_3, \phi_4, \phi_5, \phi_6, \phi_7, \phi_8)$, defining a vector space. Interestingly, there exists an isomorphic mapping between the quotient space $SU_L(3) \otimes SU_R(3)/SU_V(3)$ and the Goldstone boson fields [52]. Using this mapping, by studying the transformations of the Goldstone bosons under $SU_L(3) \otimes SU_R(3)$, the Goldstone bosons can be identified as

coordinates of a parametrization of a matrix U of $SU(3)$. A convenient parametrization is given by

$$U(x) = e^{-i\frac{\sqrt{2}}{f}\phi(x)}, \tag{2.68}$$

where

$$\begin{aligned}\phi(x) = \sum_{a=1}^{8} \theta_a \lambda_a &= \begin{pmatrix} \theta_3 + \frac{\theta_8}{\sqrt{3}} & \theta_1 - i\theta_2 & \theta_4 - i\theta_5 \\ \theta_1 + i\theta_5 & \frac{\theta_8}{\sqrt{3}} - \theta_3 & \theta_6 - i\theta_7 \\ \theta_4 + i\theta_5 & \theta_6 + i\theta_7 & \frac{-2}{\sqrt{3}}\theta_8 \end{pmatrix} \\ &= \begin{pmatrix} \pi^0 + \frac{1}{\sqrt{3}}\eta & \sqrt{2}\pi^+ & \sqrt{2}K^+ \\ \sqrt{2}\pi^- & -\pi^0 + \frac{1}{\sqrt{3}}\eta & \sqrt{2}K^0 \\ \sqrt{2}K^- & \sqrt{2}\bar{K}^0 & -\frac{2}{\sqrt{3}}\eta \end{pmatrix}. \end{aligned} \tag{2.69}$$

In Eq. (2.69), the relation between the physical fields and the cartesian components has been used. The constant f is introduced such that the argument of the exponential is dimensionless: since the boson fields have dimension of energy, f must also have dimension of energy. In fact, f can be identified with the pion decay constant in the chiral limit ($f \approx 93$ MeV).

In the next sections we will introduce the heavy quark symmetry and we will see how to use the results found here to construct an effective field theory describing the interaction of heavy hadrons with light ones. But before doing this, it is interesting to show how the spontaneous breaking of a symmetry is related to a nonzero vacuum expectation value of the fields. In fact,

$$Q_A |0\rangle \neq 0 \Rightarrow \langle 0| \bar{q}q |0\rangle \neq 0.$$

We illustrate this with the standard example of the Mexican hat potential, which, as in case of the massless QCD Lagrangian, is invariant under global phase transformations of the fields.

2.2.3 Goldstone's theorem for the mexican hat potential

A simple classical model which exhibits a continuous gauge symmetry is the one given by the Lagrangian

$$\mathscr{L} = \partial_\mu \phi \partial^\mu \phi^* - V(\phi, \phi^*), \tag{2.70}$$

with

$$V(\phi,\phi^*) = \mu^2\phi\phi^* + \frac{1}{4}\lambda(\phi\phi^*)^2, \tag{2.71}$$

and ϕ being a complex scalar field. This Lagrangian is clearly invariant under the global phase transformation

$$\phi \to e^{-i\theta}\phi, \qquad \phi^* \to e^{i\theta}\phi^*, \tag{2.72}$$

where θ is an arbitrary real constant.

At the classical level, the ground state or vacuum of the system can be found by the condition $\frac{\partial V}{\partial \phi} = 0$. From Eq. (2.71),

$$\begin{aligned}\frac{\partial V}{\partial \phi} &= \mu^2\phi^* + \frac{\lambda}{2}\phi\phi^*\phi^* = \left(\mu^2 + \frac{\lambda}{2}\phi\phi^*\right)\phi^* \\ &= \left(\mu^2 + \frac{\lambda}{2}|\phi|^2\right)\phi^*,\end{aligned} \tag{2.73}$$

when $\lambda \leq 0$, the potential has no stable minima for a finite value of ϕ. We, thus, assume $\lambda \geq 0$. Then, for $\mu^2 \geq 0$, the potential V acquires an absolute minimum at $\phi = 0$ and the vacuum has manifestly the same symmetry as the Lagrangian. But if $\mu^2 \leq 0$, the system has its lowest energy for

$$|\phi|^2 = -\frac{2\mu^2}{\lambda}. \tag{2.74}$$

That is, there is an infinite number of degenerate minima lying on a circle which has a radius given by $\sqrt{-\frac{2\mu^2}{\lambda}}$. All these minima differ from one another by a relative phase factor, but all are equivalent through the transformation in Eq. (2.72). Thus, whichever the solution is chosen it will lead to the same physics, but once the choice is made, the symmetry of the Lagrangian is broken spontaneously (since it is due to the random choice we made). For example, let us select the vacuum such that the expectation value of the field at the vacuum is given by

$$\langle\phi\rangle = \frac{v}{\sqrt{2}}, \qquad v \equiv \sqrt{-\frac{4\mu^2}{\lambda}}. \tag{2.75}$$

Within this particular choice, only the real part of ϕ acquires a nonzero vacuum expectation value, fixing the direction of the symmetry breakdown.

We now define a complex field $\chi = \chi_1 + i\chi_2$, with χ_1 and χ_2 being real fields, such that, in terms of χ, the field ϕ is written as

$$\begin{aligned}\phi &= \langle\phi\rangle + \frac{1}{\sqrt{2}}\chi \\ &= \frac{1}{\sqrt{2}}\left(v + \chi_1 + i\chi_2\right).\end{aligned} \tag{2.76}$$

In this way, the fields χ_1 and χ_2 have zero vacuum expectation value and in a quantum vision they can represent excitations of the fields from the vacuum. Particularly, excitations in the directions radial and tangential to the circle of the degenerate minima. In terms of these fields, we have, from Eqs. (2.71) and (2.76)

$$V = \left(\mu^2 + \frac{\lambda}{4}\phi\phi^*\right)(\phi\phi^*), \tag{2.77}$$

such that

$$\begin{aligned}\phi\phi^* &= \frac{1}{2}\left[(v+\chi_1)^2 + \chi_2^2\right] = \frac{1}{2}\left[v^2 + \chi_1^2 + \chi_2^2 + 2v\chi_1\right] \\ &= \frac{1}{2}\left[-4\frac{\mu^2}{\lambda} + \chi_1^2 + \chi_2^2 + 2v\chi_1\right],\end{aligned} \tag{2.78}$$

$$\Rightarrow \mu^2 + \frac{\lambda}{4}\phi\phi^* = \frac{\mu^2}{2} + \frac{\lambda}{8}\left(\chi_1^2 + \chi_2^2 + 2v\chi_1\right). \tag{2.79}$$

Then,

$$\begin{aligned}V &= \left[\frac{\mu^2}{2} + \frac{\lambda}{8}(\chi_1^2 + \chi_2^2 + 2v\chi_1)\right]\frac{1}{2}\left[v^2 + \chi_1^2 + 2v\chi_1 + \chi_2^2\right] \\ &= \frac{\mu^2 v^2}{4} + \left(\frac{\mu^2}{4} + \frac{\lambda v^2}{16}\right)(\chi_1^2 + \chi_2^2 + 2v\chi_1) + \frac{\lambda}{16}(\chi_1^2 + \chi_2^2 + 2v\chi_1)^2.\end{aligned} \tag{2.80}$$

By using Eq. (2.75), we have

$$\begin{aligned}V &= \frac{\mu^2 v^2}{4} + \frac{\lambda}{16}(\chi_1^2 + \chi_2^2 + 2v\chi_1)^2 \\ &= \frac{\mu^2 v^2}{4} + \frac{\lambda}{16}\left[\left(\chi_1^2 + \chi_2^2\right)^2 + 4v^2\chi_1^2 + 4v\chi_1(\chi_1^2 + \chi_2^2)\right] \\ &= \frac{\mu^2 v^2}{4} + \frac{\lambda}{4}v^2\chi_1^2 + \frac{\lambda}{16}(\chi_1^2 + \chi_2^2)\left[(\chi_1^2 + \chi_2^2) + 4v\chi_1\right] \\ &= -\mu^2\chi_1^2 + \frac{\lambda}{16}(\chi_1^2 + \chi_2^2)\left[4v\chi_1 + \chi_1^2 + \chi_2^2\right] + \frac{\mu^2 v^2}{4}.\end{aligned} \tag{2.81}$$

Similarly, from Eq. (2.76)

$$\partial_\mu\phi\partial^\mu\phi^* = \frac{1}{2}\left(\partial_\mu\chi_1\partial^\mu\chi_1 + \partial_\mu\chi_2\partial^\mu\chi_2\right). \tag{2.82}$$

Then the Lagrangian in Eq. (2.70), by using Eqs. (2.81) and (2.82), can be written as

$$\begin{aligned}\mathscr{L} &= \frac{1}{2}\left[\partial_\mu\chi_1\partial^\mu\chi_1 - (-2\mu^2)\chi_1^2\right] + \frac{1}{2}\partial_\mu\chi_2\partial^\mu\chi_2 \\ &\quad -\frac{\lambda}{16}\left(\chi_1^2 + \chi_2^2\right)\left[4v\chi_1 + \chi_1^2 + \chi_2^2\right] - \frac{1}{4}\mu^2 v^2,\end{aligned} \tag{2.83}$$

and the phase symmetry is not manifest, i.e., it has been broken by our choice of the vacuum, i.e., spontaneously. The field χ_1, which represents fluctuations in the direction of the symmetry breakdown, acquires a mass, but the field χ_2, which measures deviations in the direction of the symmetry conservation, remains massless. It is a Goldstone boson.

Before showing how to use the results found in the current section to construct an effective field theory describing the interaction of heavy hadrons with light ones, we need to describe some basic properties of another important symmetry to do this, which is the Heavy quark symmetry.

2.3 Heavy quark symmetry

There are several reasons for which the strong interactions of systems containing heavy quarks are easier to understand than those involving systems with light quarks. One of them is the asymptotic freedom: the coupling constant of QCD, which is related to the interaction of quarks and gluons, becomes weak in processes with large momentum transfer, i.e., at short distances. At large distances (small momentum transfer), on the other hand, the coupling becomes strong, leading to non-perturbative phenomena such as the confinement of quarks and gluons. The energy scale which separates these regions of small and large coupling is $\Lambda_{\text{QCD}} \sim 200$ MeV, a scale which is dynamically generated by QCD.

When the mass of a quark Q is much larger than Λ_{QCD}, we say that Q is a heavy quark. In this way, the quarks of the standard model can be classified as light quarks (u, d and s) and heavy quarks (c, b and t).

Consider a meson formed by a heavy and a light quarks, i.e., $Q\bar{q}$. Such a system has a typical size of the order of $\Lambda_{\text{QCD}}^{-1}$ and, considering QCD dynamics, the typical momentum transfer between the heavy and light quarks forming the meson is of the order of Λ_{QCD} [58]. In this way, the velocity of the heavy quarks remains almost unchanged: if Δp is the variation of the momentum of the heavy quark, $\Delta p \sim \Lambda_{\text{QCD}}$, while the variation of the velocity of the heavy quark is $\Delta v = \Delta p / m_Q << 1$. As a consequence, in the limit $m_Q \to \infty$, the heavy quark in the meson can be labeled by a 4-vector velocity v^μ which does not change with time. The heavy quark then behaves like a static external

source that transforms as a color triplet, and the meson dynamics reduces to that of light quarks interactions with this color source. Therefore, in the limit $m_Q \to \infty$, the mass of the heavy quark plays no role, thus, the dynamics is unchanged under the change of heavy quark flavors. This is called the heavy quark flavor symmetry.

Since the heavy quark behaves as a static source, the only strong interaction that the heavy quark can have is with gluons. In the limit $m_Q \to \infty$, this interaction is very similar to the electromagnetic interaction, with the color charge playing the role of the electric charge. The heavy quark acts as a static source of color electric field localized at the origin. Therefore, the spin of the heavy quark decouples, and the light quark and gluons cannot recognize the spin orientation of the heavy quark. In other words, the interaction does not depend on the spin of the heavy quark. This is called heavy quark spin symmetry.

In this way a meson formed by a heavy and a light quarks resembles a hydrogenlike atom in the Quantum Electrodynamics (QED). In QED, the spectrum obtained for a hydrogenlike atom is independent of the mass and spin of the nucleus: the nucleus can be treated as a static electrically charged source. In our case the heavy quark would play the role of the nucleus, and the color field would correspond to the electric field.

2.4 $SU(4)$ flavor symmetry

Another symmetry which can be used to describe interaction of mesons formed by a heavy quark, particularly a c quark, and a light quark is the $SU(4)$ symmetry: if we work with a total of 4 quarks, the heavy quark c and the light quarks u, d, s, the flavor $SU(3)$ symmetry can be extended to $SU(4)$ by considering all quarks having a similar mass. However, the mass of the charm quark (1.3 GeV) is much bigger than that of the light quarks. For this reason, $SU(4)$ cannot be considered as a good symmetry of nature. Nevertheless, it is useful in classifying and predicting the existence of hadrons having a c quark. Particularly, for mesons, since from group theory

$$4 \otimes \bar{4} = 1 \oplus 15,$$

we would expect a singlet and a 15-plet of mesons. All these mesons have been discovered (see Fig. 2.5).

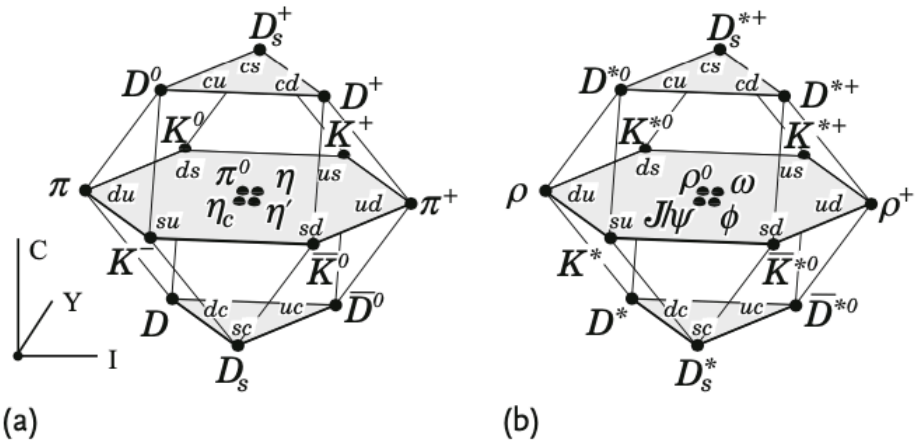

Figure 2.5: Configuration of the mesons in the $I_z - Y - C$ space ($I_z \equiv$ third isospin component, $Y \equiv$ hypercharge, $C \equiv$ charm) for pseudoscalar mesons (left) and for vector mesons (right). The central planes represent $C = 0$ mesons and, except for η_c and J/ψ, are $SU(3)$ multiplets.

2.5 An effective theory

When describing a physical system, in general, one can focus on the degrees of freedom which are relevant at the distance scales under consideration [59]. For example, it is well-know that quantum mechanics is a more fundamental theory than classical mechanics. However, it would be a cumbersome task to describe the motion of a pendulum by using quantum mechanics. The state would correspond to a complicated superposition of energy eigenstates approximating the classical motion. The description based on classical mechanics can be considered as an effective theory of the fundamental quantum mechanical description, that's it, a systematic approximation of the underlying theory, which is valid in a certain domain of energies.

Effective field theories have become a very important tool in a variety of applications such as condensed-matter, nuclear and particle physics. The unifying characteristic of an effective field theory is that they are applicable for energies which are small when compared to an energy scale of the underlying, more fundamental, theory. Since the main purpose of an effective field theory is to explain the consequences of the dynamics involved in a specific energy region, it can consider only those degrees of freedom which are relevant at that energy region and they might be different from the degrees of freedom of the underlying theory.

In our case, in which we are dealing with the strong interaction between hadrons, the fundamental theory describing such interactions is QCD. And, as mentioned in Section

2, its degrees of freedom are quarks and gluons. The running strong coupling constant $\alpha_S(Q)$ describing the strength of the interaction between quarks and gluons makes that at low energies and momenta $(Q \approx 1\text{GeV})$, $\alpha_S \approx 1$. Thus a treatment based on an expansion in powers of α_S is not valid, contrary to the situation at high energies. In view of such a situation, one can consider those degrees of freedom which are relevant to the energy domain under investigation and use them to construct a theory by means of the relevant symmetries of the underlying theory following *Weinberg's theorem* [60,61]:

Weinberg's Theorem

If one writes down the most general possible Lagrangian, including all terms consistent with assumed symmetry principles, and then calculates matrix elements with this Lagrangian to any given order in perturbation theory the result will simply be the most general possible S-matrix consistent with analyticity, perturbative unitary, cluster decomposition and the assumed symmetry principles.

Keeping in mind Weinberg's theorem, at low energies we can consider the hadrons fields as being the degrees of freedom of the theory. Such a consideration resembles the Yukawa theory of the nuclear interaction, where the interaction between two nucleons is described in terms of the exchange of pions and not by using quarks and gluons (see Fig. 2.6). In such a case, we work then with an effective field theory, i.e., a theory

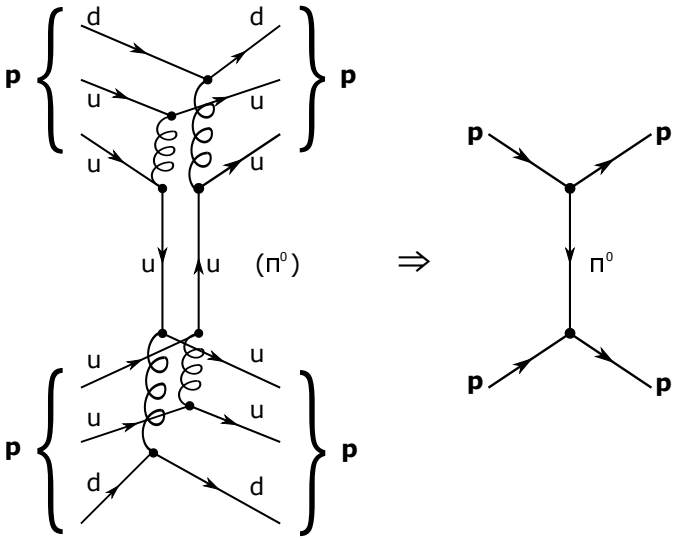

Figure 2.6: Diagrammatic representation of the nuclear interaction considering the interaction between quarks and gluons (left) and using the Yukawa theory (right), for energies around the threshold of the process.

formulated in terms of the relevant degrees of freedom for the energy region we are interested in.

If we use Weinberg's theorem to get the most general Lagrangian describing the interaction between hadrons at low energies, it will be formulated by an infinite number of terms and, thus, it does not seem too useful. For an efficient calculation, a "power-counting" scheme is established: the Lagrangian contains terms involving an increasing number of derivatives acting on the hadron fields. By using the Feynman rules, these terms are translated as powers of momentum divided by a scale, such as the mass of a particle not considered explicitly.

The Lagrangian obtained within this approach contains also the so called low-energy constants or LECs, which basically account for the missing information (degrees of freedom) not included when constructing the Lagrangian. Thus, the only way to get these LECs is by using the underlying theory (if the calculation is not cumbersome) or by fitting them to the experimental data. For the physical phenomena we want to describe, however, it is enough to consider the lowest order Lagrangian in the power of momentum. In this case, no LECs are required, gaining, thus, a predictive power.

A technical comment is here in order before proceeding further. Effective theories are non-renormalizable in the usual sense, since increasing accuracy implies including more and more terms in the Lagrangian. However, as long as one considers all terms which are permitted by the symmetries of the underlying theory, divergences that occur in calculations up to any given order of momentum/scale can be renormalized by redefining the fields and parameters (like couplings, LECs) appearing in the effective Lagrangian.

2.5.1 Effective Lagrangian based on the heavy quark symmetry

An effective field theory describing the interactions of mesons consisting of a heavy quark has been studied in detail (for instance) in Ref. [42,62,63]. In this former work, it is shown that considering the heavy quark and chiral symmetries, the scattering between Goldstone bosons and D mesons can be described by the leading order Lagrangian

$$\mathscr{L}_{\mathrm{HQ}} = D_\mu H D^\mu H^\dagger - M^2 H H^\dagger, \tag{2.84}$$

which corresponds to the kinetic and mass terms for the heavy meson, with

$$H = (D^0 \quad D^+ \quad D_s^+). \tag{2.85}$$

In Eq. (2.84) the Goldstone bosons are chirally coupled through the introduction of the covariant derivative D_μ as

$$\begin{aligned} D_\mu &= \partial_\mu + \Gamma_\mu, \\ \Gamma_\mu &= \frac{1}{2}\left(u^\dagger \partial_\mu u + u \partial_\mu u^\dagger\right), \end{aligned} \tag{2.86}$$

where

$$u^2 = U, \tag{2.87}$$

and, as we saw in section 2,

$$U = \exp\left(i\frac{\sqrt{2}\phi}{f}\right), \tag{2.88}$$

$$\phi = \begin{pmatrix} \frac{1}{\sqrt{2}}\pi^0 + \frac{1}{\sqrt{6}}\eta & \pi^+ & K^+ \\ \pi^- & -\frac{1}{\sqrt{2}}\pi^0 + \frac{1}{\sqrt{6}}\eta & K^0 \\ K^- & \bar{K}^0 & -\frac{2}{\sqrt{6}}\eta \end{pmatrix}. \tag{2.89}$$

In our work we are interested in describing a process of the type $\phi H \to \phi H$, we thus need to identify the terms involving two pseudoscalar fields and two heavy fields in the Lagrangian of Eq. (2.84). Using Eqs. (2.86) and (2.84), we obtain the terms involving two heavy hadron fields as

$$\mathscr{L}_{\mathsf{HQ}} = \partial_\mu H \Gamma^\mu H^\dagger + H\Gamma_\mu^\dagger \partial^\mu H^\dagger + H\Gamma_\mu^\dagger \Gamma^\mu H^\dagger. \tag{2.90}$$

To get now the terms up to two Goldstone boson fields, we need to make a Taylor expansion of Γ_μ up to order ϕ^2. From Eqs. (2.87) and (2.89)

$$\begin{aligned} u = e^{i\frac{\phi}{\sqrt{2}f}} &= \sum_{n=0}^{\infty} \frac{1}{n!}\left(i\frac{\phi}{\sqrt{2}f}\right)^n = 1 + i\frac{\phi}{\sqrt{2}f} - \frac{\phi^2}{4f^2} + \dots \\ \partial_\mu u &= \frac{i}{\sqrt{2}f}\partial_\mu \phi - \frac{1}{4f^2}\left(\phi\partial_\mu\phi + \partial_\mu\phi\phi\right) + \dots \end{aligned}$$

such that, up to order ϕ^2

$$\begin{aligned} \Gamma_\mu &= \frac{1}{4f^2}\left(\phi\partial_\mu\phi - \partial_\mu\phi\phi\right) = \frac{1}{4f^2}\left[\phi, \partial_\mu\phi\right], \\ \Gamma_\mu^\dagger &= \frac{1}{4f^2}\left(\partial_\mu\phi\phi - \phi\partial_\mu\phi\right) = -\Gamma_\mu. \end{aligned} \tag{2.91}$$

Using now Eq. (2.91) in Eq. (2.90), we get

$$\mathscr{L}_{\mathrm{HQ}} = \frac{1}{4f^2}\left\{\partial_\mu H[\phi,\partial^\mu\phi]H^\dagger - H\left[\phi,\partial_\mu\phi\right]\partial^\mu H^\dagger\right\}. \tag{2.92}$$

Using this Lagrangian we will obtain the lowest order amplitudes describing the interaction between a D meson and a pseudoscalar, as we will show in the next chapter.

2.5.2 Effective Lagrangian based on $SU(4)$

In Ref. [43], the interaction between heavy and light pseudoscalars is described by extending the $SU(3)$ chiral Lagrangian to $SU(4)$. Such an extension is built first by including the heavy pseudoscalars into the matrix ϕ whose elements are the Goldstone boson fields, i.e., π, K, η, such that

$$\phi = \begin{pmatrix} \frac{\pi^0}{\sqrt{2}} + \frac{\eta}{\sqrt{6}} + \frac{\eta_c}{\sqrt{12}} & \pi^+ & K^+ & \bar{D}^0 \\ \pi^- & -\frac{\pi^0}{\sqrt{2}} + \frac{\eta}{\sqrt{6}} + \frac{\eta_c}{\sqrt{12}} & K^0 & D^- \\ K^- & \bar{K}^0 & -\frac{2\eta}{\sqrt{6}} + \frac{\eta_c}{\sqrt{12}} & D_c^- \\ D^0 & D^+ & D_s^+ & -\frac{3\eta_c}{\sqrt{12}} \end{pmatrix}. \tag{2.93}$$

In this way, the Lagrangian, by analogy to the $SU(3)$ chiral Lagrangian, reads as

$$\mathscr{L} = \frac{1}{12f^2}\,\mathrm{Tr}\left(J_\mu J^\mu + M\phi^4\right), \tag{2.94}$$

where

$$M = \begin{pmatrix} m_\pi^2 & 0 & 0 & 0 \\ 0 & m_\pi^2 & 0 & 0 \\ 0 & 0 & 2m_K^2 - m_\pi^2 & 0 \\ 0 & 0 & 0 & 2m_d^2 - m_\pi^2 \end{pmatrix}, \tag{2.95}$$

with the current J^μ being

$$J^\mu = \left[\partial_\mu\phi,\phi\right]. \tag{2.96}$$

The next step consists in identifying terms in the current J_μ which could be related to the exchange of heavy vector mesons and suppress those contributions. In this way the $SU(4)$ symmetry would be broken down to $SU(3)$. For identifying those terms in the J_μ current, the authors of Ref. [43] decompose the matrix ϕ of Eq. (2.93) into its $SU(3)$ components

$$\phi = \begin{pmatrix} \phi_8 + \frac{1}{\sqrt{2}}\phi_1 I_3 & \phi_3 \\ \phi_{\bar{3}} & -\frac{3}{\sqrt{2}}\phi_1 \end{pmatrix}, \tag{2.97}$$

where

$$\phi_8 = \begin{pmatrix} \frac{\pi^0}{\sqrt{2}} + \frac{\eta}{\sqrt{6}} & \pi^+ & K^+ \\ \pi^- & -\frac{\pi^0}{\sqrt{2}} + \frac{\eta}{\sqrt{6}} & K^0 \\ K^- & \bar{K} & -\frac{2\eta}{\sqrt{6}} \end{pmatrix}, \qquad \phi_3 = \begin{pmatrix} \bar{D}^0 \\ D^- \\ D_s^- \end{pmatrix}, \qquad \phi_1 = \eta_c, \tag{2.98}$$

and I_3 is the identity matrix 3×3. Defining now currents for each of the $SU(3)$ components of ϕ, i.e.

$$J^\mu_{ab} = [\partial^\mu \phi_a, \phi_b], \qquad a,b = 1,3,\bar{3},8, \tag{2.99}$$

the term $J^\mu J_\mu$ can be written in terms of $J^\mu_{88} J_{88\mu}$, $J^\mu_{\bar{3}8} J_{38\mu}$, etc. Interestingly, terms of the type $J^\mu J_\mu$ in the chiral Lagrangian can be interpreted in terms of the hidden local symmetry approach developed in Ref. [64], as the exchange of vector mesons, like ρ, ω, ϕ, in the t-channel between two pseudoscalars, in the limit at which the 4-momentum squared of the exchanged vector mesons, q^2, is much smaller than the mass squared of the vector mesons, m_V^2 (see Fig. 2.7). Using this fact, the authors of Ref. [43] identify

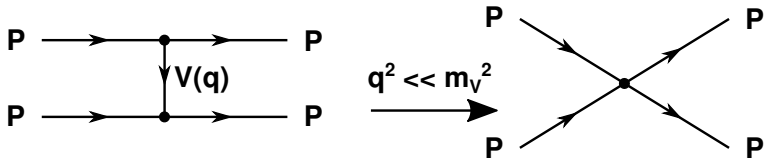

Figure 2.7: When $q^2 << m_V^2$, the propagator of the vector meson $1/(q^2 - m_V^2) \sim -1/m_V^2$ and the diagram of the left becomes a contact diagram between four pseudoscalars. In Ref. [64], the obtained contact interaction, under such a limit, is precisely the one found with the effective Lagrangian based on the chiral symmetry.

the pieces of the Lagrangian related to the exchange of charmed vector mesons by looking for those currents carrying explicitly charm quantum number. Separation of those terms related to the exchange of vector mesons with hidden charm is also required and is more subtle. We refer to the reader to Ref. [43] for more details.

Once this is done, they suppress such contributions by multiplying them by factors like

$$\gamma = \left(\frac{m_L}{m_H}\right)^2, \qquad \psi_3 = \frac{1}{3} + \frac{2}{3}\left(\frac{m_L}{m_{J/\psi}}\right), \qquad \psi_5 = -\frac{1}{3} + \frac{4}{3}\left(\frac{m_L}{m_{J/\psi}}\right)^2, \tag{2.100}$$

where, $m_L(m_H)$ is an average mass value representing the mass of the light (heavy) vector mesons, $(m_L \sim 800$ MeV$, m_H \sim 2050$ MeV$)$. In this way, the final form for the

Lagrangian is given by

$$\mathscr{L}_{SU(4)} = \frac{1}{12f^2}\left[\mathrm{Tr}\left\{J_{88\mu}J^{\mu}_{88} + 2J_{3\bar{3}\mu}J^{\mu}_{88} + J_{3\bar{3}_{\mu}}J^{\mu}_{3\bar{3}}\right\} + \frac{8}{3}\gamma J_{\bar{3}1\mu}J^{\mu}_{13} + \frac{4}{\sqrt{3}}\gamma\left(J_{\bar{3}1\mu}J^{\mu}_{83} + J_{\bar{3}8\mu}J^{\mu}_{13}\right) + 2\gamma J_{\bar{3}8\mu}J^{\mu}_{83} + \psi_5 J_{\bar{3}3\mu}J^{\mu}_{\bar{3}3} + \mathscr{L}_{\mathrm{mass}}\right]. \tag{2.101}$$

The interaction between a D^* and a Kaon, and it's coupled channels, can be obtained in a similar way by using the current [65]

$$\mathscr{J}_{\mu} = \left[\partial_{\mu}V^{\nu}, V_{\nu}\right], \tag{2.102}$$

where

$$V_{\mu} = \begin{pmatrix} \frac{\rho^0_{\mu}}{\sqrt{2}} + \frac{\omega_{\mu}}{\sqrt{6}} + \frac{J/\psi_{\mu}}{\sqrt{12}} & \rho^+_{\mu} & K^{*+}_{\mu} & \bar{D}^{*0}_{\mu} \\ \rho^{*-}_{\mu} & \frac{-\rho^0_{\mu}}{\sqrt{2}} + \frac{\omega_{\mu}}{\sqrt{6}} + \frac{J/\psi_{\mu}}{\sqrt{12}} & & \\ K^{*-}_{\mu} & \bar{K}^{*0}_{\mu} & \frac{-2\omega_{\mu}}{\sqrt{6}} + \frac{J/\psi_{\mu}}{\sqrt{12}} & D^{*-}_{s\mu} \\ D^{*0}_{\mu} & D^{*+}_{\mu} & D^{*+}_{s\mu} & \frac{-3J/\psi_{\mu}}{\sqrt{12}} \end{pmatrix}, \tag{2.103}$$

and, then, the current in Eq. (2.102) is decomposed into its $SU(3)$ components, as done in Eq. (2.97). Finally, the terms in the Lagrangian which would depend on $\mathrm{Tr}\left(\mathscr{J}_{\mu}\mathscr{J}^{\mu}\right)$, and which are related to the exchange of heavy vector mesons, are suppressed.

CHAPTER 3

Two-Body Interactions

There are many examples of two-body interactions or two-body systems in physics. A typical one is the interaction between the moon and the earth, which is important to understand the moon's orbit; another example would be a collision of two massive bodies, like two cars on a road, or we can even consider the interaction between two point-like particles.

Here, in particular, we are interested in the interactions between two hadrons. To be more specific, we are going to focus on the interaction between two mesons by using effective Lagrangians to describe the system. But before entering into the details of how to do that, let's take a look at some general aspects of the scattering theory.

3.1 Scattering: a classical view

At the classical level, when we refer to *scattering* it normally means a collision. Collisions can be classified as elastic or inelastic, depending on whether the mechanical energy related to the system of particles is conserved or not, respectively.

In the simplest version, all collision experiments start with a projectile approaching a target from a distance where the projectile can be treated as moving almost freely, and both projectile and target are considered as point particles [66]. So the idea is essentially to let two particles collide against each other and observe what comes out.

Scattering (classically)

A process in which particles are deflected

- Elastic: mechanical energy of the system is conserved.
- Inelastic: mechanical energy of the system is not conserved.

As an example, within the classical picture, one can consider a fixed target as a very massive particle, which can be modeled as a hard sphere (see Fig. 3.1), in such a way that when the projectile hits the target the latter remains basically at rest, and the trajectory of the former is deflected. If the projectile misses the target instead, it will

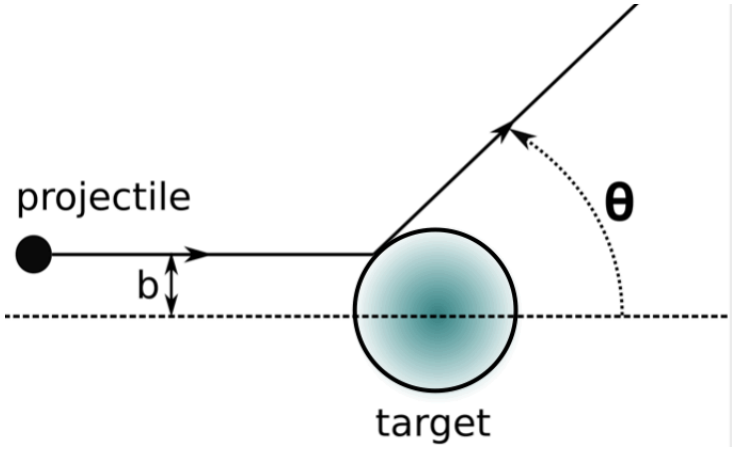

Figure 3.1: Scattering on a hard sphere.

simply pass through and there will be no deflection. Thus, in this example, there is a collision as far as the projectile can reach the area $\sigma = \pi R^2$, where R is the radius of the target. If we further model the projectile as being a hard sphere of radius r (see Fig. 3.2), instead of being a point particle, then, there will be a collision between the

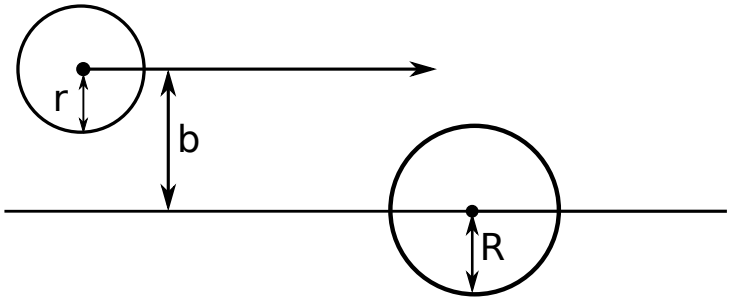

Figure 3.2: Collision between two hard spheres.

projectile and the target if the center of the projectile lies inside a circle with the center

on the target and radius $r+R$, therefore, leading to an effective area for the collision as $\sigma = \pi(r+R)^2$.

However, in atomic/nuclear physics, the target is not something that you either hit or miss but rather is something for which the closer the projectile comes the greater the deflection is: when a projectile get closer to the target, the latter exerts a force on the projectile, curving its trajectory, and moves away in a different direction (see Fig. 3.3). The projectile could also crash into the target, and depending on the properties of the target, may not re-emerge again.

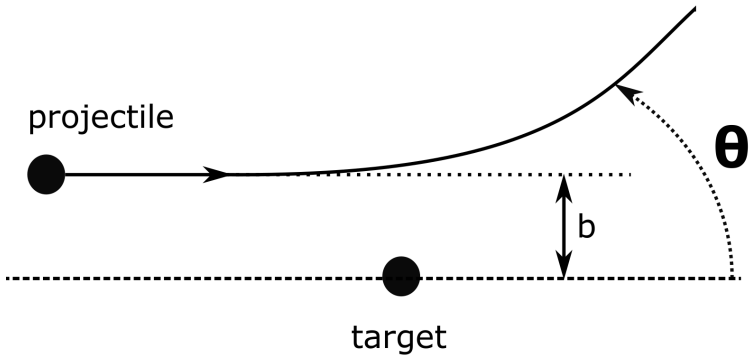

Figure 3.3: The projectile approaching the target from the left. As it proceeds it feels the presence of the target, in this case, through a repulsive interaction, curves its trajectory and moves away in a different direction.

These examples serve us to illustrate the concept of the cross section: σ depends on the properties of the target and the projectile and can be interpreted as the effective area that the target presents to the projectile for its scattering.

The observation of a projectile which has been deflected simply informs us about the presence of the target. If the same experiment is repeated, that is, many different collisions of similar projectiles and targets are studied, then it is possible to obtain information on the nature of the projectile and the target as well as their interactions.

A simple method to do this is by having many targets in a single assembly and by firing a whole beam of projectiles. Continuing with the hard-sphere example, we can consider a single projectile traveling through an assembly of hard-sphere targets (see Fig. 3.4).

Since the precise line of approach of the projectile is not know, we don't know whether the projectile will hit, or not, one of the targets. But we can determine the probability, P_{hit}, that the projectile will make a hit: if we consider targets which are ran-

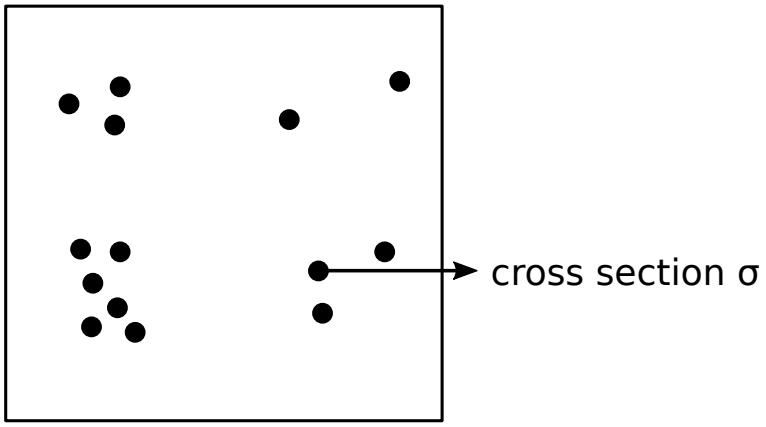

Figure 3.4: A target assembly with several hard-sphere targets, as seen head-on by the incoming projectile.

domly distributed in the assembly and that we have enough number of them, we can define a target density η_{tar}. This density corresponds to the number of targets per unit area as viewed from the incident direction. If we call A to the total area of the target assembly, we have then $\eta_{\text{tar}}A$ targets. If we denote σ to the cross section corresponding to each target, as seen from the incident direction, we have that $\eta_{\text{tar}}A\sigma$ represents the total area of all the targets. We have then

$$P_{\text{hit}} = \frac{\eta A\sigma}{A} = \eta_{\text{tar}}\sigma. \tag{3.1}$$

If we have a beam formed by a large number of incident projectiles (N_{inc}), the number of scattered projectiles (N_{sc}) in then given simply by the product of the above probability and N_{inc}

$$N_{\text{sct}} = N_{\text{inc}}\sigma\eta_{\text{tar}}, \tag{3.2}$$

since we can measure N_{sct}, N_{inc} and we know the target density, we can determine σ, which is, as shown in Eq. (3.1), related to the probability of scattering.

Considering the projectile and the target as relativistic particles doesn't change much the above description of the scattering: we simple need to take into account the contribution of the mass of the projectile and the target in the expression of their mechanical energies. But how one should describe the scattering between hadrons. We answer this question in the next section.

3.2 Scattering: a quantum mechanical view

At the quantum level, we can also classify the scattering between particles [67] as: (a) elastic, in which case two particles are simply scattered without changing their internal structure, i.e., $A+B \rightarrow A+B$; (b) inelastic, where the particles undergo a change of their internal quantum state as a consequence of the collision, for example, $A+B \rightarrow A'+B$, with A' representing the new internal state of A. In this case it is also possible that $A+B$ splits into two different particles or into a final state formed by more/less than two particles.

Now, in the quantum world, particles have a wavelength associated with them, the de Broglie wavelength, which is determined by their energies. Higher energies means smaller wavelength.

Let us consider, for example, the process $e^- + p \rightarrow e^- + p$. In function of the energy of the electron we can also have different pictures for the scattering: at very low energies, at which the de Broglie wavelength of the electron $\lambda >> r_p$, with r_p being the radius of the proton, from the point of view of the electron, the proton can be considered as a hard-sphere. In this way, the process $e^- + p \rightarrow e^- + p$ can be described as an elastic collision between an electron and a point-like proton.

If we imagine a function F describing the inner structure of the proton, this function should be related to the number of times an electron-proton scattering occurs, i.e., it should be related to the cross section of the process σ. A schematic representation of F versus the fraction of the proton which the electron "sees", χ, should look something like the plot shown in Fig. 3.5 (see Ref. [68]). If the energy of the electron is increased

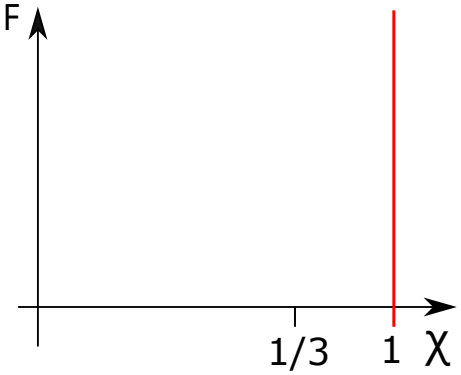

Figure 3.5: If the proton is a point-like particle, we expect $\chi = 1$ always. A logarithmic scale has been used in the abscissa axis.

such that $\lambda \approx r_p$, the electron starts to "see" the constituents of the proton, the quarks,

interacting in this way with them. As a consequence of this interaction, the final state is no longer formed by an electron and a proton, and we can have something like $e^- + p \rightarrow e^- + \gamma + X$. Since the proton is constituted by three quarks, each of them carrying one third of the momentum of the proton, we might expect the plot shown in Fig. 3.6 for F vs. χ.

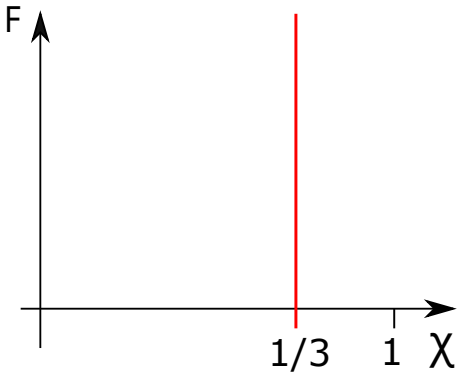

Figure 3.6: If the proton is not anymore a point-like particle and each quark carries 1/3 of its momentum, we might expect $\chi = 1/3$ always.

Note, however, that the three quarks forming the proton are inside the proton, i.e., they are bound together in the radius r_p. Thus, since we know with some precision their positions, by the Heisenberg's uncertainty relation between position and momentum, the momentum of the quarks, and, thus, χ, must be somewhat uncertain. We expect then something like the plot shown in Fig. 3.7.

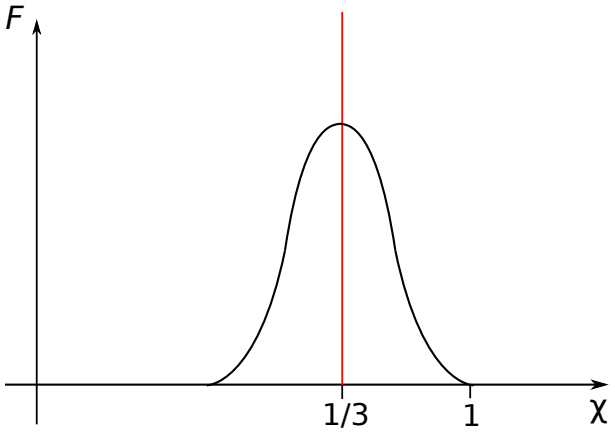

Figure 3.7: Due to the Heisenberg principle, the momentum of the quarks inside the proton should be spread out.

For highly energetic electrons, such that, $\lambda << r_p$, the electron will not simply "see" the quarks inside the proton. It would also "see" the gluons which are being exchanged between the quarks. When a quark radiates a gluon, part of the momentum of the quark

is transferred to the gluon, thus, lowering its value. But since gluons have no electric charge, the electron can not "see" them directly. The consequence is that the whole momentum, and then χ, distribution is shifted to lower values and we expect for the plot F vs. χ something like the one shown in Fig. 3.8. The closer you look, i.e., when increasing the energy of the incident electron, the bigger would be the gluon radiation and, then, the shift. In this way, the peak at $\chi = 1/3$ would be washed out.

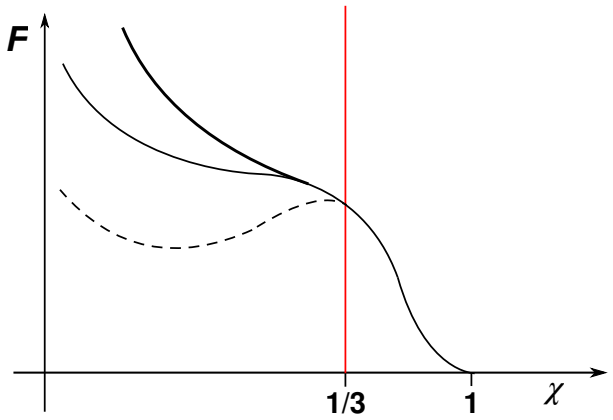

Figure 3.8: The peak at $\chi = 1/3$ becomes less pronounced when increasing the energy of the incident electron (dashed, thin, and thick lines), as a consequence of the gluon exchange between quarks

Thus, the term cross section, as in the classical description of the scattering, is used to indicate the probability that two particles will collide and react in a certain way and can be obtained as

$$\sigma = \frac{\text{number of interactions per unit time per target particle}}{\text{incident flux}}, \tag{3.3}$$

where the incident flux is the number of incident particles per unit area and unit time.

In general, we can have many possible outcomes for a given set of incident particles, and each of which have a different cross section σ_i. The total cross section is obtained by summing over all possible modes of scattering or channels

$$\sigma = \sum_{i=1}^{n} \sigma_i, \qquad \text{for } n \text{ possible channels.} \tag{3.4}$$

As we discuss in the next section, to determine theoretically the cross section for a given process we define the so called scattering matrix or the S-matrix.

3.3 Scattering matrix

Let us assume that the forces acting between two particles which interact are of sufficient short range such that the initial state before the collision, as well as the final state after the collision, can be considered to be formed of free particles [69].

The beginning of the experiment and the moment when the measurement is done, is then mathematically expressed as an infinitely remote time in the past, $t = -\infty$, and an infinitely remote time in the future, $t = +\infty$, and the scattering process is then described in terms of "in" and "out" states. We can define a state $|\psi\rangle_{\text{in}}$ corresponding to a physical system characterized by the configuration ψ at time $t = -\infty$. Since the states can be counted as free particles, we have, for example, $|0\rangle_{\text{in}}$ at $t = -\infty$ for the vacuum, $|p_1\rangle_{\text{in}}$ for one particle at $t = -\infty$, $|p_1, p_2\rangle_{\text{in}}$ for two particles at $t = -\infty$, etc., with four momenta p_1, p_2, etc. Similarly, we can write the state $|\phi\rangle_{\text{out}}$ corresponding to a system characterized by the configuration ϕ at time $t = +\infty$ and we have $|0\rangle_{\text{out}}$, $|p'_1\rangle_{\text{out}}$, $|p'_1, p'_2\rangle_{\text{out}}$ for the vacuum, one particle, two particles, etc., states with four-momenta p'_1, p'_2, etc. If a system without any particles at $t = -\infty$ will not have any particles at $t = +\infty$, we have $|0\rangle_{\text{in}} = |0\rangle_{\text{out}}$. In the same way, for one particle, we have $|p_1\rangle_{\text{in}} = |p'_1\rangle_{\text{out}}$, but for two or more particles

$$|p_1, p_2, \ldots\rangle_{\text{in}} \neq |p'_1, p'_2, \ldots\rangle_{\text{out}}, \tag{3.5}$$

if there is interaction. The probability that starting with two particles with four momenta p_1, p_2 at $t = -\infty$ we will have two particles with four momenta p'_1, p'_2 when measuring is given then by

$$\left| {}_{\text{out}}\langle p'_1\, p'_2 | p_1, p_2\rangle_{\text{in}} \right|^2. \tag{3.6}$$

Physical states are represented by unit vectors, thus, both the "in" and "out" bases are orthonormal. But this means that there should be a matrix, S, that transforms the "in" bases into the "out" basis

$$|\phi\rangle_{\text{out}} = S\,|\psi\rangle_{\text{in}}, \tag{3.7}$$

with $S \cdot S^\dagger = I$ due to the orthonormality of the "in" and "out" states. The matrix S is called scattering matrix or S-matrix, and it represents the probability amplitude for some state $|\psi\rangle$ in the distant past, where all particles emitted by the source are idealized to be non-interacting, to evolve into some other state $|\phi\rangle$ in the future, where the detector is also idealized to absorb only free, non-interacting, particles.

Most of the times in a scattering reaction, particles just zip by each other and nothing happens. To account for this, the S-matrix is commonly written as [70]

$$S_{ab} = I_{ab} - i\sqrt{\rho_a}\sqrt{\rho_b}T_{ab}, \tag{3.8}$$

where a and b are channel indices specifying all properties of the channel (four momenta, spin, etc.), ρ_a (ρ_b) is a kinematic factor related to the phase space for channel a (channel b), and T_{ab} is a matrix in the channel space which contains all the information about the scattering between the particles involved. This T_{ab} matrix is usually called the T-matrix, and it can be computed from a given theory. Observables like cross sections, decay widths, etc., are directly related to the T-matrix of the process.

So the next question should be how to calculate the T-matrix from a given theory. Particularly, our goal is to determine the T-matrix describing the interaction between a heavy pseudoscalar/vector meson (H) and a light pseudoscalar meson (ϕ) for strangeness of the system $+1$ and charm $+1$ or -1. Such T-matrices, as we will see in the next chapter, would constitute the input for solving the three-body equations for the $KD\bar{D}^*$ system.

3.4 Determination of the T-matrix

Let us consider, for example, the interaction between a heavy pseudoscalar, like the D meson, and a light pseudoscalar, like a pion or kaon. We want to describe its interaction at center of mass energies close to the threshold of the channel, i.e., close to the sum of the masses of the two hadrons. In such a situation, the momenta related to these hadrons are small when compared to their energies and their internal structure is of no relevance for understanding the interaction between them. In this way, we can consider a quantum field associated with each hadron and use an effective Lagrangian to describe the interaction.

As explained in section 2.5, such an effective Lagrangian is built by implementing the appropriate symmetries related to the system under study, like the chiral symmetry and the heavy quark symmetry. We could now ask how to determine the interaction between two hadrons like a D meson and a light pseudoscalar (represented by ϕ). A way to answer this question is to think in terms of Feynman diagrams. The simplest contribution to the scattering $D\phi \to D\phi$ is shown in the first diagram of Fig. 3.9, which is

a contact interaction between D and ϕ. Such contact interaction corresponds precisely

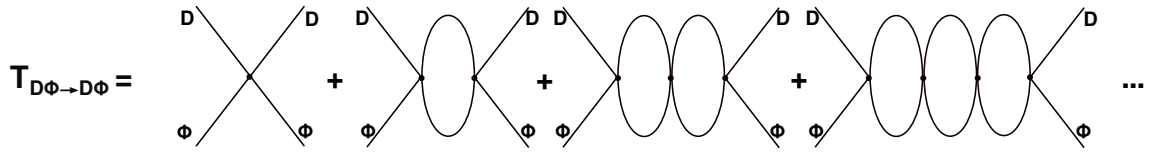

Figure 3.9: Diagrams for the calculation of the amplitude for the reaction $D\phi \to D\phi$.

to the contribution originating from the effective Lagrangian after applying the Feynman rules to it. If V represents this contribution, which is called the tree level contribution, we use the convention

$$-iV = i\mathscr{L}, \tag{3.9}$$

where $\mathscr{L}$, in general, depends on the bare masses m_i and couplings f_i.

However, we can have more possible ways of having a final $D\phi$ final state as a consequence of the interaction between a D and a ϕ in the initial state. For example, we could produce a virtual $D\phi$ state, represented as internal lines in the second diagram of Fig. 3.9, which give rise to a loop function of two propagators.

Let's evaluate the contribution of the second diagram in Fig. 3.9. In Fig. 3.10 we show the four momentum associated with each of the particles involved in the process (we denote by P the total four momentum of the system). Using the Feynman rules, as

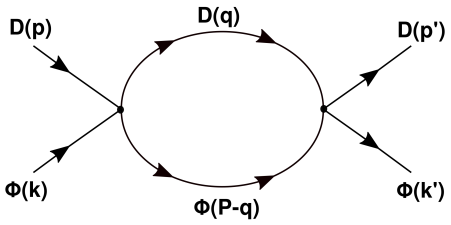

Figure 3.10: Diagram related to $T^{(2)}$. A virtual $D\phi$ state is produced.

we have discussed earlier, each vertex $D\phi \to D\phi$ in the diagram of Fig. 3.10 contributes with an amplitude V, while the loop contribute with a loop function G. Both, V and G, depend on the model we are working with, but, in general if we are only concerned about their momenta dependence, we have then $V \equiv V(p,k,q)$ and $G \equiv G(P,q)$. In this way, the diagram in Fig. 3.10 contributes to the scattering with an amplitude, $T^{(2)}$, given

by

$$
\begin{aligned}
-iT^{(2)} &= (-iV)(+iG)(-iV) = -iVGV, \\
&= -i\int \frac{d^4q}{(2\pi)^4} V(p,k,q) \frac{1}{q^2 - M^2 + i\varepsilon} \frac{1}{(P-q)^2 - m^2 + i\varepsilon} V(q,k',p'),
\end{aligned} \tag{3.10}
$$

where M (m) is the mass of the particle D (ϕ). The integration on d^4q is related to the fact of having a virtual state $D\phi$, where the momenta of D and ϕ can be anything compatible with the four momentum conservation since they are off the mass shell, or off-shell. This situation is different to the one of the particles represented by external lines in the diagram, which are on the mass shell, or simply, on-shell, i.e., $p^2 = M^2$ and $k^2 = m^2$.

The whole complication of determining the amplitude $T^{(2)}$ is in solving the integral in Eq. (3.10), which implies considering V off-shell. However, as shown in Ref. [71], we can solve Eq. (3.10) considering V on-shell. Especially when we are at center of mass energies near the threshold of the channel, as in our case, where the s-wave part of V, V_s, which is obtained as

$$
V_s = \frac{1}{2}\int_{-1}^{1} d\cos\theta\, V, \tag{3.11}
$$

with θ being the angle formed by the vectors $\vec{p}\,'$ and $\vec{k}\,'$ in the center of mass frame, is the most relevant to describe the scattering.

The argument given in Ref. [71] is the following: the amplitude $V_s(p,k,q)$ can be written as

$$
\begin{aligned}
V_s(p,k,q) &= V_s^{\text{on-shell}}(p,k) + \beta(q^2 - M^2) + \beta'[(P-q)^2 - m^2], \\
&\equiv V_s^{\text{on-shell}}(p,k) + V_s^{\text{off-shell}},
\end{aligned} \tag{3.12}
$$

where β and β' are coefficients which might appear because of the separation into on-shell and off-shell parts. In this way, if the off-shell D and ϕ particles would be placed on-shell, we would recover the on-shell amplitude, obtained from Eq. (3.9).

If we now cast Eq. (3.12) into Eq. (3.10), we get

$$
\begin{aligned}
T^{(2)} &= \int \frac{d^4q}{(2\pi)^4}(V_s^{\text{on-shell}} + V_s^{\text{off-shell}})\frac{1}{q^2-M^2+i\varepsilon}\frac{1}{(P-q)^2-m^2+i\varepsilon}(V_s^{\text{on-shell}} + V_s^{\text{off-shell}}) \\
&= V_s^{\text{on-shell}}\left[\int \frac{d^4q}{(2\pi)^4}\frac{1}{q^2-M^2+i\varepsilon}\frac{1}{(P-q)^2-m^2-i\varepsilon}\right]V_s^{\text{on-shell}} \\
&\quad + V_s^{\text{on-shell}}\int \frac{d^4q}{(2\pi)^4}\left[\frac{1}{q^2-M^2+i\varepsilon}\frac{1}{(P-q)^2-m^2-i\varepsilon}V_s^{\text{off-shell}}\right] \\
&\quad + \int \frac{d^4q}{(2\pi)^4}\left[V_s^{\text{off-shell}}\frac{1}{q^2-M^2+i\varepsilon}\frac{1}{(P-q)^2-m^2-i\varepsilon}\right]V_s^{\text{on-shell}} \\
&\quad + \int \frac{d^4q}{(2\pi)^4}\left[V_s^{\text{off-shell}}\frac{1}{q^2-M^2+i\varepsilon}\frac{1}{(P-q)^2-m^2-i\varepsilon}V_s^{\text{off-shell}}\right]. \qquad (3.13)
\end{aligned}
$$

As shown in Ref. [71], the terms involving $V_s^{\text{off-shell}}$ produce contributions with the same structure in the dynamical variables as the tree level contribution, in such a way that they can be absorbed into the parameters, like coupling constants and masses, of the Lagrangian used to get $V_s^{\text{on-shell}}$. In other words, if the Lagrangian used to get $V_s^{\text{on-shell}}$ has coupling constants given by f_i and masses given by m_i, Eq. (3.13) can be written as

$$
\begin{aligned}
T^{(2)} &= V_s^{\text{on-shell}}(f_i+\delta f_i, m_i+\delta m_i)\left[\int \frac{d^4q}{(2\pi)^4}\frac{1}{q^2-M^2+i\varepsilon}\frac{1}{(P-q)^2-m^2+i\varepsilon}\right] \\
&\quad \times V_s^{\text{on-shell}}(f_i+\delta f_i, m_i+\delta m_i). \qquad (3.14)
\end{aligned}
$$

This suggest that the contribution from the off-shell part of the amplitude V_s can be reabsorbed in f_i and m_i by renormalizing them. However, if we consider directly the physical values for the coupling constants and masses appearing in the Lagrangian used, the contribution to the scattering arising from the off-shell part of the amplitude in Eq. (3.12) would be automatically included and we can evaluate the diagram shown in Fig. 3.10 by using $V_s^{\text{on-shell}}(f_i^{\text{physical}}, m_i^{\text{physical}})$.

In this way, from Eq. (3.14), we have

$$
T^{(2)} = V_s^{\text{on-shell}}(f_i^{\text{physical}}, m_i^{\text{physical}})\cdot G \cdot V_s^{\text{on-shell}}(f_i^{\text{physical}}, m_i^{\text{physical}}), \qquad (3.15)
$$

where

$$
G = \int \frac{d^4q}{(2\pi)^4}\frac{1}{q^2-M^2+i\varepsilon}\frac{1}{(P-q)^2-m^2+i\varepsilon}. \qquad (3.16)
$$

One can proceed similarly for all the other diagrams shown in Fig. 3.9, arriving then to the conclusion that the T-matrix describing the interaction in s-wave between a D

meson and a light pseudoscalar is given by

$$T = V_s^{\text{on-shell}} + V_s^{\text{on-shell}} G V_s^{\text{on-shell}} + V_s^{\text{on-shell}} G V_s^{\text{on-shell}} G V_s^{\text{on-shell}} + \dots \tag{3.17}$$

This is a series which can be summed up and establishes that

$$T = \left[1 - V_s^{\text{on-shell}} \cdot G\right]^{-1} V_s^{\text{on-shell}}. \tag{3.18}$$

Equation (3.18) corresponds to the Bethe-Salpeter equation in its on-shell factorized form [72–74].

The Bethe-Salpeter equation describing the interaction between two particles is given by [75]

$$T = V + VGT = V + \int \frac{d^4q}{(2\pi)^4} V(p,k,q) \frac{1}{q^2 - m^2 + i\varepsilon} \frac{1}{(P-q)^2 - M^2 + i\varepsilon} T(q.p'.k'),$$

where V is the kernel of the equation. Factorizing V and, thus T, outside the integral, converts the integral equation into an algebraic equation, where

$$\begin{aligned} T = V + VGT \quad &\Rightarrow \quad (1 - VG)T = V, \\ &\Rightarrow \quad T = (1 - VG)^{-1} V, \end{aligned}$$

with G given by Eq. (3.16). Such approximation, motivated, in our case, by the use of an s-wave kernel V, and the fact that the off-shell dependence of the kernel produces loop integrals whose contributions can be absorbed in the parameters appearing in the same kernel, has been proved to be very successful when describing the interaction of mesons and baryons at energies nearby the corresponding thresholds.

So, in order to calculate the T-matrix from Eq. (3.18), we need not only the s-wave amplitude V, which is obtained from an effective Lagrangian, but also the loop function G given in Eq. (3.16). Counting the powers of q in the numerator as well as in the denominator we see that the integral in Eq. (3.16) is logarithmically divergent: as $q^2 \to \infty$, the integral behaves as $\int d^4q \frac{1}{q^4}$, which is analogous to $\int dx \frac{1}{x} = \log x$. This means that we need to regularize the integral. The regularization procedure will introduce a parameter in the theory, which can be a cut-off, if we decide to simply cut the integration after some value of the three momentum, or a subtraction constant, if dimensional regularization is used to deal with the divergence. In this thesis we have regularized the integral in

Eq. (3.16) by using dimensional regularization. This method consists of evaluating the integral in an n-dimensional space, where we are able to perform the integration, and consider the limit $n \to 4$ afterwards. In this way, Eq. (3.16) becomes

$$G_{D\theta}(\sqrt{s}) = \frac{1}{16\pi^2}\left\{ a(\mu) + \ln\frac{M^2}{\mu^2} + \frac{m^2 - M^2 + s}{2s}\ln\frac{m^2}{M^2} \right.$$
$$+ \frac{|\vec{p}_{\text{c.m}}|}{\sqrt{s}}\left[\ln\left(s - (M^2 - m^2) + 2|\vec{p}_{\text{c.m}}|\sqrt{s}\right) + \ln\left(s + (M^2 - m^2) + 2|\vec{p}_{\text{c.m}}|\sqrt{s}\right)\right.$$
$$\left.\left. - \ln\left(-s + (M^2 - m^2) + 2|\vec{p}_{\text{c.m}}|\sqrt{s}\right) - \ln\left(-s - (M^2 - m^2) + 2|\vec{p}_{\text{c.m}}|\sqrt{s}\right)\right]\right\}, \tag{3.19}$$

where μ is the regularization scale, $a(\mu)$ is the subtraction constant at this scale and $|\vec{p}_{\text{c.m}}|$ represents the center of mass momentum of the system. A change in μ produces a change in the value $a(\mu)$ since they are not independent parameters. Since the internal structure of the hadrons is not relevant in our description, a typical scale $\mu \sim 1000$ MeV is used, for which, values of $a(\mu) \sim -2$ are found in different two hadron systems when using the corresponding T-matrix to fit the data on observables like cross sections. These values of μ and $a(\mu)$ can be considered of naturals size since they are linked to cut-offs around 1000 MeV when regularizing the loop functions. Cut-offs ~ 1000 MeV also correspond to a typical average hadron size from the point of view of an effective field theory where the degrees of freedom are the hadrons and not the quarks.

Let's go back to the calculation of the T-matrix for the process $D\phi \to D\phi$. The diagram shown in Fig. 3.10 shows the interaction proceeding through a virtual $D\phi$. Note, however, that there can be other intermediate states, i.e., other two hadrons with the same quantum numbers as $D\phi$. Such that if we denote these hadrons as D' and ϕ', respectively, we can also have an intermediate $D'\phi'$ state as shown in Fig. 3.11. We say

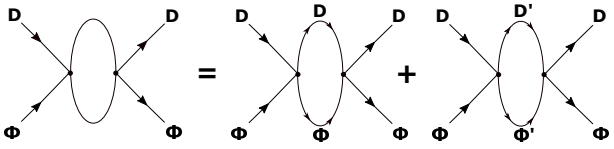

Figure 3.11: One loop contribution to the T-matrix taking in consideration the coupled channel $D'\phi'$.

that $D'\phi'$ is a coupled channel of $D\phi$. This means that to get the T-matrix related to the interaction of the two hadrons we need to consider all the relevant two-hadron coupled

channels for the energy region we want to explore. In this way the kernel $V_s^{\text{on-shell}}$ in Eq. (3.18) becomes a matrix in the coupled channel space

$$V_s^{\text{on-shell}} = \begin{pmatrix} V_{11} & V_{12} & \dots & V_{1n} \\ V_{21} & V_{22} & \dots & V_{2n} \\ \vdots & \vdots & \ddots & \vdots \\ V_{n1} & V_{n2} & \dots & V_{nn} \end{pmatrix}, \tag{3.20}$$

where V_{ij}, $i, j = 1, 2, \dots, n$, corresponds to the on-shell amplitude obtained from the Lagrangian for the transition between the channel i, constituted by a heavy mesons H_i and a light meson ϕ_i, and the channel j, formed by the mesons H_j and ϕ_j. The index n represents the total number of coupled channels considered.

Similarly, the loop function G in Eq. (3.18), which accounts for the intermediate virtual states, becomes a diagonal matrix in the coupled channel space

$$G = \begin{pmatrix} G_{11} & 0 & \dots & 0 \\ 0 & G_{22} & \dots & 0 \\ \vdots & & \ddots & \vdots \\ 0 & 0 & \dots & G_{nn} \end{pmatrix}, \tag{3.21}$$

In this way

$$T = \begin{pmatrix} T_{11} & T_{12} & \dots & T_{1n} \\ T_{21} & T_{22} & \dots & T_{2n} \\ \vdots & \vdots & & \vdots \\ T_{n1} & T_{n2} & \dots & T_{nn} \end{pmatrix}, \tag{3.22}$$

and the equation

$$T = [I - V \cdot G]^{-1} \cdot V, \tag{3.23}$$

is an algebraic matrix equation, where I is the $n \times n$ identity matrix. In this way, an element of the T-matrix is given by

$$T_{ij} = V_{ij} + \sum_{k=1}^{n} V_{ik} G_{kk} V_{kj} + \sum_{k=1}^{n} \sum_{k'=1}^{n} V_{ik} G_{kk} V_{kk'} G_{k'k'} V_{k'j} + \dots, \tag{3.24}$$

incorporating in this form the contribution from all the coupled channels via virtual states to the scattering between the particles involved in the channels i and j.

The determination of the T-matrix not only serves to calculate observables like the cross section, decay width, etc., but also to obtain information on the possible bound

states and/or resonance formed as a consequence of the dynamics involved in the interaction. In fact, if a resonance or a bound state is generated as a consequence of the interaction, the series shown in Fig. 3.9, would be equivalent to the exchange in the s-channel of the resonance/bound state formed (see Fig. 3.12)

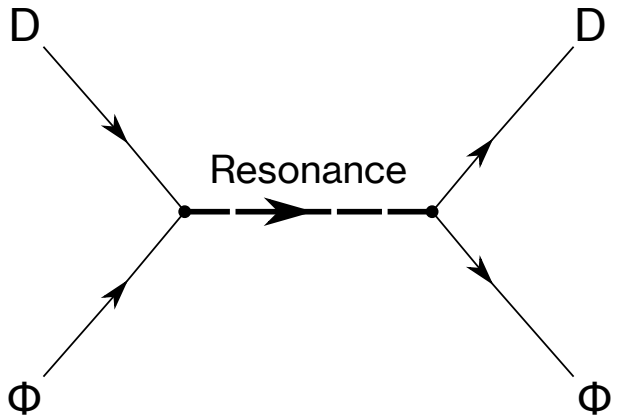

Figure 3.12: s-channel exchange of the resonance formed from the $D\phi$ interaction.

T-matrix and Unstable Particles

A particle is not necessarily stable and it can decay to other particles. Unstable particles are observed as resonances. These, in a hand-waving definition, are local maxima in the cross-section of a process as a function of the energy of the system.

Experimentally, searching for unstable particles is very similar to what is done for excited states of an atom [76]. To look for such unstable atomic states we could shine a monochromatic light beam, whose frequency can be varied, onto the atom under study. By varying the frequency, the atom initially in its ground state, can absorb a photon, producing a transition of an electron to a higher energy level, followed by the emission of a photon when the excited electron is transferred to a lower energy level of the atom. Peaks in the intensity of the emitted light will indicate the existence of excited atomic states at the corresponding energies. Similarly, to find unstable subatomic particles, in a laboratory, we collide two beams together and look for increases in the number of particles reaching the detector. In other words, we search for peaks in the cross section as a function of the energy of the system.

To be more specific, let us consider an unstable particle with mean life τ. Given a sample of these particles, the number of particles left at time t decreases exponentially with time as

$$N(t) = N_0 e^{-t/\tau}. \tag{3.25}$$

In quantum mechanics the probability of the existence of a particle is proportional to the square of its wave function. If we denote $\Psi(\vec{x},t)$ to the wave function of an unstable particle whose mean life is given by τ, we have that

$$|\Psi(\vec{x},t)|^2 \propto e^{-t/\tau}. \tag{3.26}$$

If $\Psi(\vec{x},t)$ represents the eigenstate of a Hamiltonian with energy E, the time evolution of $\psi(\vec{x},t)$ is given by the Schrödinger equation and we can write

$$\Psi(\vec{x},t) = \psi(\vec{x})e^{-iEt}, \tag{3.27}$$

by considering the method of separation of variables to solve the Schrödinger equation.

Since the probability for decay of an unstable particle is given by Eq. (3.26), by means of Eq. (3.27), we want that in some way $\psi(\vec{x})e^{-iEt} \cdot \psi^\dagger(\vec{x})e^{iEt} \propto e^{-t/\tau}$. To get this, we need E to be complex. Let us assume $E = M - i\Gamma/2$, where M is the mass of the particle and Γ its decay width ($\Gamma = \frac{1}{\tau}$).

By doing this, we have

$$\Psi(\vec{x},t) = \psi(\vec{x})e^{-iMt}e^{-\Gamma t/2}, \tag{3.28}$$

$$\Rightarrow |\Psi(\vec{x},t)|^2 = |\psi(\vec{x})|^2 e^{-\Gamma t} = |\psi(\vec{x})|^2 e^{-\frac{t}{\tau}}, \tag{3.29}$$

as desired. So, by simply extending the energies to complex energies with a negative imaginary part we are able to reproduce the existence probability. Thus, it can be said that instability of a state is equivalent to attributing it a complex energy with a negative imaginary part.

Note that if we would have considered a positive imaginary part, i.e., $E \to M + i\frac{\Gamma}{2}$, the results would have been completely different, since we would have got

$$|\Psi(\vec{x},t)|^2 = |\psi(\vec{x})|^2 e^{\frac{t}{\tau}}, \tag{3.30}$$

which is incompatible with the unstable behavior of the particle, since for $t \to \infty$ Eq. (3.30) produces an infinite probability.

Within the context of quantum mechanics we can also obtain the energy distribution of such an unstable particle. To do this, we can consider the Fourier transformation of the wave function $\Psi(\vec{x},t)$. Let us consider $\vec{x} = \vec{0}$ for simplification. Then, we have

$$\begin{aligned}\Psi(E) &= \frac{1}{\sqrt{2\pi}}\int_0^\infty dt\Psi(\vec{0},t)e^{iEt} = \frac{1}{\sqrt{2\pi}}\int_0^\infty dt\Psi(\vec{0})e^{-iMt}e^{-\frac{\Gamma}{2}t}e^{iEt}, \\ &= \frac{\Psi(\vec{0})}{\sqrt{2\pi}}\int_0^\infty dt e^{i[(E-M)+i\frac{\Gamma}{2}]t} = \frac{\Psi(\vec{0})}{\sqrt{2\pi}}\frac{i}{(E-M+i\frac{\Gamma}{2})},\end{aligned}$$

where we have used that for $t \to \infty$, $e^{-\frac{\Gamma}{2}t} \to 0$, such that $e^{i(E-M)t}e^{-\frac{\Gamma}{2}t} \to 0$ when $t \to \infty$. Then

$$\Psi(E) = \frac{\Psi(\vec{0})}{\sqrt{2\pi}}\frac{i(E-M-i\frac{\Gamma}{2})}{(E-M)^2+(\frac{\Gamma}{2})^2}. \tag{3.31}$$

So the probability density that the unstable particle has energy E is given by

$$|\Psi(E)|^2 = \frac{|\Psi(\vec{0})|^2}{2\pi}\frac{1}{(E-M)^2+(\frac{\Gamma}{2})^2}. \tag{3.32}$$

This function is a well know function called Breit-Wigner.

If an unstable particle is virtually produced as a consequence of the scattering, we expect that the cross section for the process, which, as we show in section 3.2 is related to the probability that the particles collide and react in a certain way, should have the same energy dependence as the one found in Eq. (3.32).

That's it,

$$\sigma \propto \frac{1}{(E-M)^2+(\Gamma/2)^2}. \tag{3.33}$$

Using that

$$\sigma \propto |T|^2, \tag{3.34}$$

where T is the T-matrix for the process considered, we have from Eqs. (3.33) and (3.34) that

$$T \sim \frac{1}{(E-M)+i\frac{\Gamma}{2}}. \tag{3.35}$$

Thus, by calculating T we can obtain information on the mass M and the width Γ of possible unstable states formed from the dynamics involved in the process under study.

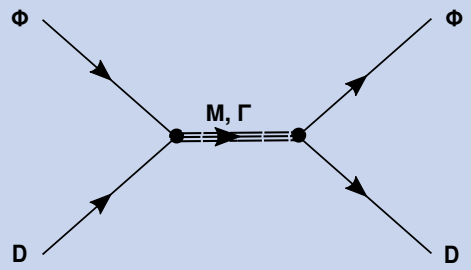

Figure 3.13: $\phi D \to \phi D$ with formation of a state with mass M and width Γ.

In such a case the diagrammatic representation of the scattering shown in Fig. 3.9 is equivalent to the one shown in Fig. 3.13, where a particle of mass M and width Γ is exchanged.

Note also that from Eq. (3.35), if we consider complex values for the energy E, the search of states generated from the dynamics involved in the system corresponds to looking for poles of the T-matrix in the complex energy plane.

3.4.1 The isospin base

Before continuing the explicit calculation of the T-matrix, let's pay attention to a detail: in the construction of the Lagrangians we have used the charge base, which is very intuitive since it allows us to work with states that represent actual measurable particles, as protons and neutrons. However, due to the almost exact isospin symmetry of the strong interaction, for many purposes, it is more convenient to work in terms of the isospin base.

Among hadrons, there are many small groups in which members have similar masses, different electric charges and it is known that the strength of the strong interaction of

such states is almost the same. Such particles form isospin multiplets, like, for example the proton and the neutron. The similarity of the properties of the proton and the neutron allows that we may treat p and n as a doublet N given by

$$N = \begin{pmatrix} p \\ n \end{pmatrix}. \tag{3.36}$$

Proton and neutron can then be interpreted as different versions of the same state, called the nucleon (N) such that the nuclear force remains unchanged under the interchange of all protons and neutrons in a system, as was precisely found by Heisenberg, in the study of mirror nuclei (same number of protons and neutrons).

As we saw in the previous chapter, the existence of such a symmetry means that there is a group related to it. If U is a matrix representation of this group, the state in Eq. (3.36) transforms as

$$N = \begin{pmatrix} p \\ n \end{pmatrix} \rightarrow N' = \begin{pmatrix} p' \\ n' \end{pmatrix} = \begin{pmatrix} a & b \\ c & d \end{pmatrix} \begin{pmatrix} p \\ n \end{pmatrix} = UN. \tag{3.37}$$

Heisenberg's finding on the nuclear force implies that the expectation value of the nuclear force (which we represent with a potential $\mathbb{V}$) does not change under the transformation in Eq. (3.37), i.e., $\langle N|\,\mathbb{V}\,|N\rangle = \langle N'|\,\mathbb{V}\,|N'\rangle$ (ignoring the effect of the electromagnetic interaction). Since

$$\langle N|N\rangle = \left\langle N'\middle|N'\right\rangle = \langle N|\,U^\dagger U\,|N\rangle = 1 \Rightarrow U^\dagger U = I, \tag{3.38}$$

U must be a unitary matrix: U then belongs to the group $SU(2)$ and we have a 2-dimensional representation of $SU(2)$. We state this fact by attributing isospin $1/2$ to the nucleon doublet and by treating the proton and neutron as states with a different third isospin component. The value of the third component of isospin, I_3, can be calculated for any particle by means of the Gell-Mann-Nishijima formula, $I_3 + \frac{Y}{2} = Q$, where Q is the electric charge and Y is the hypercharge, which is given by the sum of the strangeness S, charm C, bottomness B', topness T, and baryon number B. For example, for the neutron we have $Q = 0$ and $Y = 1$ because it has baryon number $+1$, then $I_3 = -1/2$ for the neutron. For the proton, we have $Q = +1$ and $Y = +1$ then its $I_3 = +1/2$. Particles in the multiplets are organized by decreasing order of the value of I_3. This explains the representation of the state in Eq. (3.36).

Since the Lagrangian we have derived is in the charge basis we need to find a way of relating the charge and the isospin bases. Once we realize that the isospin has the same algebra as the spin (both correspond to $SU(2)$ representations), we can use the same relations that we use in quantum mechanics to relate a state with total spin S and third spin component S_3 to the individual states $\left|s_1, s_{1,3}\right\rangle$ and $\left|s_2, s_{2,3}\right\rangle$, whose combination give rise to the state $|S, S_3\rangle$. To do this, we need to use the Clebsch-Gordan coefficients and a phase convention for the association between isospin states and the states in the charge base [77]. For example, K^+ and K^0 and D^+ and D^0 form isospin doublets, where $|K^+\rangle = |I = 1/2, I_3 = +1/2\rangle$, $\left|K^0\right\rangle = |I = 1/2, I_3 = -1/2\rangle$, $|D^+\rangle = |I = 1/2, I_3 = +1/2\rangle$ and $\left|D^0\right\rangle = -|I = 1/2, I_3 = -1/2\rangle$, and we write, by analogy to Eq. (3.36),

$$K = \begin{pmatrix} K^+ \\ K^0 \end{pmatrix}, \qquad D = \begin{pmatrix} D^+ \\ -D^0 \end{pmatrix}. \tag{3.39}$$

In this way, we can discuss the interactions of a kaon, K, with mass $m_K = \frac{m_{K^+} + m_{K^0}}{2}$, and a D meson, with mass $m_D = \frac{m_{D^0} + m_{D^+}}{2}$. Since both kaon and the D meson have isospin $1/2$, we can have a KD system with total isospin 0 or 1. By using a Clebsch-Gordan table, we have

$$|I = 0, I_3 = 0\rangle = \frac{1}{\sqrt{2}}\left[\left|I_{1,3} = \frac{1}{2}, I_{2,3} = -\frac{1}{2}\right\rangle - \left|I_{1,3} = -\frac{1}{2}, I_{2,3} = \frac{1}{2}\right\rangle\right] \tag{3.40}$$

or

$$\begin{aligned} |DK; I = 0, I_3 = 0\rangle = \frac{1}{\sqrt{2}}\Big[& \left|I_1 = 1/2, I_{1,3} = 1/2\right\rangle \otimes \left|I_2 = 1/2, I_{2,3} = -1/2\right\rangle \\ & - \left|I_1 = 1/2, I_{1,3} = -1/2\right\rangle \otimes \left|I_2 = 1/2, I_{2,3} = 1/2\right\rangle\Big], \\ = \frac{1}{\sqrt{2}}\Big[& \left|D^+\right\rangle \otimes \left|K^0\right\rangle + \left|D^0\right\rangle \otimes \left|K^+\right\rangle\Big], \end{aligned} \tag{3.41}$$

such that

$$|DK, I = 0, I_3 = 0\rangle = \frac{1}{\sqrt{2}}\left[\left|D^+K^0\right\rangle + \left|D^0K^+\right\rangle\right]. \tag{3.42}$$

Now that we know how to related the two bases, we can obtain the kernel V of the Bethe-Salpeter equation in the isospin basis from the expression of V in the charge basis. In the following discussions, the amplitude V in the isospin basis will be denoted as $V^I_{AB\to CD}$, where $AB \to CD$ is the transition we are studying and I is the total isospin of the system, while in the charge basis we will use the notation $V_{AB\to CD}$. The interactions we are interested in are those involving the charmed mesons D or D^* and a

light pseudoscalar meson, to get charm $C=+1$ and strangeness $S=+1$. This implies the following coupled channels in the isospin base: DK, $D_s\eta$, $D_s\pi$ for the interaction between a heavy and a light pseudoscalars and D^*K, $D_s^*\eta$, $D_s^*\pi$ for the interaction between a heavy vector meson and a light pseudoscalar. We also need the interaction between these mesons for total $C=-1$ and $S=+1$. In this case we study the $\bar{D}K$ and $\bar{D}^*K$ channels, respectively.

Using now Eq. (3.42), we can write

$$\begin{aligned} V^{I=0}_{DK\to DK} &= \langle DK; I=0, I_3=0|\, V\, |DK; I=0, I_3=0\rangle \\ &= \frac{1}{2}\left[\left\langle D^+K^0\right| V \left|D^+K^0\right\rangle + \left\langle D^+K^0\right| V \left|D^0K^+\right\rangle \right. \\ &\quad \left. + \left\langle D^0K^+\right| V \left|D^+K^0\right\rangle + \left\langle D^0K^+\right| V \left|D^0K^+\right\rangle\right] \\ &= \frac{1}{2}\left[V_{D^+K^0\to D^+K^0} + 2V_{D^+K^0\to D^0K^+} + V_{D^0K^+\to D^0K^+}\right]. \end{aligned} \tag{3.43}$$

Similarly, we can get $V^{I=1}_{DK\to DK}$, $V^{I=1}_{DK\to D_s\pi}$, $V^{I=0}_{DK\to D_s\eta}$, etc. Explicit calculations of different kernels are shown in Appendix A.

To obtain the amplitudes V in the charge basis, we have used two effective Lagrangians: one based on the chiral and heavy quark symmetry (which we denote as HQ) and another based on the SU(4) symmetry, which is broken in a particular way.

Let's begin first by giving the results found within the HQ Lagrangian, which we show in the next subsection, and after that we will tackle the same problem with the SU(4) Lagrangian.

3.4.2 T-matrices obtained with the HQ Lagrangian

The first step in the calculation of the T-matrix is the deduction of the amplitudes V. To do this, we use the effective Lagrangian shown in Eq. (2.92)

$$\mathscr{L}_{HQ} = \frac{1}{4f^2}\left\{\partial^\mu H\left[\phi, \partial_\mu\phi\right]H^\dagger - H\left[\phi, \partial_\mu\phi\right]\partial^\mu H^\dagger\right\} \tag{3.44}$$

where H, $H^\dagger$ and ϕ are matrices having as elements the fields shown below

$$H = \begin{pmatrix} D^0 & D^+ & D_s^+ \end{pmatrix}, \qquad H^\dagger = \begin{pmatrix} \bar{D}^0 \\ D^- \\ D_s^- \end{pmatrix},$$

$$\phi = \begin{pmatrix} \frac{1}{\sqrt{2}}\pi^0 + \frac{1}{\sqrt{6}}\eta & \pi^+ & K^+ \\ \pi^- & -\frac{1}{\sqrt{2}}\pi^0 + \frac{1}{\sqrt{6}}\eta & K^0 \\ K^- & \bar{K}^0 & -\frac{2}{\sqrt{6}}\eta \end{pmatrix},$$

and apply the Feynman rules, together with the relation $i\mathscr{L} = -iV$.

Once the amplitude for a particular channel is obtained we need to project it on s-wave. This is done by working in the center of mass frame of the system and integrating on the angle, θ, formed by the final particles with respect to the incident direction, see Fig. 3.14. By doing this, the amplitude V, which before projecting it is a function of the Mandelstam variable s, t, u, reduces to a function of the Mandelstam variable s.

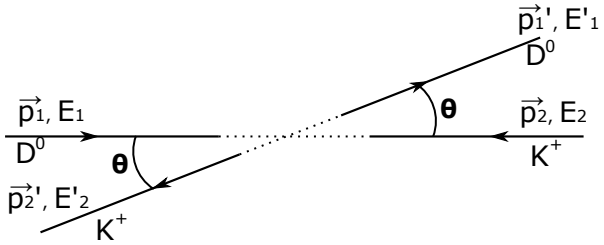

Figure 3.14: Process $D^0K^+ \to D^0K^+$ in the center of the mass frame, where $\vec{p}_1 = -\vec{p}_2$ and $\vec{p}\,'_1 = -\vec{p}\,'_2$.

An example: $D^0K^+ \to D^0K^+$

To describe the process $D^0K^+ \to D^0K^+$ we need to destroy a D^0 and a K^+ in the initial state and create a D^0 and a K^+ in the final state. Thus, we need the fields

$$H = \begin{pmatrix} D^0 & 0 & 0 \end{pmatrix}, \qquad H^\dagger = \begin{pmatrix} \bar{D}^0 \\ 0 \\ 0 \end{pmatrix}, \qquad \phi = \begin{pmatrix} 0 & 0 & K^+ \\ 0 & 0 & 0 \\ K^- & 0 & 0 \end{pmatrix}, \quad (3.45)$$

where the field D^0 annihilates the particle D^0 of the initial state, the field $\bar{D}^0$ creates the particle D^0 of the final state, the field K^+ annihilates the particle K^+ of the initial state and the field K^- creates the particle K^+ of the final state.
Substituting Eq. (3.45) in Eq. (3.44), we obtain

$$\mathscr{L}^{HQ}_{D^0K^+\to D^0K^+} = \frac{1}{4f^2}\left\{\partial_\mu D^0(K^+\partial_\mu K^- - \partial_\mu K^+K^-)\bar{D}^0 \right. \tag{3.46}$$

$$\left. -D^0(K^+\partial_\mu K^- - \partial_\mu K^+K^-)\partial_\mu \bar{D}^0\right\}. \tag{3.47}$$

Considering the momenta assignment shown in Fig. 3.14 and applying the Feynman rules, we get

$$V_{D^0K^+\to D^0K^+} = -\frac{1}{4f^2}\left[p_1(p_2+p_2') + p_1'(p_2+p_2')\right].$$

Using the Mandelstam variables, which are defined as follows

$$s=(p_1+p_2)^2, \qquad t=(p_1-p_1')^2, \qquad u=(p_1-p_2')^2,$$

we have

$$\left.\begin{aligned} p_1\cdot p_2 &= \tfrac{s-p_1^2-p_2^2}{2} \\ p_1\cdot p_2' &= \tfrac{p_1^2+p_2'^2-u}{2} \end{aligned}\right\} p_1\cdot(p_2+p_2') = \frac{s-u-p_2^2+p_2'^2}{2}, \tag{3.48}$$

$$\left.\begin{aligned} p_1'\cdot p_2 &= \tfrac{p_1'^2+p_2^2-u}{2} \\ p_1'\cdot p_2' &= \tfrac{s-p_1'^2p_2'^2}{2} \end{aligned}\right\} p_1'\cdot(p_2+p_2') = \frac{s-u-p_2'^2+p_2^2}{2}, \tag{3.49}$$

thus

$$V_{D^0K^+\to D^0K^+} = -\frac{1}{4f^2}(s-u). \tag{3.50}$$

In the center of mass frame of the system (see Fig. 3.14)

$$s=(E_1+E_2)^2=(E_1'+E_2')^2, \quad u=m_1^2+m_2'^2-2E_1E_2-2|\vec{p}_1||\vec{p}_1'|\cos\theta, \tag{3.51}$$

where m_i (m_i'), $i=1,2$, is the mass of the particle with momentum $\vec{p}_i$ ($\vec{p}_i'$) and we have used $p_1^2=m_1^2$ and $p_2'^2=m_2'^2$.

In this way $V_{D^0K^+\to D^0K^+}$ can be expressed as

$$V_{D^0K^+\to D^0K^+} = -\frac{1}{4f^2}\left(s - m_1^2 - m_2^2 + 2E_1E_2' + 2|\vec{p}_1||\vec{p}_1'|\cos\theta\right). \tag{3.52}$$

Once we have found the expression of Eq. (3.52), we can project it on s-wave and obtain

$$\begin{aligned} V^{\text{s-wave}}_{D^0K^+\to D^0K^+} &= \frac{1}{2}\int d\cos\theta V_{D^0K^+\to D^0K^+} \\ &= -\frac{1}{4f^2}\int d\cos\theta\left(s - m_1^2 - m_2^2 + 2E_1E_2' + 2|\vec{p}_1||\vec{p}_1'|\cos\theta\right) \\ &= \frac{1}{4f^2}\left(m_1^2 + m_2'^2 - 2E_1E_2' - s\right), \end{aligned}$$

where, in the CM frame, $E_1 = \frac{s+m_1^2-m_2^2}{2\sqrt{s}}$, $E_2' = \frac{s-m_1'^2+m_2'^2}{2\sqrt{2}}$ and then $2E_1E_2 = \frac{(s+m_1^2-m_2^2)(s-m_1'^2+m_2'^2)}{2s}$, finding then

$$V^{\text{s-wave}}_{D^0K^+\to D^0K^+} = \frac{1}{8f^2}\left[(m_1^2 + m_1'^2 + m_2^2 + m_2'^2) - 3s + (m_1^2 - m_2^2)(m_1'^2 - m_2'^2)\right].$$

The explicit calculation of the amplitudes V, and the s-wave projection, for all coupled channels can be found in Appendix B. As shown there, the results obtained can be written in a compact form as

$$V^{s\text{-wave}}_{H_i\phi_i\to H_j\phi_j} = \frac{\alpha_{ij}}{8f^2}\left[-3s + M_i^2 + M_j^2 + m_i^2 + m_j^2 + (M_i^2 - m_i^2)\cdot(M_j^2 - m_j^2)\right], \tag{3.53}$$

with M_i (M_j) and m_i (m_j) being the masses of the heavy and light mesons, respectively, in the initial (final) state. The coefficients α_{ij} are given in table 3.1.

Table 3.1: Coefficients α_{ij} for the coupled channels with charge $+1$, charm $+1$ and strangeness $+1$ (left) and charge 0, charm -1 and strangeness $+1$ (right). In case of charm -1 and charge $+1$, $\alpha_{\bar{D}^0K^+\to\bar{D}^0K^+} = -1$.

	D^0K^+	D^+K^0	$D_s^+\pi^0$	$D_s^+\eta$
D^0K^+	1	1	$-\frac{1}{\sqrt{2}}$	$-\sqrt{\frac{3}{2}}$
D^+K^0	1	1	$\frac{1}{\sqrt{2}}$	$-\sqrt{\frac{3}{2}}$
$D_s^+\pi^0$	$-\frac{1}{\sqrt{2}}$	$\frac{1}{\sqrt{2}}$	0	0
$D_s^+\eta$	$-\sqrt{\frac{3}{2}}$	$-\sqrt{\frac{3}{2}}$	0	0

	$\bar{D}^0K^0$	D^-K^+
$\bar{D}^0K^0$	0	-1
D^-K^+	-1	0

Using the relation between the charge and the isospin bases, the s-wave projection of the amplitudes V in the isospin basis has the same form as the one shown in

Eq. (3.53), except that now the masses appearing in Eq. (3.53) correspond to isospin average masses and the coefficients α_{ij} in the isospin basis are given in Tables 3.2 and 3.3.

Table 3.2: Coefficients α_{ij} for charm $+1$ and strangeness $+1$ and total isospin $+1$ (left) or total isospin 0 (right).

	DK	$D_s\pi$
DK	0	1
$D_s\pi$	1	0

	DK	$D_s\eta$
DK	2	$-\sqrt{3}$
$D_s\eta$	$-\sqrt{3}$	0

Table 3.3: Coefficients α_{ij} for charm -1 and strangeness $+1$ and total isospin $+1$ (left) or total isospin 0 (right).

	$\bar{D}K$
$\bar{D}K$	-1

	$\bar{D}K$
$\bar{D}K$	1

Once we have all the amplitudes V necessary to obtain the T-matrix, the next step is to calculate the loop function for the different coupled channels [see Eq. (3.19)]. In

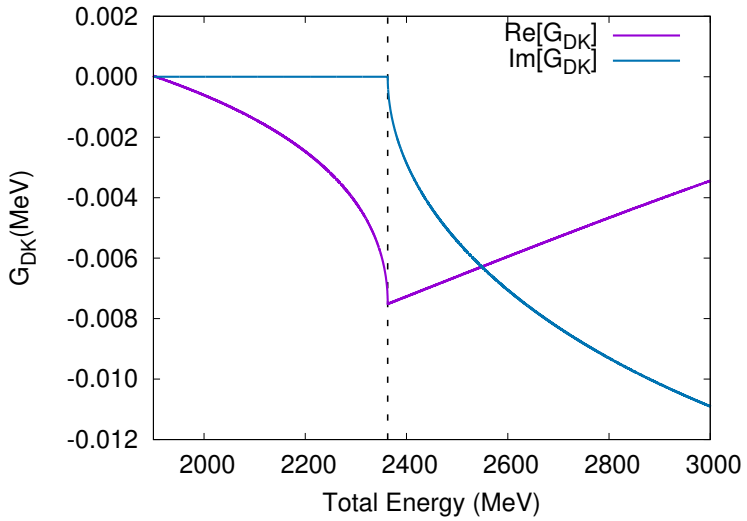

Figure 3.15: Real and imaginary part of G_{DK}. The dashed-line indicates the DK threshold position.

Fig. 3.15 we show the loop function for the DK system by using average masses for the members of the same isospin multiplet ($M_D = 1867.21$ MeV, $m_K = 495.644$ MeV). As can be seen, the imaginary part of G is zero below the threshold of the channel (i.e., for energies below $M_D + m_k = 2362,85$MeV). This is a consequence of the unitarity of the S-matrix.

Unitarity in coupled channels

From Eq. (3.8), considering the same channel in the initial and final states

$$\begin{aligned} S_{aa}S_{aa}^{\dagger} &= (1-i\rho_a T_{aa})\left(1+i\rho_a T_a^{\dagger}\right), \\ &= 1+i\rho_a(T_{aa}^{\dagger}-T_{aa})+\rho_a^2 T_{aa}T_{aa}^{\dagger}, \\ &= 1. \end{aligned} \tag{3.54}$$

Then, if $T_{aa} = \mathrm{Re}\{T_{aa}\} + i\,\mathrm{Im}\{T_{aa}\}$, we have that $T_{aa}T_{aa}^{\dagger} = |T_{aa}|^2$ and $T_{aa}^{\dagger} - T_{aa} = -2i\,\mathrm{Im}\{T_{aa}\}$, such that from Eq. (3.54)

$$2\rho_a\,\mathrm{Im}\{T_{aa}\} = -\rho_a^2|T_{aa}|^2 \Rightarrow \mathrm{Im}\{T_{aa}\} = -\frac{\rho_a}{2}|T_{aa}|^2. \tag{3.55}$$

From the Bethe-Salpeter equation

$$\begin{aligned} T = (1-VG)^{-1}V \Rightarrow T^{-1} &= V^{-1}(1-VG), \\ &= V^{-1} - G. \end{aligned}$$

In this way, since V is real,

$$\mathrm{Im}\left\{T_{aa}^{-1}\right\} = -\,\mathrm{Im}\{G_{aa}\}. \tag{3.56}$$

Using that

$$T_{aa}^{-1} = \frac{1}{T_{aa}} = \frac{T_{aa}^*}{|T_{aa}|^2} = \frac{\mathrm{Re}\{T_{aa}\} - i\,\mathrm{Im}\{T_{aa}\}}{|T_{aa}|^2},$$

we have, by taking the imaginary part of the above equation,

$$\mathrm{Im}\left\{T_{aa}^{-1}\right\} = -\frac{\mathrm{Im}\{T_{aa}\}}{|T_{aa}|^2}.$$

From Eq. (3.55)

$$\mathrm{Im}\left\{T_{aa}^{-1}\right\} = \frac{\rho_a}{2},$$

and using Eq. (3.56), we get

$$\mathrm{Im}\{G_{aa}\} = -\frac{\rho_a}{2} = -\frac{|\vec{p}_a|}{8\pi\sqrt{s}}, \tag{3.57}$$

where $|\vec{p}_a| = \frac{\lambda^{1/2}(s,M_a^2,m_a^2)}{2\sqrt{s}}$ is the center os mass momentum of the particles in the channel a.

With these ingredients, we can solve Eq. (3.18) using coupled channels and obtain

the T-matrices in the isospin base. In Fig. 3.16 we show $|T^{I=0}_{DK\to DK}|^2$ (upper panel, left side) and $|T^{I=1}_{DK\to DK}|^2$ (upper panel, right side) as function of the center of mass energy of the system. As shown in Ref. [78], we know that the interaction of a K with a D

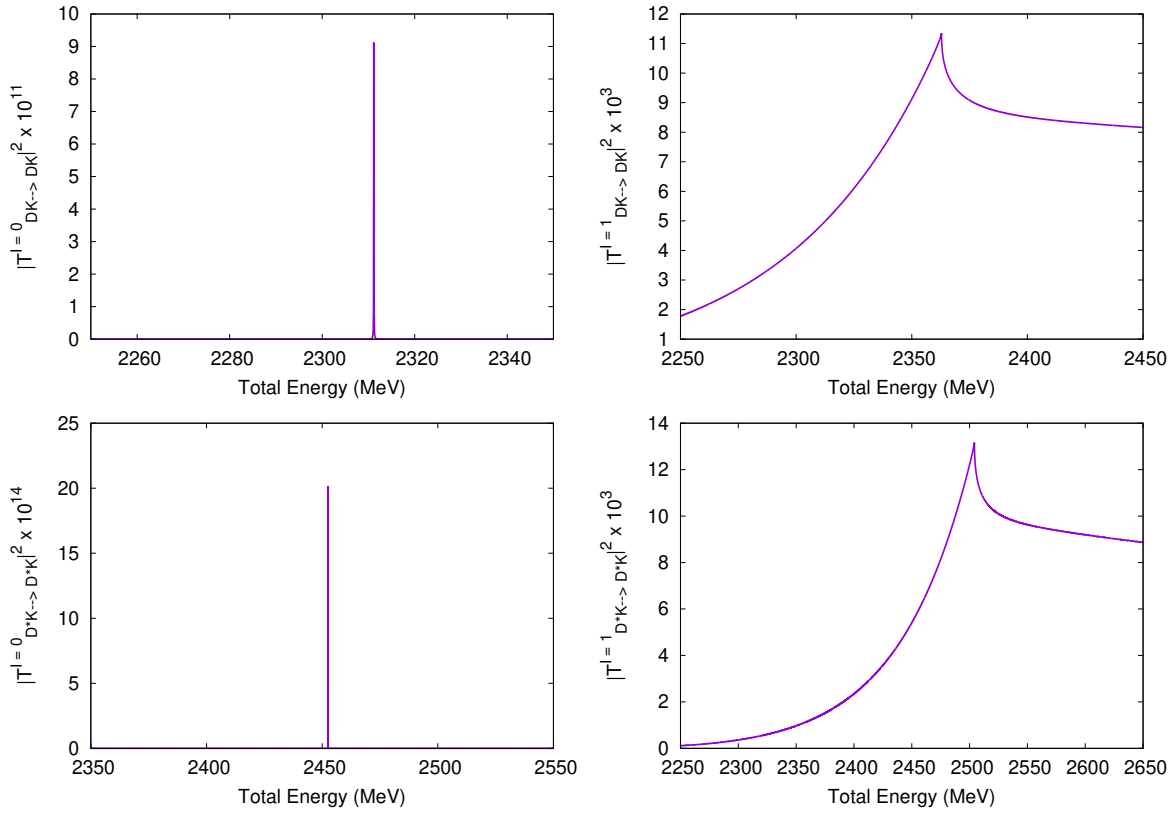

Figure 3.16: T-matrices obtained by using the Lagrangian based on the HQ symmetry. Upper panel: $|T_{KD\to KD}|^2$ for isospin 0 (left) and isospin 1 (right). Lower panel: $|T_{KD^*\to KD^*}|^2$ for isospin 0 (left) and isospin 1 (right).

in isospin 0 is attractive and generates the bound state $D^*_{s0}(2317)$. As can be seen in Fig. 3.16 (upper panel on the left), a peak of zero width is found at 2317 MeV which can be associated with $D^*_{s0}(2317)$. The isospin 1 interaction, however, does not form any state and we simply observe a cusp at the threshold, which corresponds to the opening of the DK channel.

We can repeat the same procedure for the D^*K system and coupled channels. As shown in Fig. 3.16, the D^*K interaction in isospin 0 (lower panel, left side) is attractive and forms a bound state at energy of 2460 MeV, which can be related to the state $D^*_{s1}(2460)$ [78]. As in case of the DK system, in isospin 1, as can be seen in Fig. 3.16 (lower panel, right side), no state is formed and we simply observe a cusp at the D^*K threshold.

As mentioned in section 3.2, if the peaks observed in the modulus squared of the T-matrix correspond to a state formed by the interaction between the hadrons considered, we should be able to find a pole in the T-matrix when going to the complex energy plane. When doing this, we need to take care of the branch cut that the loop function has when the threshold of a channel is opened. As shown in Ref. [72–74], this can be achieved by using

$$G_{aa} = \begin{cases} G^I_{aa}(\sqrt{s}), & \text{for Re}\{\sqrt{s}\} < (m_a + M_a) \\ G^I_{aa}(\sqrt{s}) - 2i\,\text{Im}\{G^I_{aa}\}, & \text{for Re}\{\sqrt{s}\} \geqslant (m_a + M_a). \end{cases} \tag{3.58}$$

with G^I_{aa} being the same expression as the one of Eq. (3.19) for the channel a.

Analytical Continuation of the T-matrix

The loop function appearing in Eq. (3.19) is an analytic function in the Mandelstam variable s up to its branch cuts, which appear whenever there is a channel opening.

In order to make an analytical continuation of G to the complex plane we need to cross the branch cuts. To do this, it is useful to visualize the branch cut as the connection between different complex energy planes, and $G(z)$ as a mapping from these planes onto a single complex energy plane. Each of these complex planes is called a Riemann sheet [79]. In particular, for the loop function there are two Riemann sheets for each channel.

The origin of these two sheets is because in the complex energy plane the mapping between the modulus of the three-momentum in the center of mass frame of the particles and s is not unique. The physical sheet or first Riemann sheet is associated with the physical region, i.e.,

$$|\vec{p}_a|^I = +\frac{\lambda^{1/2}(s, M_a^2, m_a^2)}{2\sqrt{s}}, \tag{3.59}$$

while the unphysical sheet, also called second Riemann sheet, is associated with

$$|\vec{p}_a|^{II} = -\frac{\lambda^{1/2}(s, M_a^2, m_a^2)}{2\sqrt{s}}, \tag{3.60}$$

To pass from one sheet to another, we can use the Schwarz's reflection principle [80], which states that if a function $f(z)$ is analytic in a region of the complex z-plane including a portion on the real axis in which f is real, then $f(z) = [f(z^*)]^*$. The loop function satisfies these conditions, therefore, in the complex energy plane, for a channel a, whenever $\mathrm{Re}\{\sqrt{s}\} \geq M_a + m_a$, we have, close to the real axis,

$$\begin{aligned} G_{aa}(\sqrt{s} - i\varepsilon) &= \left[G_{aa}(\sqrt{s} + i\varepsilon)\right]^*, \\ &= G_{aa}(\sqrt{s} + i\varepsilon) - 2i\,\mathrm{Im}\left\{G_{aa}(\sqrt{s} + i\varepsilon)\right\}. \end{aligned} \tag{3.61}$$

Since the beginning of the second Riemann sheet should match the end of the first Riemann sheet, we have

$$G^{II}_{aa}(\sqrt{s} - i\varepsilon) = G^{I}_{aa}(\sqrt{s} + i\varepsilon), \tag{3.62}$$

and from Eq. (3.61),

$$G^{II}_{aa} = (\sqrt{s} + i\varepsilon) = G^{I}_{aa}(\sqrt{s} + i\varepsilon) - 2i\,\mathrm{Im}\left\{G^{I}_{aa}\right\}$$

where, as we saw in Eq. (3.57)

$$\mathrm{Im}\left\{G^{I}_{aa}(\sqrt{s} + i\varepsilon)\right\} = -\frac{|\vec{p}_a|^I}{8\pi\sqrt{s}}, \tag{3.63}$$

and G^I_{aa} is given by Eq. (3.19). On the real axis $G(\sqrt{s}) = \lim_{\varepsilon \to 0} G^I(\sqrt{s} + i\varepsilon)$, which is compatible with the Feynman's prescription for obtaining physical amplitudes by attributing a small negative imaginary part to the mass of each particle in any internal line of a Feynman diagram. Then, for a complex energy z, we can write

$$G^{II}_{aa}(z) = G^{I}_{aa}(z) - 2i\,\mathrm{Im}\left\{G^{I}_{aa}(z)\right\}. \tag{3.64}$$

Bound states formed by the dynamics appear as poles of the T-matrix on the real axis and below the lowest threshold, i.e., in the first Riemann sheet of the lightest coupled channel. Unstable particles, i.e., those with a finite width, generated by the dynamics of the system appear as poles of the T-matrix in the second Riemann sheet.

A simple way to see this is by considering a Breit-Wigner form for the T-matrix

$$T \sim \frac{1}{s - M_R^2 + iM_R\Gamma_R}, \tag{3.65}$$

with M_R (Γ_R) being the mass (width) of the unstable particle formed, which is also called resonance. The decay width Γ_R is a function of the energy, particularly, of the center of mass momentum $|\vec{p}|$ of the system. In the first Riemann sheet, for complex values of s, the term $M_R\Gamma_R$ develops an imaginary part which has the same sign as the imaginary part of s. Thus, we can never have that the denominator of Eq. (3.65) becomes zero. Only in the unphysical or second Riemann sheet the imaginary part of s and that of $M_R\Gamma_R$ can be opposite and we can have a null denominator.

With this new definition of $G(\sqrt{s})$, we calculate the T-matrix in the complex energy plane. In Fig. 3.17 we show the modulus squared of the T-matrices related to $DK \to DK$ (left) and $D^*K \to D^*K$ (right) in isospin 0 in the complex energy plane. Poles at $\sqrt{s} = 2318 - i0$ MeV and $\sqrt{s} = 2450 - i0$ MeV are found, which correspond to the states $D_{s0}^*(2317)$ and $D_{s1}^*(2460)$, respectively [78].

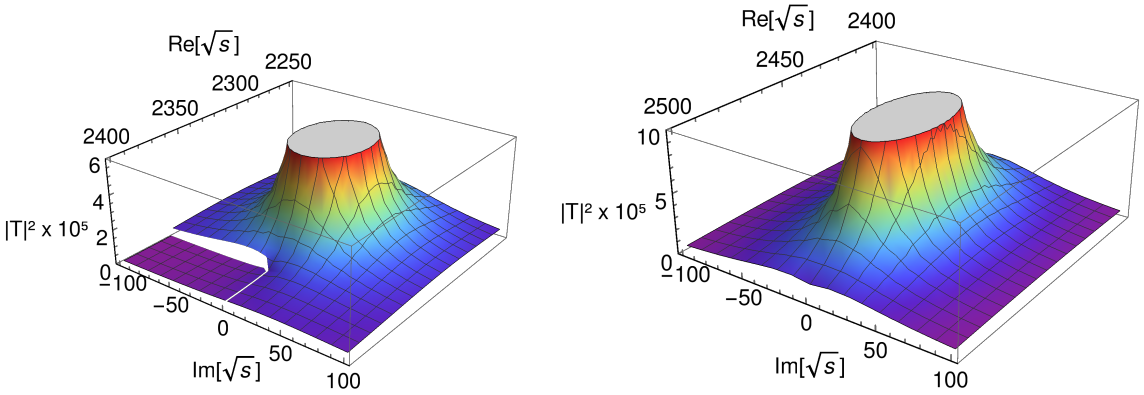

Figure 3.17: $|T^{I=0}_{DK\to DK}|^2$ (left) and $|T^{I=0}_{D^*K\to D^*K}|^2$ (right) in the complex energy plane within the HQ model. A pole at $\sqrt{s} = 2318 - i0$ MeV (left) and at $\sqrt{s} = 2450 - i0$ MeV (right) is found. These poles are related to the states $D_{s0}^*(2317)$ and $D_{s1}^*(2460)$, respectively.

In the next section we show the results obtained by using the SU(4) Lagrangian to determine the amplitudes V.

3.4.3 T-matrices obtained with the $SU(4)$ Lagrangian

We can also determine the amplitudes V for the DK and D^*K systems by using the Lagrangians shown in section 2.5.2, which are based on the $SU(4)$ symmetry with a particular way of breaking it. The results found for V are given in the Appendix B.

An example: $V_{D^0K^+\to D^0K^+}$

In this case, we have

$$\phi_3 = \begin{pmatrix} \bar{D}^0 \\ 0 \\ 0 \end{pmatrix}, \quad \phi_{\bar{3}} = \begin{pmatrix} D^0 & 0 & 0 \end{pmatrix}, \quad \phi_8 = \begin{pmatrix} 0 & 0 & K^+ \\ 0 & 0 & 0 \\ K^- & 0 & 0 \end{pmatrix}, \tag{3.66}$$

such that the Lagrangian of Eq. (2.101) reads

$$\begin{aligned} \mathscr{L}_{SU(4)} = \frac{1}{6f^2}\{&(\partial_\mu \bar{D}^0 D^0 - \bar{D}^0 \partial_\mu D^0)(\partial^\mu K^+ K^- - K^+ \partial^\mu K^-) \\ &+\gamma(\partial_\mu D^0 K^+ - D^0 \partial_\mu K^+)(\partial^\mu K^- \bar{D}^0 - K^- \partial^\mu \bar{D}^0)\}. \end{aligned} \tag{3.67}$$

Using the Feynman rules, we get, for the process $D^0(p_1)K^+(p_2) \to D^0(p_1')K^+(p_2')$, the following amplitude

$$V_{D^0K^+\to D^0K^+} = -\frac{1}{6f^2}\{(p_1'+p_1)(p_2+p_2') + \gamma(p_1-p_2)(p_2'-p_1')\}. \tag{3.68}$$

In terms of the Mandelstam variable

$$V_{D^0K^+\to D^0K^+} = -\frac{1}{6f^2}\{s-u+\gamma(t-s)+m_K^2+M_D^2\}. \tag{3.69}$$

This expression is further projected on s-wave, obtaining

$$V_{K^+D^0\to K^+D^0} = -\frac{1}{6f^2}\left[\frac{3s}{2} + \frac{(M_D^2-m_K^2)^2}{2s} - \gamma\left(\frac{3s}{2} + \frac{(M_D^2-m_K^2)^2}{2s} - M_D^2 - m_K^2\right)\right]. \tag{3.70}$$

As done in subsection 3.4.2, the loop functions are regularized using dimensional regularization and we consider the same subtraction as used in Ref. [43]: $\mu = 1500$ MeV, $a(\mu) = -1,5$.

In Fig. 3.18 we show the modulus squared of the T-matrix for $DK \to DK$ in isospin 0 (upper panel, left side) and isospin 1 (upper panel, right side) on the real axis. As in case of the results found in subsection 3.4.2, a peak around 2317 MeV is observed in

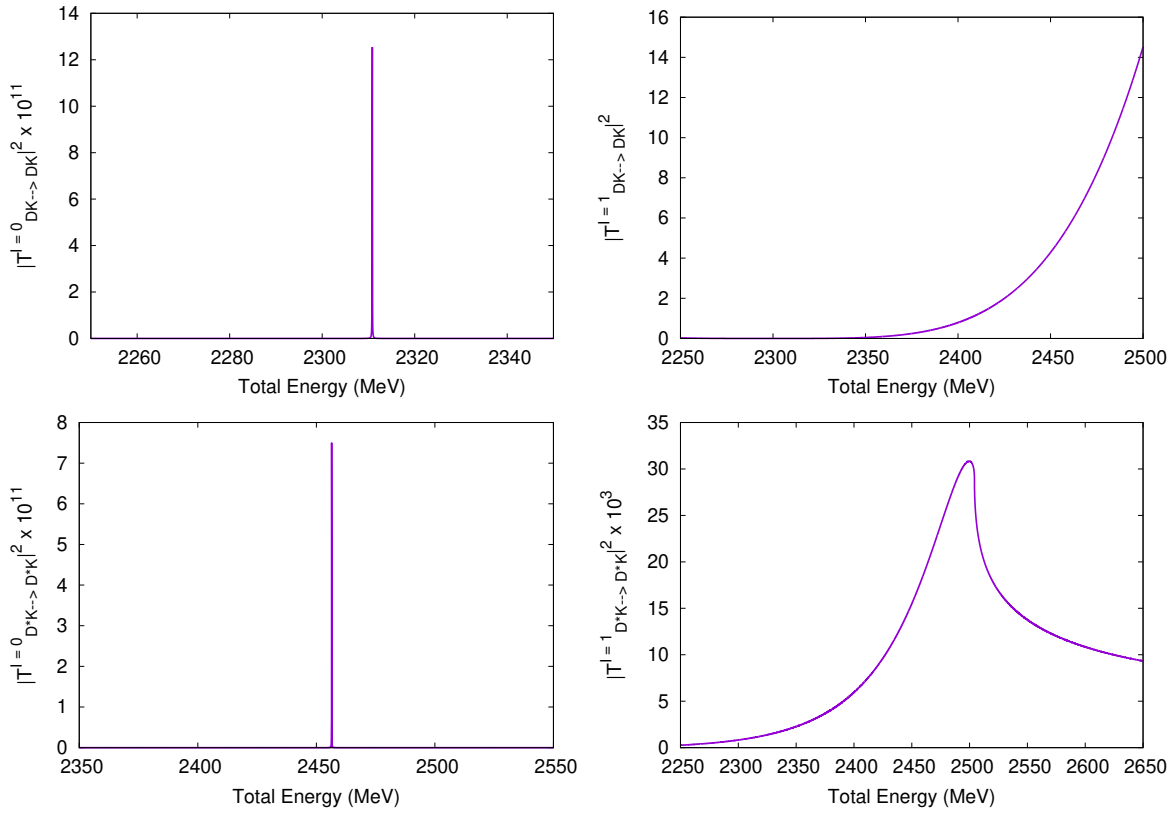

Figure 3.18: T-matrices determined by using the Lagrangian based on the $SU(4)$ symmetry. Upper panel: $|T_{DK\to DK}|^2$ for isospin 0 (left) and isospin 1 (right). Lower panel: $|T_{D^*K\to D^*K}|^2$ for isospin 0 (left) and isospin 1 (right).

the isospin 0, while the isospin 1 T-matrix does not show any structure. A pole in the complex energy plane is also formed for the isospin 0 case, which can be identified with the $D_{s0}^*(2317)$ [78].

As in case of the DK system, on the real axis, the modulus squared of the D^*K T-matrix in isospin 0 shows a peak at 2460 MeV with 0 width (see the lower panel, left side, of Fig. 3.18), while the isospin 1 T-matrix simply shows a cusp at the D^*K threshold (lower panel, right side).

In the complex energy plane, the T-matrices for the DK and D^*K systems in the isospin 0 configuration show the formation of poles which can be associated with $D_{s0}^*(2317)$ and $D_{s0}^*(2460)$, respectively (see Fig. 3.19).

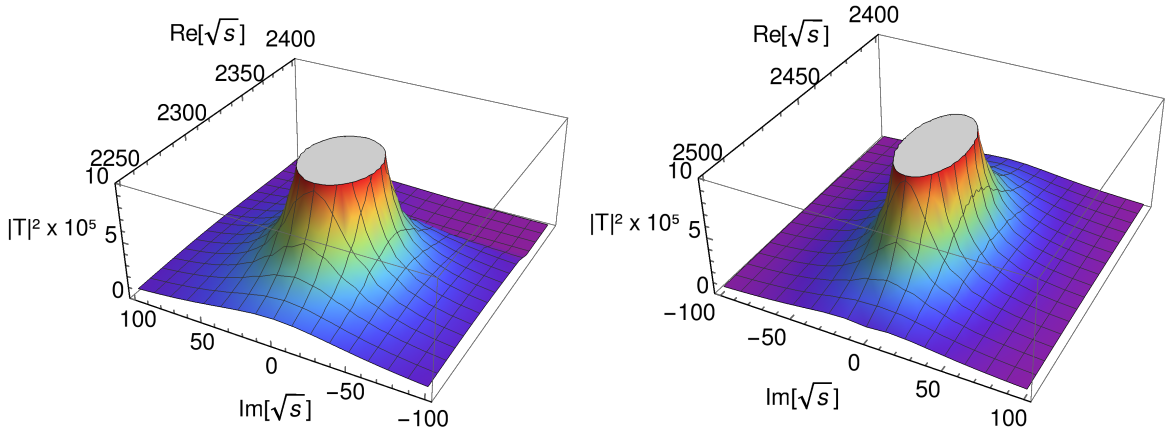

Figure 3.19: $|T^{I=0}_{DK\to DK}|^2$ (left) and $|T^{I=0}_{D^*K\to D^*K}|^2$ (right) in the complex energy plane within the $SU(4)$ model. A pole at $\sqrt{s} = 2318 - i0$ MeV (left) and at $\sqrt{s} = 2450 - i0$ MeV (right) is found. These poles are related to the states $D^*_{s0}(2317)$ and $D^*_{s1}(2460)$, respectively.

CHAPTER 4

Three-body Interactions and the $KD\bar{D}^*$ System

In the previous chapter we presented the formalism to determine the T-matrices describing the interaction between the DK and $\bar{D}^*K$ systems within a coupled channel approach. Using these results, we are now able to study the three-body system formed by $KD\bar{D}^*$ and investigate the possible formation of bound states or resonances as a consequence of the dynamics involved in the system.

4.1 The Faddeev equations

As in case of a two-body system, to investigate the generation of states in a three-body system we need to obtain the T-matrix for the system. To do this we can determine the different Feynman diagrams which can contribute to the scattering between three particles. If we label the particles involved as particles 1, 2 and 3, respectively, the simplest contribution to the scattering is the one where two of the particles interact and the other remains as a spectator. In Fig. 4.1 we show the corresponding diagrams. The blobs in Fig. 4.1 represent an infinite series of interactions between the particles involved [see Fig. 4.2]. In other words, t_1, t_2 and t_3 are the T-matrices obtained from the resolution of the Bethe-Salpeter equation computed in a coupled channel approach describing the interaction between the particles 2 and 3, 1 and 3, 1 and 2, respectively.

We can proceed further and continue adding interactions between the different pairs

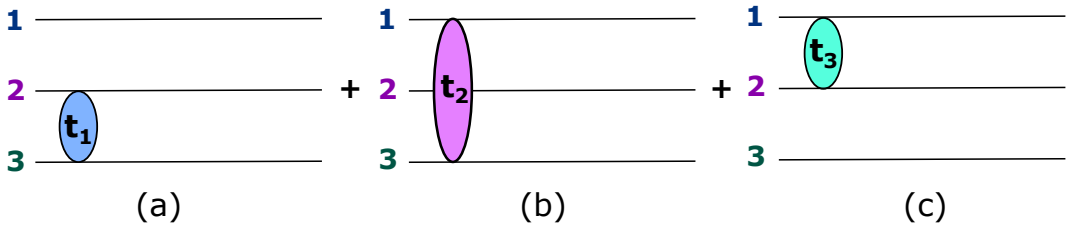

Figure 4.1: Diagrammatic representation of the simplest contributions to the scattering of 3 particles.

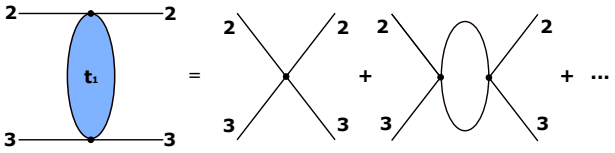

Figure 4.2: Diagrammatic representation of the Bethe-Salpeter equation for the scattering between particles 2 and 3.

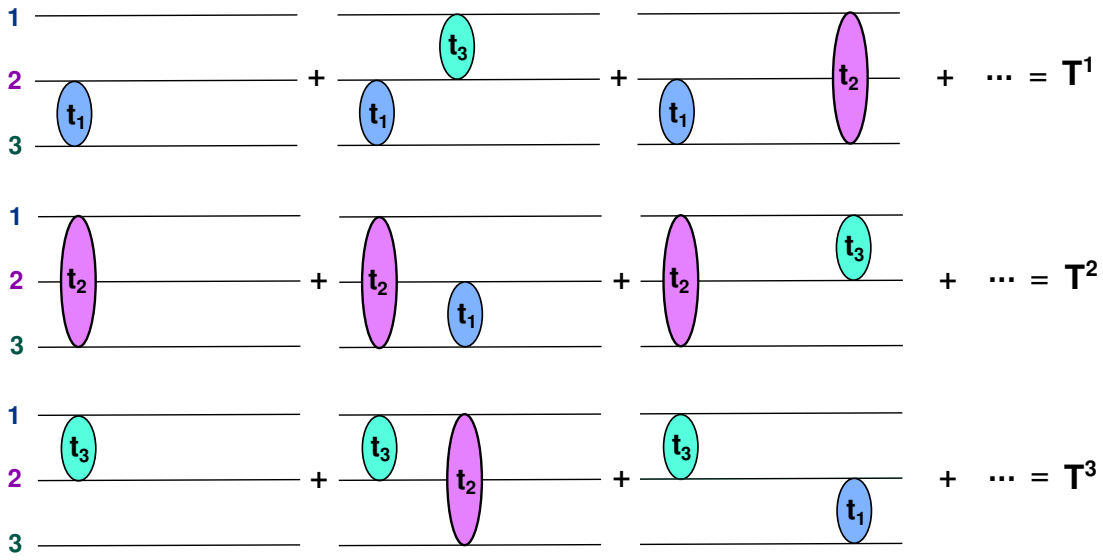

Figure 4.3: Diagrammatic representation of the interaction between three particles

of particles to the diagrams shown in Fig. 4.1 [see Fig. 4.3]. In this way, we get three series which can be written mathematically as

$$T_1 = t_1 + t_1 G[t_2 + t_2 G t_1 + \ldots] + t_1 G[t_3 + t_3 G t_1 + \ldots],$$

$$T_2 = t_2 + t_2 G[t_1 + t_1 G t_2 + \ldots] + t_2 G[t_3 + t_3 G t_2 + \ldots],$$

$$T_3 = t_3 + t_3 G[t_1 + t_1 G t_3 + \ldots] + t_3 G[t_2 + t_2 G t_3 + \ldots],$$

or, in a more compact form, as

$$\begin{aligned} T_1 &= t_1 + t_1 G [T_2 + T_3] , \\ T_2 &= t_2 + t_2 G [T_1 + T_3] , \\ T_3 &= t_3 + t_3 G [T_1 + T_2] , \end{aligned} \tag{4.1}$$

where G represents the Green function or propagator of the three particles. This set of coupled equations are the so called Faddeev equations [81]. These equations, as in case of the Bethe-Salpeter equations, are integral equations, but now, we have a set of integral coupled equations. An exact computation of the Faddeev equations [Eq. (4.1)], which is to obtain the T-matrix for the three-body system, i.e., $T = T_1 + T_2 + T_3$, is an extremely arduous task and, for practical calculations, it is customary to resort to some approximations applicable to a given system. In our case, we are going to consider the fixed center approximation (FCA) to solve Eq. (4.1).

4.2 Fixed center approximation to the Faddeev equations

Our goal is to obtain the T-matrix for the $KD\bar{D}^*$ system. This system has certain interesting characteristics which allows us to consider simplifications when dealing with Eq. (4.1): the $D\bar{D}^*$ interaction in s-wave is attractive in nature and it generates the $X(3872)$ in isospin 0 and the $Z_c(3900)$ in isospin 1 [43, 82–84]. Thus, when studying the $KD\bar{D}^*$ system we can consider that we have a kaon interacting with a cluster of two particles, $D\bar{D}^*$. And since the mass of the cluster formed is much bigger than that of the particle interacting with it, and we are interested in studying the three-body dynamics at low energies (very close to the three-body threshold), we can assume that the cluster remains unaltered during the scattering. In other words, D and $\bar{D}^*$ always cluster as $X(3872)$ or as $Z_c(3900)$. Then the whole scattering is analogous to the scattering of a particle by a fixed center of force.

Let us describe the scattering between a particle 3 and a cluster B formed by the particles 1 and 2. As done earlier, we start with the simplest contribution to the scattering, which is represented diagrammatically in Fig. 4.4. An analogous diagram will be the one where particle 3 interacts with particle 2, while particle 1 stays as a spectator.

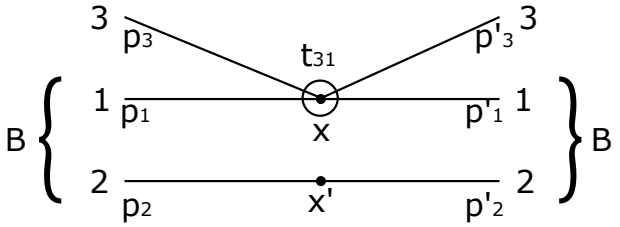

Figure 4.4: Diagrammatic representation of the $3+B \to 3+B$ scattering in which particle 3 interacts with particle 1 of the cluster.

In the following we will first obtain a mathematical description for the diagrams of a series where the first interaction is always between particles 3 and 1. Subsequently, we will write the expression for the other series of diagrams, where the first interaction is always between particles 3 and 2. Coming back to the diagram shown in Fig. 4.4, if we call $S^{(1)}$ to the contribution to the S-matrix of the process, we have

$$S^{(1)} = \frac{1}{V}\prod_{i=1}^{3}\sqrt{\frac{N_i}{2E_i}}\prod_{j=1}^{3}\sqrt{\frac{N_j}{2E'_j}}\Big[\int d^4x \int d^4x' e^{-i\left(p_3-p'_3+p_1-p'_1\right)x}\phi_1(\vec{x})\phi_2(\vec{x}\,')$$
$$\times e^{-i\left(p_2-p'_2\right)x'}\phi_1^*(\vec{x})\phi_2^*(\vec{x}\,')\Big](-it_{31}), \tag{4.2}$$

where N_i is a normalization factor (which is 1 for mesons and $2m_i$ for baryons of mass m_i), E_i (E'_j) represents the energy of the particle in the initial (final) state, and t_{31} describes the interaction between particles 3 and 1 at the vertex x. To write Eq. (4.2) we have considered a finite volume $V$and normalized the wave functions in this volume. In Eq. (4.2), $\phi_i(\vec{x})$ represents the wave function of the particle $i=1,2$ in the cluster B. Let us introduce the variables

$$\vec{R} = \frac{\vec{x}+\vec{x}\,'}{2}, \quad \vec{r} = \vec{x}-\vec{x}\,' \tag{4.3}$$

which represent the center of mass coordinate (for $m_1 \sim m_2$, as in our case) and the relative position between particles 1 and 2.

If we consider that particles 1 and 2 form a cluster of momentum $\vec{p}_B$ with wave function $\phi_B(\vec{r})$, we can use as ansatz for $\phi_1(\vec{x})\phi_2(\vec{x}\,')$ the expression

$$\phi_1(\vec{x})\phi_2(\vec{x}\,') = \frac{1}{\sqrt{V}}e^{-i\vec{p}_B\cdot\vec{R}}\phi_B(\vec{r}) \tag{4.4}$$

where we have separated the motion of the center of mass of the system from the relative motion of the particles in the cluster. By doing this, the integrations in d^3x and

d^3x' get replaced by integrations in d^3R and d^3r, whose contributions can be separated and we find

$$S^{(1)} = \frac{1}{V^2}\prod_{i=1}^{3}\sqrt{\frac{N_i}{2E_i}}\prod_{j=1}^{3}\sqrt{\frac{N_j}{2E'_j}}(2\pi)^4\delta^{(4)}\Big(\sum_{i=1}^{3}p_i-\sum_{j=1}^{3}p'_j\Big)(-it_{31})\,F_B\left(\frac{\vec{p}'_3-\vec{p}_3}{2}\right), \tag{4.5}$$

where

$$F_B\left(\frac{\vec{p}'_3-\vec{p}_3}{2}\right) = \int d^3r\, e^{-\frac{i}{2}(\vec{p}'_3-\vec{p}_3)\,\vec{r}}\,|\phi_B(\vec{r})|^2. \tag{4.6}$$

To get Eq. (4.6) we have considered that $\vec{p}_1 \sim \vec{p}'_1$ since $m_3 << m_1$. For scattering at low energies (around the threshold m_3+m_B), we can also approximate

$$F_B\left(\frac{\vec{p}'_3-\vec{p}_3}{2}\right) \sim F_B(0) = \int d^3r|\phi_B(\vec{r})|^2 = 1. \tag{4.7}$$

In this way, Eq. (4.5) can be written as

$$S^{(1)} = \frac{1}{V^2}\prod_{i=1}^{3}\sqrt{\frac{N_i}{2E_i}}\prod_{j=1}^{3}\sqrt{\frac{N_j}{2E'_j}}(2\pi)^4\delta^{(4)}\left(\sum_{i=1}^{3}p_i-\sum_{j=1}^{3}p'_j\right)(-it_{31}). \tag{4.8}$$

Let us consider the next contribution to the scattering, which we represented diagrammatically in Fig. 4.5, where the particle 3, after interacting with particle 1 of the cluster, propagates and interacts with particle 2 of the cluster. If we call $S^{(2)}$ to the

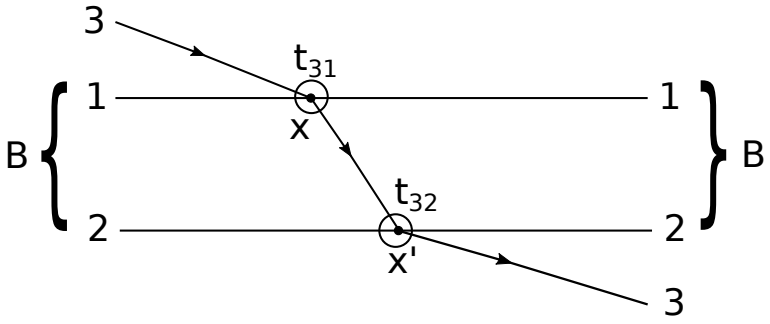

Figure 4.5: Diagrammatic representation of the scattering $3+B \to 3+B$ in which the particle 3 propagates in the cluster.

contribution to the S-matrix related to the diagram in Fig. 4.5, we have

$$\begin{aligned} S^{(2)} = \frac{1}{V}\prod_{i=1}^{3}\sqrt{\frac{N_i}{2E_i}}\prod_{j=1}^{3}\sqrt{\frac{N_j}{2E'_j}}\int d^4x\int d^4x' e^{-ip_3x}e^{-ip_1x}e^{ip'_1x}\phi_1(\vec{x})\phi_1^*(\vec{x}\,') \\ \times e^{-ip_2x'}e^{ip'_2x'}\phi_2(\vec{x}\,')\phi_2^*(\vec{x}\,')\int\frac{d^4q}{(2\pi)^4}i\frac{e^{iq(x-x')}}{q^2-m_3^2+i\varepsilon}(-it_{31})(-it_{32}), \end{aligned} \tag{4.9}$$

where t_{32} represents the interaction between particles 3 and 2 at the vertex x'. Writing $\int d^4x$ and $\int d^4x'$ as $\int dx^0\int d^3x$ and $\int dx'^0\int d^3x'$, respectively, using Eq. (4.4) and relating

$\int d^3x$ and $\int d^3x'$ to $\int d^3R$ and $\int d^3r$, we can write Eq. (4.9) as

$$S^{(2)} = -i\frac{(2\pi)^4}{V^2}\delta^4\left(\sum_{i=1}^{3} p_i - \sum_{j=1}^{3} p'_j\right)\prod_{i=1}^{3}\sqrt{\frac{N_i}{2E_i}}\prod_{j=1}^{3}\sqrt{\frac{N_j}{2E'_j}}t_{31}Gt_{32}, \tag{4.10}$$

where

$$G = \int \frac{d^3q}{(2\pi)^3}\frac{F_B(\vec{q})}{q^{0^2} - \vec{q}^2 - m_3^2 + i\varepsilon}, \tag{4.11}$$

with $q^0 = E'_3 + E'_2 - E_2$, represents the propagator of particle 3 in the cluster. The function $F_B(\vec{q})$, which is given by

$$F_B(\vec{q}) = \int d^3r e^{-i\vec{q}\cdot\vec{r}}|\phi_B(\vec{r})|^2, \tag{4.12}$$

as shown in Ref. [85], corresponds to a form factor associated with the cluster B and can be written in the momentum space as

$$F_B(\vec{q}) = \frac{1}{\mathcal{N}}\int d^3k \frac{\Theta(\Lambda - |\vec{k}|)}{E_B - E_1(\vec{k}) - E_2(\vec{k})}\frac{\Theta(\Lambda - |\vec{k} - \vec{q}|)}{E_B - E_1(\vec{k} - \vec{q}) - E_2(\vec{k} - \vec{q})}, \tag{4.13}$$

where $\mathcal{N}$ is a normalization factor such that $F_B(\vec{q} = \vec{0}) = 1$ and Θ represents the Heaviside Θ-function.

If we continue further, we can have contributions to the S-matrix from higher order diagrams (of the series) like those shown in Fig. 4.6, such that the S-matrix describing the interactions between particle 3 and the cluster constituted by particles 1 and 2 can be written as

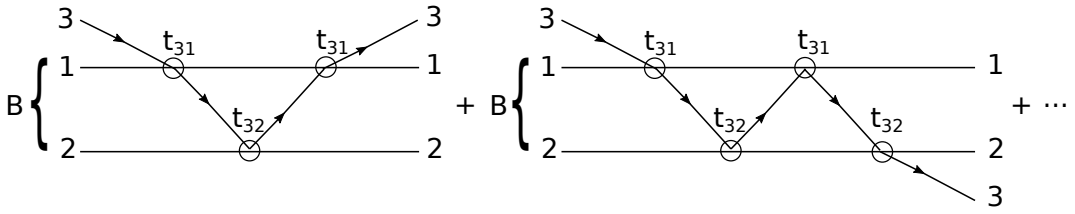

Figure 4.6: Other contributions to the scattering between particle 3 and the cluster B formed by particles 1 and 2.

$$S = S^{(0)} + S^{(1)} + S^{(2)} + \ldots \tag{4.14}$$

where $S^{(0)}$ represents the trivial case where there is no interactions at all, i.e.,

$$S^{(0)} = \delta_{\vec{p}_3,\vec{p}'_3}\delta_{\vec{p}_1,\vec{p}'_1}\delta_{\vec{p}_2,\vec{p}'_2}. \tag{4.15}$$

Then, we arrive to

$$S = \delta_{\vec{p}_3,\vec{p}'_3}\delta_{\vec{p}_1,\vec{p}'_1}\delta_{\vec{p}_2,\vec{p}'_2} - i\frac{(2\pi)^4}{V^2}\delta^4\left(\sum_{i=1}^{3} p_i - \sum_{j=1}^{3} p'_j\right)\prod_{i=1}^{3}\sqrt{\frac{N_i}{2E_i}}$$
$$\times\prod_{j=1}^{3}\sqrt{\frac{N_j}{2E'_j}}\left[t_{31} + t_{31}Gt_{32} + \ldots\right]. \tag{4.16}$$

In this way, the T-matrix related to the series of contributions which start with the interaction between particles 3 and 1 is given by

$$T_{31} = t_{31} + t_{31}Gt_{32} + t_{31}Gt_{32}Gt_{31} + \ldots \tag{4.17}$$

Similarly, as mentioned earlier, we can also have contributions to the scattering as those shown diagrammatically in Fig. 4.7, where particle 3 interacts first with particle 2 of the cluster and then rescatters. In this case, the T-matrix related to the process

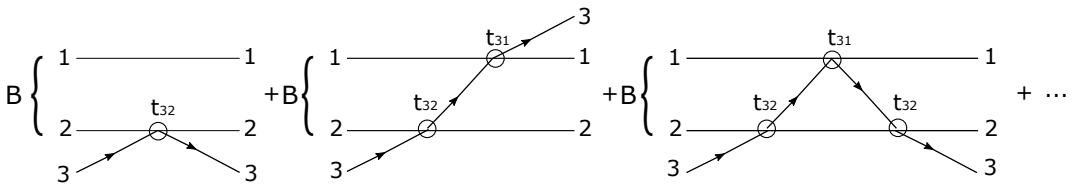

Figure 4.7: Contributions to the scattering between particle 3 and the cluster starting from the interaction between particle 3 and particle 2 of the cluster.

shown in Fig. 4.7 is given by

$$T_{32} = t_{32} + t_{32}Gt_{31} + t_{32}Gt_{31}Gt_{32} + \ldots \tag{4.18}$$

and the final T-matrix corresponds to the sum of T_{31} and T_{32}. Equations (4.17) and (4.18) can be written in a more compact form as a set of two coupled equations

$$T_{31} = t_{31} + t_{31}GT_{32},$$
$$T_{32} = t_{32} + t_{32}GT_{31}. \tag{4.19}$$

Since we are going to consider energies close to the threshold of the system, such that the representation of the scattering as a particle interacting with a cluster (which remains unperturbed) is meaningful, the particles in the triangular loops shown in Fig. 4.6 and 4.7 can not be too off-shell. In this way, we can approximate the two-body T-matrices involved in the triangular loops shown in Figs. 4.6 and 4.7 by the on-shell ones and factorize them outside the integration on the loop variable. By doing this, Eq. (4.19) becomes a set of algebraic coupled equations which can be easily solved.

A comment is here in order. For a process $3+B \to 3+B$, the S-matrix associated with it would be related to the T-matrix as

$$S_{3+B} = \delta_{\vec{p}_3,\vec{p}'_3}\delta_{\vec{p}_B,\vec{p}'_B} - i\frac{(2\pi)^4}{V^2}\delta^{(4)}\left(p_3+p_B-p'_3-p'_B\right) \times \sqrt{\frac{N_3}{2E_3}}\sqrt{\frac{N_B}{2E_B}}\sqrt{\frac{N_3}{2E'_3}}\sqrt{\frac{N_B}{2E'_B}}T_{3+B}, \tag{4.20}$$

which has a different normalization than the expression obtained in Eq. (4.16). This issue, which is related to the normalizations of the fields, can be solved by replacing

$$\begin{aligned} t_{31} \to \tilde{t}_{31} &= \sqrt{\frac{2E_B}{N_B}}\sqrt{\frac{2E'_B}{N_B}}\sqrt{\frac{2E_1}{N_1}}\sqrt{\frac{2E'_1}{N_1}}t_{31}, \\ t_{32} \to \tilde{t}_{32} &= \sqrt{\frac{2E_B}{N_B}}\sqrt{\frac{2E'_B}{N_B}}\sqrt{\frac{2E_2}{N_2}}\sqrt{\frac{2E'_2}{N_2}}t_{32}, \\ G \to \tilde{G} &= \sqrt{\frac{N_B}{2E_B}}\sqrt{\frac{N_B}{2E'_B}}G. \end{aligned} \tag{4.21}$$

Normalization factors in Eq. (4.21)

The contributions of the diagram in Fig. 4.4 to the S-matrix describing the interactions of particle 3 and the cluster B can be written as

$$\tilde{S}^{(1)} = -i\frac{(2\pi)^4}{V^2}\delta^{(4)}(p_3+p_B-p'_3-p'_B)\sqrt{\frac{N_3}{2E_3}}\sqrt{\frac{N_3}{2E'_3}}\sqrt{\frac{N_B}{2E_B}}\sqrt{\frac{NB3}{2E'_B}}\tilde{t}_{31}, \tag{4.22}$$

which is compatible with the expression found in Eq. (4.8) in terms of t_{31} as far as t_{31} and $\tilde{t}_{31}$ are related through Eq. (4.21). Similarly, for the contribution of the diagram in Fig. 4.5, we have

$$\tilde{S}^{(2)} = -i\frac{(2\pi)^4}{V^2}\delta^{(4)}(p_3+p_B-p'_3-p'_B)\sqrt{\frac{N_3}{2E_3}}\sqrt{\frac{N_3}{2E'_3}}\sqrt{\frac{N_B}{2E_B}}\sqrt{\frac{N_B}{2E'_B}}\tilde{t}_{31}\tilde{G}\tilde{t}_{32}, \tag{4.23}$$

which is compatible with the result obtained in Eq. (4.10).

In summary, we need to solve the coupled equations

$$\begin{aligned} \tilde{T}_{31} &= \tilde{t}_{31} + \tilde{t}_{31}\tilde{G}\tilde{T}_{32}, \\ \tilde{T}_{32} &= \tilde{t}_{32} + \tilde{t}_{32}\tilde{G}\tilde{T}_{31}, \end{aligned} \tag{4.24}$$

and determine the T-matrix for the scattering between particle 3 and a cluster B, which is formed as a consequence of the interaction between particles 1 and 2, as

$$\tilde{T} = \tilde{T}_{31} + \tilde{T}_{32}. \tag{4.25}$$

We are interested in calculating the T-matrix for the $KD\bar{D}^*$ system where the $D\bar{D}^*$ subsystem clusters as $X(3872)$ in isospin 0 or as $Z_c(3900)$ in isospin 1. In this way we can study the $KX(3872)$ and $KZ_c(3900)$ configurations of the $KD\bar{D}^*$ system. While the $KX(3872)$ system can only have total isospin $1/2$, the $KZ_c(3900)$ system can have total isospin $1/2$ and $3/2$. Thus, for total isospin $1/2$ we have two coupled channels, $KX(3872)$ and $KZ_c(3900)$, while in total isospin $3/2$ we have only one channel. The $\tilde{t}_{31}$, $\tilde{t}_{32}$ and $\tilde{G}$ in Eq. (4.24) are then matrices in the coupled channel space

$$\tilde{t}_{31} = \begin{bmatrix} (\tilde{t}_{31})_{11} & (\tilde{t}_{31})_{12} \\ (\tilde{t}_{31})_{21} & (\tilde{t}_{31})_{22} \end{bmatrix}, \quad \tilde{t}_{32} = \begin{bmatrix} (\tilde{t}_{32})_{11} & (\tilde{t}_{32})_{12} \\ (\tilde{t}_{32})_{21} & (\tilde{t}_{32})_{22} \end{bmatrix},$$
$$\tilde{G} = \begin{bmatrix} (\tilde{G})_{11} & 0 \\ 0 & (\tilde{G})_{22} \end{bmatrix}. \tag{4.26}$$

The element (11) in the above equations represents the $KX \to KX$ transition, the element (12) $KX \to KZ$, and so on and so forth. The elements $(\tilde{t}_{31})_{11}$, $(\tilde{t}_{31})_{12}$, etc., are given in terms of the two-body T-matrices of the KD and $K\bar{D}^*$ subsystems in the isospin base and we calculate them in the next section.

4.3 Determination of the $\tilde{t}_{31}$ and $\tilde{t}_{32}$ two-body T-matrices

To calculate $(\tilde{t}_{31})_{11}$ we need first to write the state $|KX(3872)\rangle$ with total isospin $I = 1/2$ and third isospin component, for example, $I_3 = 1/2$, which we represent as $\left|KX;\frac{1}{2},\frac{1}{2}\right\rangle$, and then determine

$$\left\langle KX;\frac{1}{2},\frac{1}{2}\right| t_{31} \left|KX;\frac{1}{2},\frac{1}{2}\right\rangle. \tag{4.27}$$

The state $\left|KX;\frac{1}{2},\frac{1}{2}\right\rangle$ is deduced as

$$\begin{aligned} \left|KX;\frac{1}{2},\frac{1}{2}\right\rangle &= \left|K^+;\frac{1}{2},\frac{1}{2}\right\rangle \otimes |D\bar{D}^*;0,0\rangle \\ &= \left|I_3^K = \frac{1}{2}\right\rangle \otimes \frac{1}{\sqrt{2}}\left[\left|I_3^D = \frac{1}{2}, I_3^{\bar{D}^*} = -\frac{1}{2}\right\rangle - \left|I_3^D = -\frac{1}{2}, I_3^{\bar{D}^*} = \frac{1}{2}\right\rangle\right], \end{aligned} \tag{4.28}$$

where we have used the Clebsch-Gordan coefficients to write the state $|D\bar{D}^*;0,0\rangle$ in terms of the states $\left|I_3^D, I_3^{\bar{D}^*}\right\rangle$. Since the $\tilde{t}_{31}$ two-body T-matrix describes the interaction between particles 3 and 1 of the cluster, which in this case correspond to the K and D,

respectively, it is convenient to write Eq. (4.28) in terms of the total isospin of the KD system. Using once more the Clebsch-Gordan coefficients, we can write

$$\left|KX;\frac{1}{2},\frac{1}{2}\right\rangle = \left[\left|I^{KD}=1,I_3^{KD}=1\right\rangle\otimes\left|I_3^{\bar{D}^*}=-\frac{1}{2}\right\rangle - \frac{1}{\sqrt{2}}\left(\left|I^{KD}=1,I_3^{KD}=0\right\rangle+\left|I^{KD}=0,I_3^{KD}=0\right\rangle\right)\otimes\left|I_3^{\bar{D}^*}=\frac{1}{2}\right\rangle\right]. \quad (4.29)$$

Further, using Eqs. (4.27) and (4.29), we get

$$\begin{aligned}\left\langle KX;\frac{1}{2},\frac{1}{2}\right|t_{31}\left|KX;\frac{1}{2},\frac{1}{2}\right\rangle &= \frac{1}{2}\Bigg[\left\langle I^{KD}=1,I_3^{KD}=1\right|t_{31}\left|I^{KD}=1,I_3^{KD}=1\right\rangle \\ &+\frac{1}{2}\Bigg(\left\langle I^{KD}=1,I_3^{KD}=0\right|t_{31}\left|I^{KD}=1,I_3^{KD}=0\right\rangle \\ &+\left\langle I^{KD}=0,I_3^{KD}=0\right|t_{31}\left|I^{KD}=0,I_3^{KD}=0\right\rangle\Bigg)\Bigg] = \frac{1}{2}\left[t_{KD}^{I=1}+\frac{1}{2}\left(t_{KD}^{I=1}+t_{KD}^{I=0}\right)\right] \\ &= \frac{1}{4}(3t_{KD}^{I=1}+t_{KD}^{I=0}),\end{aligned}$$

with t_{KD}^{I} being the two-body T-matrix for the KD system in a given isospin I. Using this result and Eq. (4.21) we have

$$(\tilde{t}_{31})_{11} = \frac{M_X}{4m_D}(3t_{KD}^{I=1}+t_{KD}^{I=0}), \quad (4.30)$$

where we have used the non-relativistic approximation of $E_X \sim M_X$ and $E_D \sim m_D$, which is valid since we are interested in energies close to the threshold of the KX system.

Similarly, to calculate $(\tilde{t}_{32})_{11}$ we need to write the state in Eq. (4.28) in terms of the isospin of the $K\bar{D}^*$ system by using Clebsch-Gordan coefficients. The result found for $(\tilde{t}_{32})_{11}$ is analogous to the one in Eq. (4.30) and can be obtained by replacing $t_{KD}^{I=1}\to t_{K\bar{D}^*}^{I=1}$ and $t_{KD}^{I=0}\to t_{K\bar{D}^*}^{I=0}$ as

$$(\tilde{t}_{32})_{11} = \frac{M_X}{4m_D}(3t_{K\bar{D}^*}^{I=1}+t_{K\bar{D}^*}^{I=0}). \quad (4.31)$$

We can also obtain now the $\left|KZ_c;\frac{1}{2},\frac{1}{2}\right\rangle$ state and evaluate the rest of elements in Eq. (4.26). The results obtained can be written in a compact form by introducing the vectors

$$\vec{t}_{\,31} = \left(t_{KD}^{I=1},t_{KD}^{I=0}\right), \quad \vec{t}_{\,32} = \left(t_{K\bar{D}^*}^{I=1},t_{K\bar{D}^*}^{I=0}\right),$$

such that

$$\begin{aligned}(t_{31})_{ij} &= \vec{\omega}_{31}^{\,i\to j}\cdot\vec{t}_{\,31}, \\ (t_{32})_{ij} &= \vec{\omega}_{32}^{\,i\to j}\cdot\vec{t}_{\,32},\end{aligned} \quad (4.32)$$

Table 4.1: Vector $\vec{\omega}_{31}^{i\to j}$ appearing in Eq. (4.32) for total isospin $1/2$ and for the transition $i \to j$. The vector $\vec{\omega}_{32}^{i\to j} = a\vec{\omega}_{31}^{i\to j}$ where $a = 1$ (-1) for $i = j$ $(i \neq j)$.

	KX	KZ
KX	$\frac{1}{4}(3,1)$	$\frac{\sqrt{3}}{4}(1,-1)$
KZ	$\frac{\sqrt{3}}{4}(1,-1)$	$\frac{1}{4}(1,3)$

where the vectors $\vec{\omega}_{31}^{i\to j}$ and $\vec{\omega}_{32}^{i\to j}$ are given in Table 4.1.

Before proceeding further, a comment regarding $Z_c(3900)$ is here in order. The nature of $Z_c(3900)$ is still under debate. Experimental investigations seem to report two states with $J^P = 1^+$ around 3900 MeV, $Z_c(3900)$ [86–88] and $Z_c(3885)$ [89, 90]. It is still not clear if these states are two different ones or are the same. The lattice investigations [91–93], on the other hand, do not seem to find an evidence for the existence of a molecular state around 3900 MeV. However, the analysis made in Ref. [94] shows that the lattice data is compatible with the existence of the $Z_c(3900)$ resonance. Further, the latest experimental investigations continue to find signals of a state with mass near 3900 MeV in different processes, such as B-decays [95], $\eta_c\rho$ invariant mass spectra [96], etc. In spite of the debate, both experimental and theoretical investigations indicate that the $D\bar{D}^*$ interaction in isospin 1, spin-parity 1^+ is attractive in nature and produces a peak in the cross sections of the relevant processes. In our study, the $Z_c(3900)$ we refer to is the state arising from the $D\bar{D}^*$ and coupled channel dynamics found in Ref. [46].

4.4 Results

In Fig. 4.8 we show the results for the modulus squared of the T-matrix for the $KX \to KX$ transition, T_{XX}, for total isospin $1/2$, as a function of the center of mass energy. The left (right) panel corresponds to the results obtained by using the HQ [$SU(4)$] Lagrangian when solving the Bethe-Salpeter equation to determine the input $\tilde{t}_{31}$ and $\tilde{t}_{32}$. In both cases, to begin with, we do not consider KZ_c as a coupled channel to KX in the isospin $1/2$ configuration. As can be seen, in both HQ and $SU(4)$ approaches, a peak around 4307 MeV with zero width is found as a consequence of the dynamics involved in the system. In Fig. 4.8 we also show the dependence of the results with the cut-off Λ by varying it in the range 700 - 750 MeV. This cut-off is necessary to regularize the loop integral appearing in Eq. (4.11).

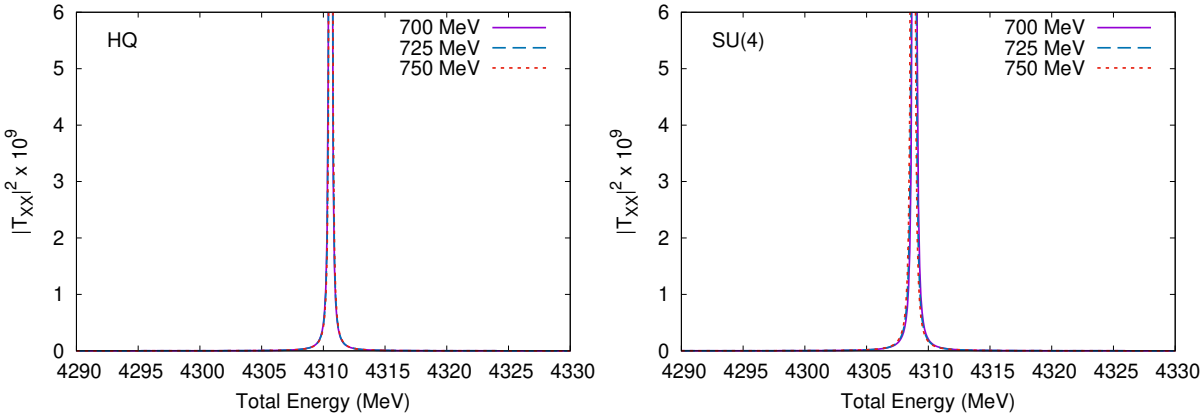

Figure 4.8: Modulus squared of the T_{XX} matrix as a function of the total energy in the center of mass frame. (Left side) Results found describing the interaction in the two-body subsystems by means of an effective Lagrangian based on heavy-quark symmetry. (Right side) In this case, we use the $SU(4)$ symmetry and a particular way of breaking it instead of the heavy-quark symmetry to obtain the T-matrices related to the two-body subsystems.

In Fig. 4.9 we show the results found for the modulus squared of the T-matrix related to the $KZ_c \to KZ_c$ transition, T_{ZZ}, within both approaches, i.e., the one based on the heavy-quark symmetry (left side) and the one based on the $SU(4)$ symmetry (right side), as a function of the center of mass energy. These results are obtained by disconsidering the width (for the time being) for $Z_c(3900)$, which is around 28 MeV [97]. As can be seen, in both cases, a bound state around 4307 MeV is formed. The width of the $Z_c(3900)$ can

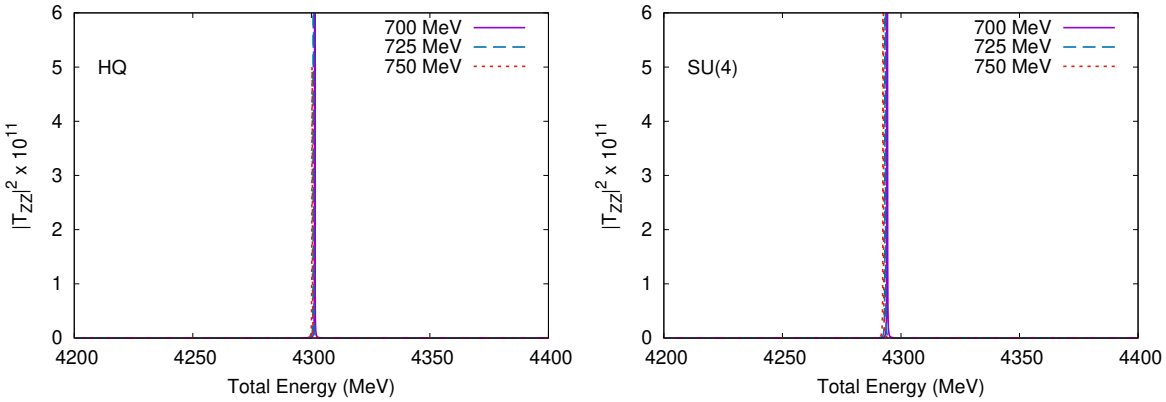

Figure 4.9: Same as in Fig. 4.8 but for the $KZ_c \to KZ_c$ transition.

be incorporated in our formalism by substituting in Eq. (4.13) $E_B \to E_B - i\frac{\Gamma_B}{2}$, where Γ_B is the width related to the cluster formed. The results obtained are shown in Fig. 4.10.

We can now couple the KX and KZ_c systems and find how the results change as compared to those shown in Figs. 4.8 and 4.10. In Fig. 4.11 we show the results found

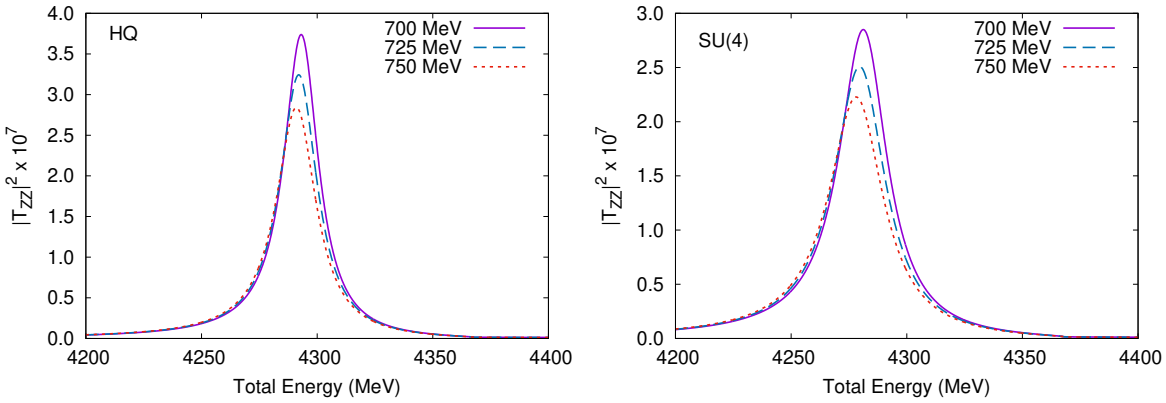

Figure 4.10: Same as in Fig. 4.9 but considering $\Gamma_z = 28$ MeV.

by considering the coupled channel dynamics. As can be seen, a peak around 4307 MeV continues to appear with a width around 18 MeV as a consequence of the incorporation of the Γ_Z in our calculation.

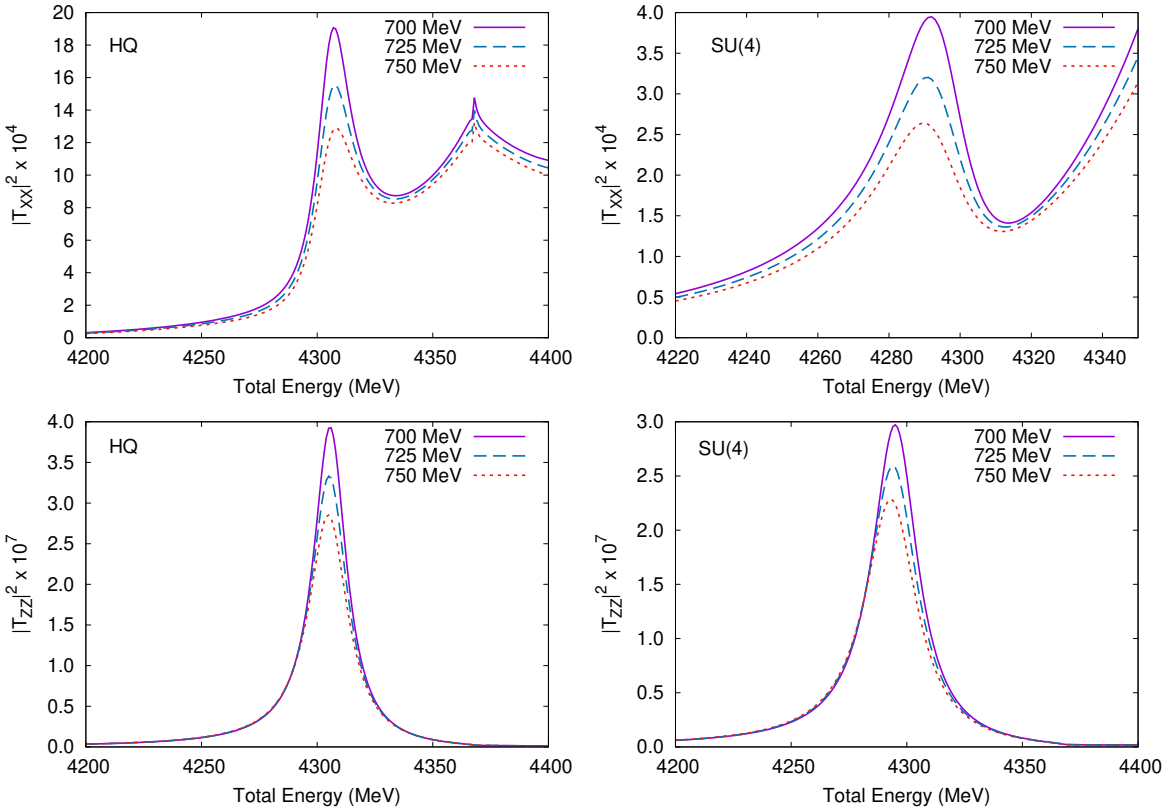

Figure 4.11: Results found for $|T_{XX}|^2$ (top) and $|T_{ZZ}|^2$ (bottom) as a function of the center of mass energy. (Left) Results obtained with the HQ approach. (Right) Results found with the $SU(4)$ approach.

In this way, we find that the dynamics involved in the $KD\bar{D}^*$ system compels the generation of a state with mass around 4307 MeV and width of 18 MeV with essentially $KX(3872)$ and $KZ_c(3900)$ components in its wave-function. This state has a hidden

charm, isospin $1/2$, strangeness $+1$ and spin-parity 1^-. Thus, it can be identified as a K^* meson. The mass and quantum numbers of the state invoke a clear non quark-antiquark structure for it. So far, according to the PDG [97], the last excited state of a K/K^* meson corresponds to the $K(3100)$. Thus, the results found constitute a prediction for a K^* state with hidden charm and mass around 4307 MeV and should serve as a motivation for conducting experimental investigations of this state. Having this in mind, in the next chapter we investigate the two-body decay mechanisms of this state.

For the sake of completeness, we must mention that in the total isospin $3/2$ no state is obtained, as can be seen in Fig. 4.12

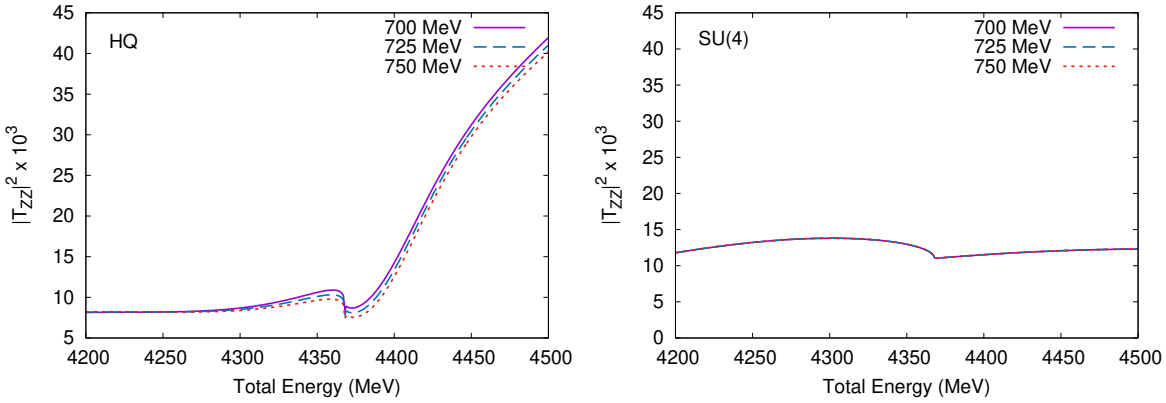

Figure 4.12: Results found for $|T_{ZZ}|^2$ as a function of the center of mass energy. (Left) Results obtained with the HQ approach. (Right) Results found with the $SU(4)$ approach.

Finally, to end the chapter, we can say that the formation of a K^*-state is found within two different models considered in our work, thus, making the claim for the existence of such a state more robust. Although one of the models is based on the $SU(4)$ symmetry, which could be thought to be less reliable than the HQ model, even if a symmetry breaking mechanism has been taking into account, the main conclusions continue to be the same. Indeed, as can be seen in Fig. 4.11, based on the magnitude of the three-body T-matrices, the KZ_c dynamics dominates the formation of the $K^*(4307)$, and, this happens in both models. Also, the $KZ_c \to KZ_c$ amplitude within the two models [HQ and $SU(4)$] is similar, which would result in compatible findings for observables like cross sections, decay widths, etc. This is the reason for which in the next chapter, where we calculate further properties of the $K^*(4307)$, we will restrict the discussion to the HQ model.

CHAPTER 5

On the two-body decay widths of $K^*(4307)$

In the previous chapter, we showed that a K^* resonance with hidden charm content arises from the $KD\bar{D}^*$ dynamics, where the $D\bar{D}^*$ system is treated as $Z_c(3900)$ in the isospin 1 configuration or as $X(3872)$ in the isospin 0. With the motivation of determining its further properties, which can be observed in experiments, we now present a calculation of the decay processes of this K^*, denoted as $K^*(4307)$, to two-body channels. To be more specific, we consider the decay channels $J/\psi K^*(892)$, $\bar{D}D_s$, $\bar{D}D_s^*$ and $\bar{D}^*D_s^*$.

The mechanisms of the decay to these channels involve triangular loops and are a consequence of the internal structure of the state. Thus, the values found for the decay widths of the proposed $K^*(4307)$ are related to its nature and should be valuable and motivating for an experimental investigation of the $K^*(4307)$.

5.1 Theoretical framework

As we have seen in the previous chapter, the re-scattering of a kaon with the D and $\bar{D}^*$, which cluster to form $X(3872)$ in the isospin 0 and $Z_c(3900)$ in the isospin 1, generates a $I(J^P) = 1/2\ (1^-)$ K^* state with a mass around 4307 MeV, which is below the $KD\bar{D}^*$ threshold, thus, it is a bound state [29]. When considering the width of $Z_c(3900)$, which is around 28 MeV, a width close to 18 MeV is found for the $K^*(4307)$ state. A K^* state with such an internal structure can naturally decay to three-body channels, like $J/\psi\pi K$,

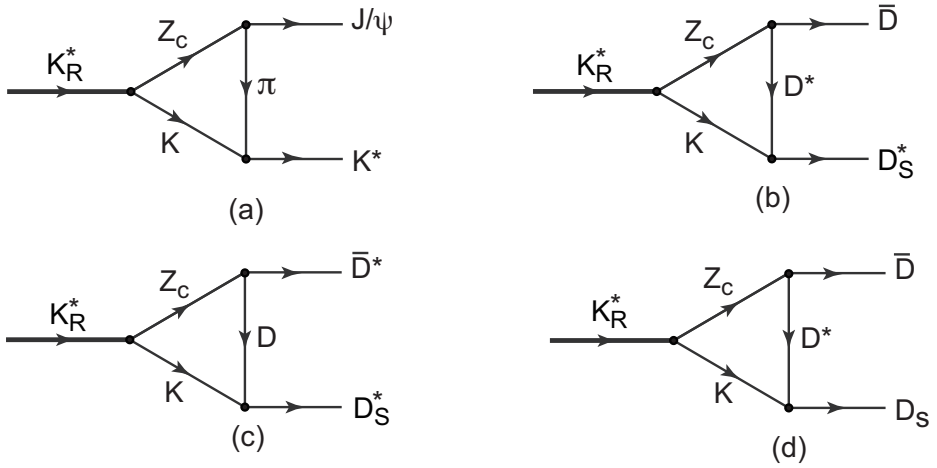

Figure 5.1: Main two-body decay channels for the K_R^* state found.

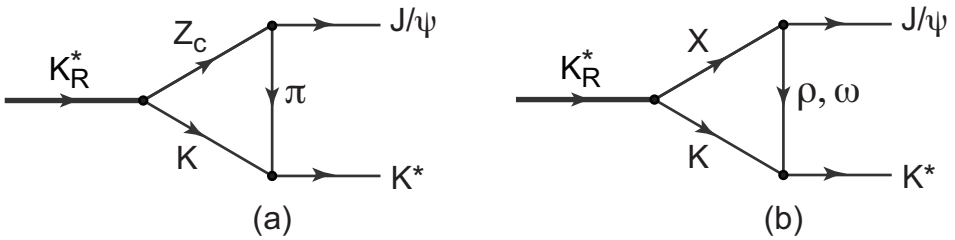

Figure 5.2: Decay mechanism of K_R^* to the $J/\psi K^*$ channel. The vertex $X \to J/\psi\rho\ (\omega)$ on the diagram (b) involves yet another triangular loop, as shown in Fig. 5.3.

since the state itself is obtained as a consequence of the three-body dynamics involved in the $KD\bar{D}^*$ system. However, it can also decay to two-body channels. In this latter case, due to the nature found for $K^*(4307)$, such a decay mechanism can proceed through triangular loops and we can have as main decay channels $J/\psi K^*(892)$, $\bar{D}D_s^*$, $\bar{D}^*D_s^*$, and $\bar{D}D_s$ (see Fig. 5.1). In order to avoid confusion between $K^*(4307)$ and $K^*(892)$ and to simplify the notation, we shall, henceforth, denote the former as K_R^* and the latter as K^*.

From the results of the T-matrices shown in the previous chapter, and considering a Breit-Wigner form for them, the coupling of K_R^* to $KZ_c(3900)$ is around 4 times bigger than that to $KX(3872)$. Thus, for calculating the decay width of K_R^* (which is proportional to the squared coupling of K_R^* to KZ_c or KX), the contribution arising from the diagram shown in Fig. 5.2(b) is negligible when compared to the one coming from the diagram in Fig. 5.2(a). On top of that, for the decay process $K_R^* \to J/\psi K^*$, the vertex $X \to J/\psi\rho(\omega)$ shown in Fig. 5.2(b) involves yet another triangular loop [98] (see Fig. 5.3) and such a vertex produces a contribution much smaller than that of the vertices $Z_c \to J/\psi\pi$, $\bar{D}D^*$,

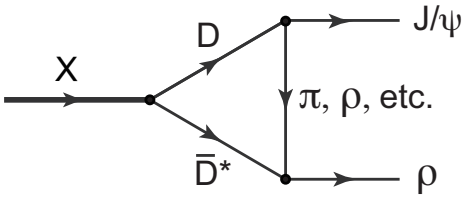

Figure 5.3: Decay mechanism of X to the $J/\psi\rho$ channel in an approach in which X is obtained from the $D\bar{D}^*$ interaction [98].

$\bar{D}^*D$, since $Z_c(3900)$ couples directly to $J/\psi\pi$, $\bar{D}D^* - $c.c (where c.c means complex conjugate) [46], at the tree level. It is also interesting to notice that, with the internal structure found for K_R^*, the decay process $K_R^* \to \bar{D}^*D_s$ could also be contemplated, but it would involve a three pseudoscalar vertex (see Fig. 5.4), resulting in a null amplitude.

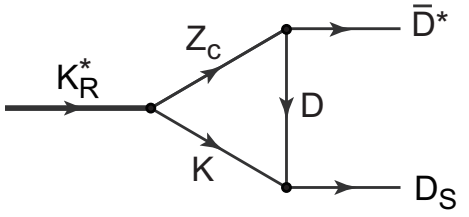

Figure 5.4: Decay process of K_R^* into the $\bar{D}^*D_s$ channel.

5.1.1 Determination of the vertices

Let us start evaluating the contribution arising from the diagrams shown in Fig. 5.1. Considering the decay of a neutral K_R^{*0} into a J/ψ and a K^0, we have two diagrams contributing to each of the processes shown in Fig. 5.1: in one of the diagrams, the primary vertex is $K_R^{*0} \to K^0 Z_c^0$ while in the other it is the vertex $K^{*0} \to K^+ Z_c^-$. We illustrate these two contributions in Fig. 5.5 for the decay process $K_R^{*0} \to J/\psi K^{*0}$.

To evaluate these diagrams, we need several vertices involving vector and pseudoscalar mesons. The contribution for the $K_R^* \to KZ_c$ vertices in Fig. 5.5 can be written

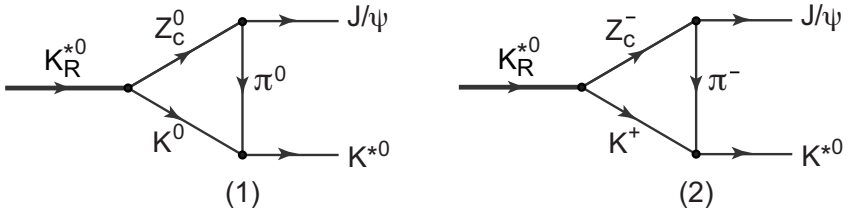

Figure 5.5: Contributions related to the diagram (a) of Fig. 5.1 for the decay mechanism $K_R^{*0} \to J/\psi K^{*0}$.

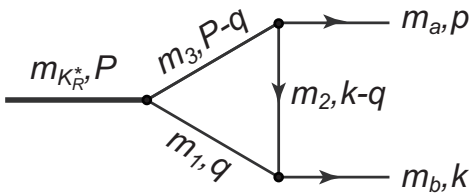

Figure 5.6: Momenta and mass assignment in the decay process of the K_R^* state.

in terms of the polarization vectors $\varepsilon^{\mu}_{K_R^*}$ and $\varepsilon^{\mu}_{Z_c}$ associated with the vector mesons K_R^* and Z_c, respectively, and the coupling of K_R^* to the $KZ_c(3900)$ channel as

$$\begin{aligned} t_{K_R^{*0}\to K^0 Z_c^0} &= g_{K_R^{*0}\to K^0 Z_c^0}\,\varepsilon_{K_R^{*0}}(P)\cdot\varepsilon_{Z_c^0}(P-q), \\ t_{K_R^{*0}\to K^+ Z_c^-} &= g_{K_R^{*0}\to K^+ Z_c^-}\,\varepsilon_{K_R^{*0}}(P)\cdot\varepsilon_{Z_c^-}(P-q), \end{aligned} \tag{5.1}$$

where the four momenta and masses assigned to the particles are as shown in Fig. 5.6. The couplings $g_{K_R^{*0}\to K^0 Z_c^0}$ and $g_{K_R^{*0}\to K^+ Z_c^-}$ in Eq. (5.1) can be obtained from the isospin 1/2 scattering matrix, $T_{(KZ_c)_{\frac{1}{2}}}$, determined in the previous chapter. To do this, we consider, a Breit-Wigner expression for this T-matrix in an energy region around the mass $m_{K_R^*}$ of the state, i.e.,

$$T_{(KZ_c)_{\frac{1}{2}}} \simeq \frac{g^2_{K_R^*\to(KZ_c)_{\frac{1}{2}}}}{s - M^2_{K_R^*} + iM_{K_R^*}\Gamma_{K_R^*}}\,\vec{\varepsilon}_{Z_c}\cdot\vec{\varepsilon}_{Z_c} \equiv \tilde{T}_{Z_cK}\,\vec{\varepsilon}_{Z_c}\cdot\vec{\varepsilon}_{Z_c}, \tag{5.2}$$

and we can get $g_{K_R^*\to(KZ_c)_{\frac{1}{2}}}$, i.e., the coupling of K_R^* to the isospin 1/2 state KZ_c, from the residue of $T_{(KZc)_{\frac{1}{2}}}$ at the pole position in the complex energy plane. Alternatively, since the decay width of K_R^* is proportional to $|g_{K_R^*\to(KZ_c)_{\frac{1}{2}}}|^2$, we can estimate such a value directly from Eq. (5.2), by considering the limit $s \to M^2_{K_R^*}$ [99]

$$|g_{K_R^*\to(KZ_c)_{\frac{1}{2}}}| = \left|\sqrt{iM_{K_R^*}\Gamma_{K_R^*}\tilde{T}_{(KZ_c)_{\frac{1}{2}}}}\right| \simeq 22143 \text{ MeV}. \tag{5.3}$$

Once we have the value of $g_{K_R^*\to(KZ_c)_{\frac{1}{2}}}$, the couplings $g_{K_R^{*0}\to K^0 Z_c^0}$ and $g_{K_R^{*0}\to K^+ Z_c^-}$ can be related to $g_{K_R^*\to(KZ_c)_{\frac{1}{2}}}$ by using the fact that

$$|KZ_c; I=\frac{1}{2}, I_3=-\frac{1}{2}\rangle = -\frac{1}{\sqrt{3}}|K^0 Z_c^0\rangle + \sqrt{\frac{2}{3}}|K^+ Z_c^-\rangle, \tag{5.4}$$

where we use the phase convention $|K^-\rangle = -|\frac{1}{2}, -\frac{1}{2}\rangle$. In this way, from Eq. (5.4),

$$\begin{aligned} g_{K_R^{*0}\to K^0 Z_c^0} &= -\frac{1}{\sqrt{3}} g_{K_R^*\to(KZ_c)_{\frac{1}{2}}}, \\ g_{K_R^{*0}\to K^+ Z_c^-} &= \sqrt{\frac{2}{3}} g_{K_R^*\to(KZ_c)_{\frac{1}{2}}}. \end{aligned} \tag{5.5}$$

Using isospin average masses for the particles belonging to the same isospin multiplet and Eq. (5.5), we can write Eq. (5.1) as

$$t_{K_R^*\to KZ_c} = C_{KZ_c}\, g_{K_R^*\to (KZ_c)_{\frac{1}{2}}}\, \varepsilon_{K_R^*}(P)\cdot\varepsilon_{Z_c}(P-q), \tag{5.6}$$

with

$$C_{KZ_c} = \begin{cases} -1/\sqrt{3} & \text{for } K_R^{*0}\to K^0 Z_c^0, \\ \sqrt{2/3} & \text{for } K_R^{*0}\to K^+ Z_c^-. \end{cases} \tag{5.7}$$

Next, we need the vertices $Z_c\to J/\psi\pi$, $\bar{D}D^*$, $\bar{D}^*D$ for different charge combinations. As shown in Ref. [46], a state with mass around 3872 MeV and 30 MeV of width is generated from the dynamics present in the $D\bar{D}^*+$c.c. (c.c. means complex conjugate) and $J/\psi\pi$ coupled channel system in isospin 1 and positive G-parity. This state can be related to $Z_c(3900)$ [46].

Following the approach of Ref. [46], we can write

$$\begin{aligned} t_{Z_c\to J/\psi\pi} &= C_{J/\psi\pi} g_{Z_c\to (J/\psi\pi)_1}\, \varepsilon_{Z_c}(P-q)\cdot\varepsilon_{J/\psi}(p), \\ t_{Z_c\to \bar{D}D^*} &= C_{\bar{D}D^*} g_{Z_c\to (\bar{D}D^*)_1}\, \varepsilon_{Z_c}(P-q)\cdot\varepsilon_{D^*}(p), \\ t_{Z_c\to \bar{D}^*D} &= C_{\bar{D}^*D} g_{Z_c\to (\bar{D}D^*)_1}\, \varepsilon_{Z_c}(P-q)\cdot\varepsilon_{\bar{D}^*}(p), \end{aligned} \tag{5.8}$$

where we have defined

$$g_{Z_c\to(\bar{D}D^*)_1} = \frac{1}{\sqrt{2}} g_{Z_c\to\frac{1}{\sqrt{2}}[(\bar{D}D^*)_1+\text{c.c}]}. \tag{5.9}$$

The subscript 1 in the above equation indicates the total isospin of the $\bar{D}D^*$ system. The $C_{\bar{D}D^*}$ and $C_{\bar{D}^*D}$ coefficients in Eq. (5.8), which relate the Z_c state to the $\bar{D}D^*$ and $D\bar{D}^*$ states in the charge basis, are given by

$$C_{\bar{D}D^*(\bar{D}^*D)} = \begin{cases} 1, & \text{for } Z_c^+\to \bar{D}^0 D^{*+}\,(\bar{D}^{*0}D^+), \\ 1/\sqrt{2}, & \text{for } Z_c^0\to D^- D^{*+}\,(D^{*-}D^+), \\ -1/\sqrt{2}, & \text{for } Z_c^0\to \bar{D}^0 D^{*0}\,(\bar{D}^{*0}D^0), \\ -1, & \text{for } Z_c^-\to D^- D^{*0}\,(D^{*-}D^0), \end{cases} \tag{5.10}$$

where we have used the isospin phase convention $|D^{*0}\rangle = -|\frac{1}{2},-\frac{1}{2}\rangle$ and $|D^0\rangle = -|\frac{1}{2},-\frac{1}{2}\rangle$. In case of pions, we follow the isospin phase convention $|\pi^+\rangle = -|1,1\rangle$. In this way, $C_{J/\psi\pi}=1$ for the processes $Z_c^0\to J/\psi\pi^0$ and $Z_c^-\to J/\psi\pi^-$.

The couplings in Eq. (5.8) can be obtained from the residue of the isospin 1 two-body scattering matrix determined in Ref. [46] in the complex energy plane. We have calculated them and obtain

$$|g_{Z_c\to(J/\psi\pi)_1}| \simeq 3715 \text{ MeV}, \quad |g_{Z_c\to\frac{1}{\sqrt{2}}[(\bar{D}D^*)_1+\text{c.c.}]}| \simeq 8149 \text{ MeV}. \tag{5.11}$$

Other vertices needed to evaluate the contribution of the diagrams shown in Fig. 5.1 are $K\pi \to K^*$, $D^*K \to D_s$ and $DK \to D_s^*$. To determine these contributions, we use the effective Lagrangian $\mathscr{L}_{PPV}$ [64, 100] involving two pseudoscalars and a vector meson

$$\mathscr{L}_{PPV} = -ig\langle V^\mu [P, \partial_\mu P]\rangle, \tag{5.12}$$

with V^μ and P being matrices containing the corresponding vectors and pseudoscalar fields,

$$V_\mu = \begin{pmatrix} \frac{\omega+\rho^0}{\sqrt{2}} & \rho^+ & K^{*+} & \bar{D}^{*0} \\ \rho^- & \frac{\omega-\rho^0}{\sqrt{2}} & K^{*0} & D^{*-} \\ K^{*-} & \bar{K}^{*0} & \phi & D_s^{*-} \\ D^{*0} & D^{*+} & D_s^{*+} & J/\psi \end{pmatrix}_\mu ,$$

$$P = \begin{pmatrix} \frac{\eta}{\sqrt{3}} + \frac{\eta'}{\sqrt{6}} + \frac{\pi^0}{\sqrt{2}} & \pi^+ & K^+ & \bar{D}^0 \\ \pi^- & \frac{\eta}{\sqrt{3}} + \frac{\eta'}{\sqrt{6}} - \frac{\pi^0}{\sqrt{2}} & K^0 & D^- \\ K^- & \bar{K}^0 & -\frac{\eta}{\sqrt{3}} + \sqrt{\frac{2}{3}}\eta' & D_s^- \\ D^0 & D^+ & D_s^+ & \eta_c \end{pmatrix}, \tag{5.13}$$

respectively. The coupling g in Eq. (5.12) is given by $m_V/(2f_\pi) \simeq 4.41$, with $m_V \simeq 815$ MeV being an average mass for the vector mesons ρ, ω and K^* and $f_\pi = 92.4$ MeV being the pion decay constant. While this value of the coupling produces a theoretical width of the K^{*+} meson, which comes basically from the decay processes $K^{*+} \to K^0\pi^+$, $K^+\pi^0$, compatible with the experimental result, it underestimates the width of the D^{*+} meson, obtained from the processes $D^{*+} \to D^0\pi^+$, $D^+\pi^0$. In this latter case, as shown in Ref. [101], arguments based on the heavy quark symmetry establish that $g \to m_{D^*}g/m_{K^*} \simeq 9.9$ when using the Lagrangian in Eq. (5.12) for describing processes involving heavy pseudoscalar and vector mesons. Having this in mind and using Eq. (5.12), we get the

following amplitudes for the above mentioned vertices

$$\begin{aligned} t_{K\pi\to K^*} &= -2C_{K\pi}\, g_L\, q\cdot\varepsilon_{K^*}(k), \\ t_{KD\to D_s^*} &= -2C_{KD}\, g_H\, q\cdot\varepsilon_{D_s^*}(k), \\ t_{KD^*\to D_s} &= C_{KD^*}\, g_H\, (k+q)\cdot\varepsilon_{D_s^*}(k-q). \end{aligned} \tag{5.14}$$

In the above equations, $g_L = 4.41$ and $g_H = 9.9$, and the coefficients $C_{K\pi}$, C_{KD} and C_{KD^*} are given by

$$C_{K\pi} = \begin{cases} 1/\sqrt{2}, & \text{for } K^0\pi^0 \to K^{*0}, \\ -1, & \text{for } K^+\pi^- \to K^{*0}, \end{cases} \tag{5.15}$$

$$C_{KD\,(KD^*)} = \begin{cases} -1, & \text{for } K^+D^0 \to D_s^{*+}\ (K^+D^{*0} \to D_s^+), \\ -1, & \text{for } K^0D^+ \to D_s^{*+}\ (K^0D^{*+} \to D_s^+). \end{cases} \tag{5.16}$$

The last vertex whose contribution needs to be determined corresponds to $D^*K \to D_s^*$. To do this, we consider the effective Lagrangian $\mathscr{L}_{VVP}$ [64,102] involving two vectors and a pseudoscalar meson

$$\mathscr{L}_{VVP} = \frac{G'}{\sqrt{2}}\varepsilon^{\mu\nu\alpha\beta}\langle\partial_\mu V_\nu \partial_\alpha V_\beta P\rangle, \tag{5.17}$$

where the coupling G' is given by $\frac{3g'^2}{4\pi^2 f_\pi}$ with $g' = -\frac{M_\rho}{2f_\pi} = -4.14$. Using Eq. (5.17), we can write

$$t_{KD^*\to D_s^*} = C_{KD^*}G'\,\varepsilon^{\mu\nu\alpha\beta}\,(k-q)_\mu\, k_\alpha\, \varepsilon_{D^*,\nu}(k-q)\,\varepsilon_{D_s^*,\beta}(k), \tag{5.18}$$

with

$$C_{KD^*} = \begin{cases} -\frac{1}{\sqrt{2}}, & \text{for } K^+D^{*0} \to D_s^{*+}, \\ -\frac{1}{\sqrt{2}}, & \text{for } K^0D^{*+} \to D_s^{*+}. \end{cases} \tag{5.19}$$

5.1.2 Triangular loops

Once we have all the vertices associated with the decay mechanisms of K_R^*, we can evaluate the contributions related to the diagrams in Fig. 5.1. We start with the process shown in Fig. 5.1(a) and the two Feynman diagrams shown in Fig. 5.5 (for the K_R^{*0} decay). Using the vertices given in Eqs. (5.1), (5.8), (5.14), the corresponding amplitude

can be written as,

$$
\begin{aligned}
t_a = t_a^{(1)} + t_a^{(2)} &= i\sqrt{6}\, g_{K_R^*\to(KZ_c)_{\frac{1}{2}}}\, g_{Z_c\to(J/\psi\pi)_1}\, g_L\, \varepsilon^{\mu}_{K_R^*}(P)\, \varepsilon^{\nu}_{J/\psi}(p)\, \varepsilon^{\alpha}_{K^*}(k) \\
&\times \int \frac{d^4q}{(2\pi)^4} \frac{\left(-g^{\mu\nu} + \frac{(P-q)^\mu (P-q)^\nu}{m_{Z_c}^2}\right) q^\alpha}{(q^2 - m_K^2 + i\varepsilon)[(k-q)^2 - m_\pi^2 + i\varepsilon][(P-q)^2 - m_{Z_c}^2 + i\varepsilon]} \\
&= i\sqrt{6}\, g_{K_R^*\to(KZ_c)_{\frac{1}{2}}}\, g_{Z_c\to(J/\psi\pi)_1}\, g_L\, \varepsilon^{\mu}_{K_R^*}(P)\, \varepsilon^{\nu}_{J/\psi}(p)\, \varepsilon^{\alpha}_{K^*}(k) \\
&\times \left[-g_{\mu\nu} I^1_\alpha - \frac{P_\nu}{m_{Z_c}^2} I^2_{\mu\alpha} + \frac{1}{m_{Z_c}^2} I^3_{\mu\nu\alpha} \right],
\end{aligned}
\tag{5.20}
$$

where we have introduced the three tensor integrals $I^1_\alpha, I^2_{\mu\nu}, I^3_{\mu\nu\alpha}$, which are defined as

$$
I^N_{\mu_1\mu_2,\ldots,\mu_N} = \int \frac{d^4q}{(2\pi)^4} \frac{q_{\mu_1} q_{\mu_2} \cdots q_{\mu_N}}{(q^2 - m_1^2 + i\varepsilon)[(k-q)^2 - m_2^2 + i\varepsilon][(P-q)^2 - m_3^2 + i\varepsilon]}, \tag{5.21}
$$

with m_1, m_2 and m_3 being the masses of the particles in the triangular loops shown in Fig. 5.1 (see Fig. 5.6 for the corresponding four momenta labels).

Based on the Lorentz covariance, Eq. (5.21) can be written in terms of the external momentum P and k. In particular, we have

$$
\begin{aligned}
I^1_\alpha &= a^1_1 P_\alpha + a^1_2 k_\alpha, \\
I^2_{\mu\alpha} &= a^2_1 g_{\mu\alpha} + a^2_2 P_\mu P_\alpha + a^2_3 (P_\mu k_\alpha + k_\mu P_\alpha) + a^2_4 k_\mu k_\alpha, \\
I^3_{\mu\nu\alpha} &= a^3_1 (g_{\mu\nu} P_\alpha + g_{\mu\alpha} P_\nu + g_{\nu\alpha} P_\mu) + a^3_2 (g_{\mu\nu} k_\alpha + g_{\mu\alpha} k_\nu + g_{\nu\alpha} k_\mu) \\
&\quad + a^3_3 P_\mu P_\nu P_\alpha + a^3_4 (P_\mu P_\nu k_\alpha + P_\mu k_\nu P_\alpha + k_\mu P_\nu P_\alpha) \\
&\quad + a^3_5 k_\mu k_\nu k_\alpha + a^3_6 (k_\mu k_\nu P_\alpha + k_\mu P_\nu k_\alpha + P_\mu k_\nu k_\alpha),
\end{aligned}
\tag{5.22}
$$

which correspond to the standard Passarino-Veltman decomposition for tensor integrals [103]. The coefficients a^i_j are scalars to be determined. Considering the Lorenz gauge and using $P = p + k$, the amplitude t_a in Eq. (5.20) can be further simplified to

$$
\begin{aligned}
t_a = i\sqrt{6} m_{Z_c}^2\, g_{K_R^*\to(KZ_c)_{\frac{1}{2}}}\, g_{Z_c\to(J/\psi\pi)_1}\, g_L \Big[&(-m_{Z_c}^2 a^1_1 + a^3_1) \varepsilon_{K_R^*}(P) \cdot \varepsilon_{J/\psi}(p)\, p \cdot \varepsilon_{K^*}(k) \\
&+ (-a^2_1 + a^3_1 + a^3_2) \varepsilon_{K_R^*}(P) \cdot \varepsilon_{K^*}(k)\, k \cdot \varepsilon_{J/\psi}(p) + a^3_2 k \cdot \varepsilon_{K_R^*}(P)\, \varepsilon_{J/\psi}(p) \cdot \varepsilon_{K^*}(k) \\
&+ (-a^2_3 + a^3_4 + a^3_6) k \cdot \varepsilon_{K_R^*}(P)\, k \cdot \varepsilon_{J/\psi}(p)\, p \cdot \varepsilon_{K^*}(k) \Big],
\end{aligned}
\tag{5.23}
$$

and we need to determine seven coefficients, a^1_1, a^2_1, a^2_3, a^3_1, a^3_2, a^3_4, and a^3_6. To do this, the way of proceeding is: first, by using Eq. (5.22), we can contract the expressions in Eq. (5.22) with the different Lorentz structures present there and get a system of coupled

equations which can be solved. For example, from the expression of I^1_α in Eq. (5.22), we have

$$\begin{aligned} P\cdot I^1 &= a^1_1 P^2 + a^1_2 P\cdot k, \\ k\cdot I^1 &= a^1_1 k\cdot P + a^1_2 k^2. \end{aligned} \tag{5.24}$$

By solving this system of coupled equations, we can write a^1_1 as

$$a^1_1 = \frac{k^2(\mathbb{PI}^1) - (k\cdot P)(\mathbb{KI}^1)}{k^2P^2 - (k\cdot P)^2}, \tag{5.25}$$

where

$$\mathbb{PI}^1 \equiv P^\mu I^1_\mu, \quad \mathbb{KI}^1 \equiv k^\mu I^1_\mu, \quad \mathbb{GI}^2 \equiv g^{\mu\alpha} I^2_{\mu\alpha}. \tag{5.26}$$

Equation (5.25) clearly shows that the a^i_j coefficients depend on the mass of the decaying particle, $m_{K^*_R}$, the masses of the particles in the loops, m_1, m_2 and m_3, and the masses m_a and m_b of the particles to which K^*_R can decay (see Fig. 5.6). For all the diagrams shown in Fig. 5.1, $m_1 = m_K$ and $m_3 = m_{Z_c}$, and for the particular case of the diagram in Fig. 5.1(a), $m_2 = m_\pi$, $m_a = m_{J/\psi}$ and $m_b = m_{K^*}$. The next step consists in calculating the Lorentz scalar terms appearing in Eq. (5.26) directly from the definition in Eq. (5.21). For example, using Eq. (5.21), $\mathbb{PI}^1$ is given by

$$\mathbb{PI}^1 = \int \frac{dq^0}{2\pi} \int \frac{d^3q}{(2\pi)^3} \frac{P^0 q^0}{(q^{0^2} - \omega_1^2 + i\varepsilon)[(k^0-q^0)^2 - \omega_2^2 + i\varepsilon][(P^0-q^0)^2 - \omega_3^2 + i\varepsilon]}, \tag{5.27}$$

with

$$\omega_1 = \sqrt{\vec{q}^{\,2} + m_1^2}, \quad \omega_2 = \sqrt{(\vec{k}-\vec{q})^2 + m_2^2}, \quad \omega_3 = \sqrt{\vec{q}^{\,2} + m_3^2}, \tag{5.28}$$

where we have used the rest frame of the decaying particle, for which $P^\mu = (P^0, \vec{0}) = (m_{K^*_R}, \vec{0})$ and

$$k^0 = \frac{P^{0^2} - m_a^2 + m_b^2}{2P^0}, \quad |\vec{k}| = \frac{\lambda^{1/2}(P^{0^2}, m_a^2, m_b^2)}{2P^0}. \tag{5.29}$$

Next, we can use the Cauchy's theorem to determine the q^0 integration of Eq. (5.27), and we get

$$\begin{aligned} \mathbb{PI}^1 = -i \int \frac{d^3q}{(2\pi)^3} P^0\omega_1 \Big\{ & -k^{0^2}P^0\omega_2 + k^0\omega_3[(\omega_1+\omega_3)(\omega_1+2\omega_2+\omega_3) - P^{0^2}] \\ & + P^0\omega_2(\omega_1+\omega_2)(\omega_1+\omega_2+2\omega_3)\Big\} \frac{1}{2\,\omega_1\,\omega_2\,\omega_3\,(k^0+\omega_1+\omega_2)} \\ & \times \frac{1}{P^0+\omega_1+\omega_3} \frac{1}{\omega_1 - k^0 + \omega_2 - i\varepsilon} \frac{1}{\omega_1 - P^0 + \omega_3 - i\varepsilon} \\ & \times \frac{1}{k^0 - P^0 + \omega_2 + \omega_3 - i\varepsilon} \frac{1}{P^0 - k^0 + \omega_3 + \omega_2 - i\varepsilon}. \end{aligned} \tag{5.30}$$

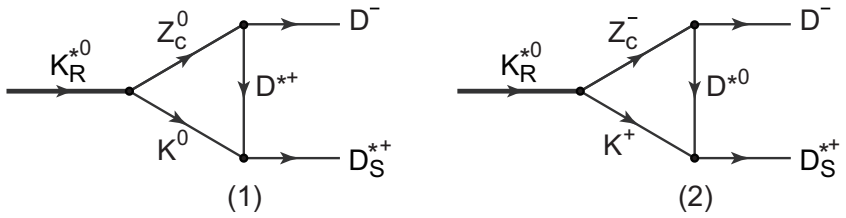

Figure 5.7: Contributions associated with the diagram (b) of Fig. 5.1 for the decay mechanism $K_R^{*0} \to D^- D_s^{*+}$.

Similarly, we can continue with the evaluation of the other a_j^i coefficients of Eq. (5.23). The results are given in the appendix C. Note that some of these a_j^i coefficients, after performing the integration on the q^0 variable, involve integrals in d^3q which are divergent. In such a case, we regularize the corresponding integral by introducing a cutoff $\Lambda = 700$ MeV, which corresponds to the value used in the previous chapter (and in Ref. [29]) to study the generation of the resonance K_R^* from the three-body $KD\bar{D}^*$ system. It is also interesting to notice that for the cases in which the d^3q integration does not involve divergences, the upper limit for such integration is also naturally provided [104], in this case, by the value of the cut-off used when regularizing the two-body loops involved in the generation of the Z_c state from the interaction of $D\bar{D}^*$ and coupled channels, and which is also $\sim$700 MeV [46]. In any case, as in the previous chapter, we vary this value of the cut-off and estimate the error induced by it in our final results.

Let us consider now the decay mechanism shown in Fig. 5.1(b) and the two Feynman diagrams contributing to it, which are shown in Fig. 5.7. In this case, considering Eqs. (5.1), (5.8) and (5.18), the amplitude describing the process is given by

$$\begin{aligned} t_b = t_b^{(1)} + t_b^{(2)} &= i\frac{\sqrt{3}}{2} g_{K_R^* \to (KZ_c)_{\frac{1}{2}}} g_{Z_c \to (\bar{D}D^*)_1} G' \, \varepsilon^{\mu}_{K_R^*}(P) \, \varepsilon_{D_s^*,\beta}(k) \\ &\times \int \frac{d^4q}{(2\pi)^4} \left(-g^{\mu\nu} + \frac{(P-q)^\mu (P-q)^\nu}{m_{Z_c}^2} \right) \left(-g_{\nu\lambda} + \frac{(k-q)_\nu (k-q)_\lambda}{m_{D^*}^2} \right) \\ &\times \frac{\varepsilon^{\sigma\lambda\alpha\beta} \, (k-q)_\sigma \, k_\alpha}{(q^2 - m_K^2 + i\varepsilon)[(k-q)^2 - m_{D^*}^2 + i\varepsilon][(P-q)^2 - m_{Z_c}^2 + i\varepsilon]} \\ &= i\frac{\sqrt{3}}{2} g_{K_R^* \to (KZ_c)_{\frac{1}{2}}} g_{Z_c \to (\bar{D}D^*)_1} G' \, \varepsilon^{\mu}_{K_R^*}(P) \, \varepsilon_{D_s^*,\beta}(k) \, \varepsilon^{\sigma\lambda\alpha\beta} \left[g_{\mu\lambda} k_\alpha I_\sigma^1 + \frac{1}{M_{Zc}^2} P_\lambda k_\alpha I_{\mu\sigma}^2 \right], \end{aligned} \quad (5.31)$$

where the Lorenz gauge and the antisymmetric properties of the Levi-Civita tensor have been used to get the last line. Using the decomposition in Eq. (5.22) and considering once again the antisymmetric properties of the Levi-Civita tensor, Eq. (5.31) can be

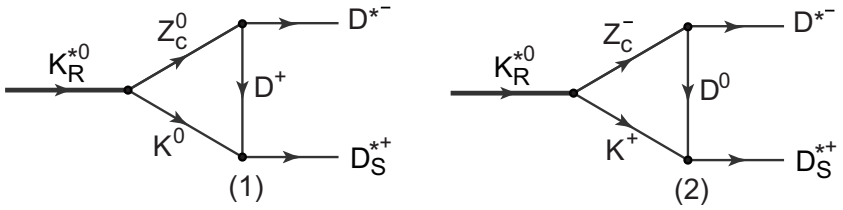

Figure 5.8: Contributions associated with the diagram (c) of Fig. 5.1 for the decay mechanism $K_R^{*0} \to D^{*-} D_s^{*+}$.

written as

$$t_b = i\frac{\sqrt{3}}{2} g_{K_R^* \to (KZ_c)_{\frac{1}{2}}} g_{Z_c \to (\bar{D}D^*)_1} G' \, \varepsilon^{\mu}_{K_R^*}(P) \, \varepsilon_{D_s^*,\beta}(k) \, \varepsilon^{\sigma\lambda\alpha\beta} \left[g_{\mu\lambda} P_\sigma a_1^1 + \frac{1}{M_{Zc}^2} P_\lambda g_{\mu\sigma} a_1^2 \right] k_\alpha, \tag{5.32}$$

where the coefficient a_1^1 can be obtained from Eq. (5.25), where now, from Fig. 5.1(b), $m_3 = m_{D^*}$, $m_a = m_{\bar{D}}$, $m_b = m_{D_s^*}$, and the expression for a_1^2 can be found in the appendix C.

Next, we continue with the evaluation of the process depicted in Fig. 5.1(c). In this case, considering the diagrams shown in Fig. 5.8 and using the results in Eqs. (5.1), (5.8), (5.14), the amplitude associated with such decay mechanism reads as

$$\begin{aligned} t_c = t_c^{(1)} + t_c^{(2)} &= -i\sqrt{6} g_{K_R^* \to (KZ_c)_{\frac{1}{2}}} g_{Z_c \to (\bar{D}D^*)_1} g_H \, \varepsilon^{\mu}_{K_R^*}(P) \, \varepsilon^{\mu}_{\bar{D}^*}(P-k) \, \varepsilon^{\alpha}_{D_s^*}(k) \\ &\times \int \frac{d^4q}{(2\pi)^4} \frac{\left(-g_{\mu\nu} + \frac{(P-q)_\mu (P-q)_\nu}{m_{Z_c}^2} \right) q_\alpha}{(q^2 - m_K^2 + i\varepsilon)[(k-q)^2 - m_D^2 + i\varepsilon][(P-q)^2 - m_{Z_c}^2 + i\varepsilon]} \\ &= -i\sqrt{6} g_{K_R^* \to (KZ_c)_{\frac{1}{2}}} g_{Z_c \to (\bar{D}D^*)_1} g_H \, \varepsilon^{\mu}_{K_R^*}(P) \, \varepsilon^{\nu}_{\bar{D}^*}(P-k) \, \varepsilon^{\alpha}_{D_s^*}(k) \\ &\times \left[-g_{\mu\nu} I_\alpha^1 - \frac{1}{m_{Z_c}^2} P_\nu I_{\mu\alpha}^2 + \frac{1}{m_{Z_c}^2} I_{\mu\nu\alpha}^3 \right]. \end{aligned} \tag{5.33}$$

Note that the above expression is analogous (up to a phase) to the expression of t_a in Eq. (5.20) changing $g_L \to g_H$, $J/\psi \to \bar{D}^*$, $\pi \to D$, $K^* \to D_s^*$ in the couplings and in the products of four momenta, i.e., we have now $m_2 = m_D$ (instead of m_π), $m_a = m_{\bar{D}^*}$ (instead of $m_{J/\psi}$) and $m_b = m_{D_s^*}$ (instead of m_{K^*}). This result is expected since we are, basically, changing a light pseudoscalar (the pion) by a heavy pseudoscalar (the D meson) and light vector mesons (J/ψ and K^*) by heavy ones ($\bar{D}^*$ and D_s^* respectively).

At last, considering the vertices in Eqs. (5.1), (5.8), (5.14) and the diagrams in Fig. 5.9, we get the following amplitude for the description of the process shown in

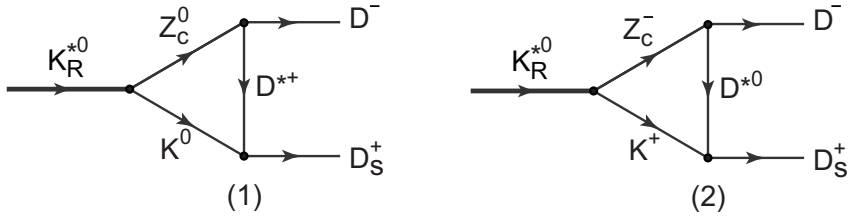

Figure 5.9: Contributions related to the diagram (d) of Fig. 5.1 for the decay mechanism $K_R^{*0} \to D^{*-} D_s^{*+}$.

Fig. 5.1(d),

$$t_d = t_d^{(1)} + t_d^{(2)} = i\sqrt{\frac{3}{2}}\, g_{K_R^* \to (KZ_c)_{\frac{1}{2}}}\, g_{Z_c \to (\bar{D}D^*)_1}\, g_H\, \varepsilon_{K_R^*,\mu}(P) \times \int \frac{d^4q}{(2\pi)^4} \frac{\left(-g^{\mu\nu} + \frac{(P-q)^\mu (P-q)^\nu}{m_{Z_c}^2}\right)\left(-g_{\nu\alpha} + \frac{(k-q)_\nu (k-q)_\alpha}{m_{D^*}^2}\right)(k+q)^\alpha}{(q^2 - m_K^2 + i\varepsilon)[(k-q)^2 - m_{D^*}^2 + i\varepsilon][(P-q)^2 - m_{Z_c}^2 + i\varepsilon]}. \tag{5.34}$$

Using the Lorenz gauge, we can write Eq. (5.34) as

$$\begin{aligned} t_d = i\sqrt{\frac{3}{2}}\, & g_{K_R^* \to (KZ_c)_{\frac{1}{2}}}\, g_{Z_c \to (\bar{D}D^*)_1}\, g_H\, \varepsilon_{K_R^*,\mu}(P) \\ & \times \left[k^\mu \left(1 - \frac{k^2}{m_{D^*}^2}\right) I_0 + \left(1 + \frac{k^2}{m_{D^*}^2} + \frac{P\cdot k}{m_{Z_c}^2} - \frac{k^2 P\cdot k}{m_{D^*}^2 m_{Z_c}^2}\right) I_1^\mu + \frac{k^\mu}{m_{D^*}^2} g_{\alpha\beta} I_2^{\alpha\beta} \right. \\ & + \left(\frac{(P-k)_\sigma}{m_{Z_c}^2} + \frac{k^2 (P+k)_\sigma}{m_{D^*}^2 m_{Z_c}^2}\right) I_2^{\mu\sigma} - \left(\frac{1}{m_{D^*}^2} + \frac{1}{m_{Z_c}^2} + \frac{k^2 - P\cdot k}{m_{D^*}^2 m_{Z_c}^2}\right) g_{\alpha\beta} I_3^{\mu\alpha\beta} \\ & \left. - \frac{(P+k)_\sigma}{m_{D^*}^2 m_{Z_c}^2} g_{\alpha\beta} I_4^{\mu\alpha\beta\sigma} + \frac{1}{m_{D^*}^2 m_{Z_c}^2} g_{\alpha\beta} g_{\sigma\lambda} I_5^{\mu\alpha\beta\sigma\lambda} \right]. \end{aligned}$$

We could proceed as in the previous cases and use the Lorentz covariance to write the tensor integrals in terms of the the possible Lorentz structures and some a_j^i coefficients. However, the presence of the tensor integrals $I_4^{\mu\alpha\beta\sigma}$ and $I_5^{\mu\alpha\beta\sigma\lambda}$ makes such a method inconvenient, since many different Lorentz structures would appear. We adopt then a different strategy: although the particles in the triangular loop are off-shell, their interactions give rise to the K_R^* and Z_c states. In such a situation, the momenta associated with the particles generating such states are much smaller as compared to their energies. In this way, the temporal component of the polarization vector (of the order momentum/mass) is negligible as compared to the spatial components. Thus, when summing over the internal polarizations of the particles, if we call Q^μ and m the four-momentum and mass, respectively, of the vector meson whose interaction with the corresponding

pseudoscalar generates K_R^* or Z_c, we write

$$-g^{\mu\nu} + \frac{Q^\mu Q^\nu}{m^2} \to \delta_{ij}, \tag{5.35}$$

with i and j being spatial indices. Considering such an approach, the amplitude in Eq. (5.34) can be written as

$$\begin{aligned} t_d &= i\sqrt{\frac{3}{2}}\, g_{K_R^*\to(KZ_c)_{\frac{1}{2}}}\, g_{Z_c\to(\bar{D}D^*)_1}\, g_H\, \vec{\varepsilon}_{K_R^*}(P) \\ &\times \int \frac{d^4q}{(2\pi)^4} \frac{\vec{k}+\vec{q}}{(q^2-m_K^2+i\varepsilon)[(k-q)^2-m_{D^*}^2+i\varepsilon][(P-q)^2-m_{Z_c}^2+i\varepsilon]} \\ &= i\sqrt{\frac{3}{2}}\, g_{K_R^*\to(KZ_c)_{\frac{1}{2}}}\, g_{Z_c\to(\bar{D}D^*)_1}\, g_H\, \vec{\varepsilon}_{K_R^*}(P)(I^0\vec{k} + \vec{I}^{\,1}), \end{aligned} \tag{5.36}$$

where I^0 is given by Eq. (5.21) (with $m_1 = m_K$, $m_2 = m_{D^*}$ and $m_3 = m_{Z_c}$) and

$$\vec{I}^{\,1} \equiv \int \frac{d^4q}{(2\pi)^4} \frac{\vec{q}}{(q^2-m_K^2+i\varepsilon)[(k-q)^2-m_{D^*}^2+i\varepsilon][(P-q)^2-m_{Z_c}^2+i\varepsilon]}. \tag{5.37}$$

Note that the approach shown in Eq. (5.35) could have also been used when calculating the amplitudes in the diagrams depicted in Fig. 5.1(a)-(c). There, however, such an approach would not lead to a significant simplification in the calculations, and we have not implemented it. In any case, for completeness, in section. 5.2, we discuss the validity of such an approach by comparing the results obtained with and without the substitution of Eq. (5.35) for the diagram shown in Fig. 5.1(a).

The next step to get t_d consists of performing the q^0 integration in Eq. (5.37). The details of this integration are given in the appendix C. After that, since in the rest frame of the decaying particle $\vec{P} = \vec{0}$, the integral in Eq. (5.37) is a function of $\vec{k}$. In such a case, to perform the integration in d^3q, it is more convenient to introduce the dot product between $\vec{q}$ and $\vec{k}$, which can be done by replacing

$$\int d^3q\, \vec{q} \to \vec{k} \int d^3q\, \frac{\vec{q}\cdot\vec{k}}{\vec{k}^2}. \tag{5.38}$$

5.2 Results and discussions

The decay width of the K_R^* state to the two-body channels shown in Fig. 5.1 can be obtained from the amplitudes determined in the previous section as

$$\Gamma_i = \int \frac{d\Omega}{4\pi^2} \frac{1}{8M_{K_R^*}^2} \frac{p_{\text{c.m.}}}{3} \sum |t_i|^2 = \frac{p_{\text{c.m.}}}{24\pi M_{K_R^*}^2} \sum |t_i|^2, \tag{5.39}$$

where the index $i = a,\ b,\ c,\ d$ is associated with the processes shown in Fig. 5.1 ($a \equiv K_R^* \to J/\psi K^*$, $b \equiv K_R^* \to \bar{D}D_s^*$, $c \equiv K_R^* \to \bar{D}^* D_s^*$, $d \equiv \bar{K}_R^* \to \bar{D}D_s$), $d\Omega$ represents the solid angle, $p_{\text{c.m}}$ is the center of mass momentum of the particles in the final state, the factor 3 has its origin in the average over the K_R^* meson polarizations and the symbol $\sum$ indicates summation over the polarizations of the initial and final states.

Considering Eq. (5.39) and Eqs. (5.23), (5.32), (5.33), (5.36), we get, when regularizing the integrals present in the a_j^i coefficients with a cut-off $\Lambda = 700$ MeV,

$$\Gamma_a = 6.70 \text{ MeV}, \quad \Gamma_b = 0.47 \text{ MeV}, \quad \Gamma_c = 0.47 \text{ MeV}, \quad \Gamma_d = 0.98 \text{ MeV}. \tag{5.40}$$

It is interesting to notice that the process depicted in Fig. 5.1(b) involves an anomalous vertex [105, 106], the $D^* D_s^* K$ vertex, whose contribution is given by the Lagrangian in Eq. (5.17). It is sometimes argued that processes involving anomalous vertices should give smaller contributions than those in which no anomalous vertices are involved. However, the importance of the anomalous vertices in different contexts, like in the determination of production and absorption cross sections of several processes, calculation of radiative decays of scalar and axial resonances and kaon photo-production, has been shown [107–114]. In the present work, as can be seen, the decay width found for the $\bar{D}D_s^*$ channel, which, as stated above, involves an anomalous vertex, is comparable to the result obtained for the $\bar{D}^* D_s^*$ channel, which does not involve anomalous vertices, but has smaller phase space than $\bar{D}D_s^*$.

We can study the sensitivity of the results to the cut-off used when regularizing the integrals appearing in the a_j^i coefficients of Eqs. (5.23), (5.32), (5.33), (5.36). Changing Λ in the range 700-800 MeV, we get the following values for the decay widths

$$\begin{aligned} &\Gamma_a = 6.97 \pm 0.27 \text{ MeV}, \quad \Gamma_b = 0.54 \pm 0.08 \text{ MeV}, \\ &\Gamma_c = 0.54 \pm 0.07 \text{ MeV}, \quad \Gamma_d = 1.14 \pm 0.17 \text{ MeV}. \end{aligned} \tag{5.41}$$

We can also study the uncertainty produced in the results under changes in the coupling constant of $K_R^* \to K Z_c$. If we allow a variation of $\pm 1\%$ in this coupling, for a fixed cut-off $\Lambda = 700$ MeV, we get

$$\begin{aligned} &\Gamma_a = 6.71 \pm 0.14 \text{ MeV}, \quad \Gamma_b = 0.47 \pm 0.02 \text{ MeV}, \\ &\Gamma_c = 0.47 \pm 0.01 \text{ MeV}, \quad \Gamma_d = 0.98 \pm 0.02 \text{ MeV}. \end{aligned} \tag{5.42}$$

In case of the diagram shown in Fig. 5.1(a), when calculating the decay width of $K_R^* \to J/\psi K^*$, we can also consider the fact that the K^* meson has a width $\Gamma_{K^*} \sim 47$ MeV from its decay to the $K\pi$ channel. This can be done by convoluting the expression in Eq. (5.39) with the spectral function associated with the K^* meson, in which case

$$\Gamma_a = \frac{1}{N} \int_{(m_{K^*}-2\Gamma_{K^*})^2}^{(m_{K^*}+2\Gamma_{K^*})^2} d\tilde{m}^2 \, \mathrm{Im}\left[\frac{1}{\tilde{m}^2 - m_{K^*}^2 + i\Gamma_{K^*}(\tilde{m}^2)\tilde{m}}\right] \Gamma_a(\tilde{m}^2)\Theta(m_{K_R^*} - m_{J/\psi} - \tilde{m}), \quad (5.43)$$

where

$$N = \int_{(m_{K^*}-2\Gamma_{K^*})^2}^{(m_{K^*}+2\Gamma_{K^*})^2} d\tilde{m}^2 \, \mathrm{Im}\left[\frac{1}{\tilde{m}^2 - m_{K^*}^2 + i\Gamma_{K^*}(\tilde{m}^2)\tilde{m}}\right], \quad (5.44)$$

the expression for $\Gamma_a(\tilde{m}^2)$ in Eq. (5.43) is given by Eq. (5.39), and

$$\Gamma_{K^*}(\tilde{m}^2) = \Gamma_{K^*}\left[\frac{p_{\mathrm{c.m}}(\tilde{m}^2, m_K^2, m_\pi^2)}{p_{\mathrm{c.m}}(m_{K^*}^2, m_K^2, m_\pi^2)}\right]^3. \quad (5.45)$$

Note, however, that since the mass of the K_R^* resonance is far from the $J/\psi K^*$ threshold, even when the width of K^* is taken into account, a significant change in the results is not expected. We indeed find almost the same value for the decay width Γ_a.

It is also interesting to establish the validity of the approach in Eq. (5.35). If we would have considered such an approach when determining the amplitude in Eq. (5.20), the terms related to the coefficients different to a_1^1 would have vanished. In such a case, we would have got for Γ_a the value of 6.66 MeV instead of the result in Eq. (5.40). This clearly shows that the approach in Eq. (5.35) is, in fact, reliable.

Chapter 6

Conclusions

In this dissertation we predict the existence of an exotic $K^*(4307)$ meson with isospin $1/2$ and spin-parity 1^- which can be understood as a meson arising from the three-body dynamics involved in the $KD\bar{D}^*$ system. With the idea of motivating experimental investigations of such state we have studied several two-body decay channels of this K^*: **a)** $J/\psi K^*(892)$, **b)** $\bar{D}D_s$, **c)** $\bar{D}D_s^*$ and **d)** $\bar{D}^*D_s^*$.

As future prospects we find it important to study different processes where a signal for $K^*(4307)$ can be looked for in future works. A process which can be particularly interesting to explore the evidence of this state is the decay $B \to J/\psi\pi K\pi\pi$, which was used by the Belle collaboration to observe the $X(3872)$ in the $J/\psi\pi\pi$ invariant mass distribution [115]. However, the $J/\psi\pi K$ invariant mass distribution was not reconstructed by the Belle collaboration. The $K^*(4307)$, with a dominant $KZ_c(3900)$ component in its wave function, can naturally decay to a final state formed by $KJ/\psi\pi$, with J/ψ and π coming from the decay of the $Z_c(3900)$. In this way, a reconstruction of the $J/\psi\pi K$ invariant mass could posses a signal of $K^*(4307)$ and confirm its existence.

Besides studying possible processes that generates the $K^*(4307)$ we also plan to use the formalism of the present work to describe other systems. Recently, the LHCb collaboration has claimed the existence of baryon states whose properties can not be understood in terms of 3 quarks [116, 117]. They are called P_c states, and since they are baryons with hidden charm the minimal quark content is that of 5 quarks. Presently, there is a large discussion in the community on the nature of these states, if the states can be understood as compact pentaquark states or as meson-baryon molecules arising as a consequence of the dynamics involved in the $\Sigma_c^{(*)}\bar{D}^{(*)}$ coupled channels. The

quantum numbers of these P_c states have not been determined yet, however, theoretical studies suggest that the spin-parity of the state $P_c(4312)$ is $1/2^-$, while for $P_c(4380)$, $P_c(4440)$ and $P_c(4457)$ is $3/2^-$.

These states can be understood as nucleons with hidden charm. If the present P_c states are negative parity baryons, then similar states with positive parity must exist. Keeping in mind that the $D\bar{D}^*$ interaction is attractive in s-wave in both isospins 0 and 1 and give rise to the formation of the states $X(3782)$ and $Z_c(3900)$, adding a nucleon to the system can produce positive parity nucleon states with hidden charm which arise from three-body dynamics. The masses of such states should be around 4800 MeV, slightly above the current P_c states found by the LHCb collaboration. The s-wave interaction of the DN system and coupled channels is also attractive in nature and is known to produce the state $\Lambda_c(2595)$ [118, 119]. In this way, we will have attraction in both $D\bar{D}^*$ and DN subsystems and the chances of generating a three-body state in the $ND\bar{D}^*$ are high. Thus, the study of the three-body system $ND\bar{D}^*$ and coupled channels can bring information on the generation of nucleon resonances with hidden charm and positive parity, in other words, positive parity partners of the recently discovered P_c states.

Appendix A

Kernels V: isospin vs. charge

In this appendix we give the expression of the amplitudes V (appearing in the Bethe-Salpeter equation) in the isospin base in terms of the amplitudes V in the charge base for the different systems studied. All the two-body systems considered have strangeness $S=+1$, but they can have different isospin I and charm C quantum numbers. We follow the isospin phase convention given in Ref. [77], such that $|K^-\rangle$, $|D^0\rangle$ and $|D^{*0}\rangle$ are identified with the state $-|I=1/2,I_3=-1/2\rangle$, and $|\pi^+\rangle=-|I=1,I_3=-1\rangle$. To simplify the notation, we omit the labels I and I_3 in the ket $|I,I_3\rangle$, and whenever there could be a confusion to which particle the state $|I,I_3\rangle$ is being associated with, we include the particle we are referring to via a subindex in the ket $|I,I_3\rangle$. In this way, for example, $|K^-\rangle=-|1/2,-1/2\rangle_K$ and $|D^0\rangle=-|1/2,-1/2\rangle_D$.

A.1 $C=+1$ and $I=0,\ 1$

In this case, we have two coupled channels, DK and $D_S\eta$, such that for $I=0$, we have

$$\begin{aligned}|DK;0,0\rangle &= \frac{1}{\sqrt{2}}\left[|1/2,1/2\rangle_D\otimes|1/2,-1/2\rangle_K-|1/2,-1/2\rangle_D\otimes|1/2,1/2\rangle_K\right]\\ &= \frac{1}{\sqrt{2}}\left[\left|D^+\right\rangle\otimes\left|K^0\right\rangle+\frac{1}{\sqrt{2}}\left|D^0\right\rangle\otimes\left|K^+\right\rangle\right]=\frac{1}{\sqrt{2}}\left[\left|D^+K^0\right\rangle+\left|D^0K^+\right\rangle\right],\\ |D_s\eta;0,0\rangle &= \left|D_s^+\eta\right\rangle. \end{aligned} \tag{A.1}$$

Using these equations, we get

$$
\begin{aligned}
V^{I=0}_{DK\to DK} &= \langle DK;0,0|\,V\,|DK;0,0\rangle = \frac{1}{2}\Big[\left\langle D^+K^0\right|V\left|D^+K^0\right\rangle + 2\left\langle D^+K^0\right|V\left|D^0K^+\right\rangle \\
&\quad + \left\langle D^0K^+\right|V\left|D^0K^+\right\rangle\Big] = \frac{1}{2}\left[V_{D^+K^0\to D^+K^0} + 2V_{D^+K^0\to D^0K^+} + V_{D^0K^+\to D^0K^+}\right], \\
V^{I=0}_{DK\to D_s\eta} &= \langle DK;0,0|\,V\,|D_s\eta;0,0\rangle = \frac{1}{\sqrt{2}}\left[\left\langle D^+K^0\right|V\left|D_S^+\eta\right\rangle + \left\langle D^0K^+\right|V\left|D_S^+\eta\right\rangle\right] \\
&= \frac{1}{\sqrt{2}}\left[V_{D^+K^0\to D_S^+\eta} + V_{D^0K^+\to D_S^+\eta}\right], \\
V^{I=0}_{D_s\eta\to D_s\eta} &= \langle D_s\eta;0,0|\,V\,|D_s\eta;0,0\rangle = V_{D_s^+\eta\to D_s^+\eta}.
\end{aligned}
\tag{A.2}
$$

In case of $I=1$,

$$
\begin{aligned}
|DK;1,0\rangle &= \frac{1}{\sqrt{2}}\Big[|1/2,1/2\rangle\otimes|1/2,-1/2\rangle + |1/2,-1/2\rangle\otimes|1/2,1/2\rangle\Big] \\
&= \frac{1}{\sqrt{2}}\Big[\left|D^+\right\rangle\otimes\left|K^0\right\rangle - \left|D^0\right\rangle\otimes\left|K^+\right\rangle\Big] = \frac{1}{\sqrt{2}}\left[\left|D^+K^0\right\rangle - \left|D^0K^+\right\rangle\right], \\
|D_s\pi;1,0\rangle &= |0\,0\rangle\otimes|1\,0\rangle = \left|D_s^+\pi^0\right\rangle.
\end{aligned}
\tag{A.3}
$$

Thus,

$$
\begin{aligned}
V^{I=1}_{DK\to DK} &= \langle DK;1,0|\,V\,|DK;1,0\rangle = \frac{1}{2}\Big[\left\langle D^+K^0\right|V\left|D^+K^0\right\rangle - 2\left\langle D^+K^0\right|V\left|D^0K^+\right\rangle \\
&\quad + \left\langle D^0K^+\right|V\left|D^0K^+\right\rangle\Big] = \frac{1}{2}\left[V_{D^+K^0\to K^+D^0} - 2V_{D^0K^+\to D^+K^0} + V_{D^0K^+\to D^0K^+}\right], \\
V^{I=1}_{DK\to D_s\pi} &= \langle DK;1,0|\,V\,|D_s\pi;1,0\rangle = \frac{1}{\sqrt{2}}\left[\left\langle D^+K^0\right|V\left|D_s^+\pi^0\right\rangle - \left\langle D^0K^+\right|V\left|D_s^+\pi^0\right\rangle\right] \\
&= \frac{1}{\sqrt{2}}\left[V_{D^+K^0\to D_s^+\pi} - V_{D^0K^+\to D_s^+\pi^0}\right], \\
V^{I=1}_{D_s\pi\to D_s\pi} &= \langle D_s\pi;1,0|\,V\,|D_s\pi;1,0\rangle = \left\langle D_s^+\pi^0\right|V\left|D_s^+\pi^0\right\rangle = V_{D_s^+\pi^0\to D_s^+\pi^0}.
\end{aligned}
\tag{A.4}
$$

A.2 $C=-1$ and $I=0,\ 1$

The only possible channel is $\bar{D}K$, with

$$
\begin{aligned}
|\bar{D}K;0,0\rangle &= \frac{1}{\sqrt{2}}\Big[|1/2\ 1/2\rangle_{\bar{D}}\otimes|1/2\ -1/2\rangle_K - |1/2\ -1/2\rangle_{\bar{D}}\otimes|1/2\ 1/2\rangle_K\Big] \\
&= \frac{1}{\sqrt{2}}\Big[\left|\bar{D}^0\right\rangle\otimes\left|K^0\right\rangle - \left|D^-\right\rangle\otimes\left|K^+\right\rangle\Big] = \frac{1}{\sqrt{2}}\left[\left|\bar{D}^0K^0\right\rangle - \left|D^-K^+\right\rangle\right], \\
|\bar{D}K;1,1\rangle &= |1/2,1/2\rangle_{\bar{D}}\otimes|1/2,1/2\rangle_K = \left|\bar{D}^0K^+\right\rangle.
\end{aligned}
\tag{A.5}
$$

In this way,

$$V^{I=0}_{\bar{D}K\to\bar{D}K} = \langle \bar{D}K;0,0|\,V\,|\bar{D}K;0,0\rangle = \frac{1}{2}\Big[\left\langle \bar{D}^0K^0\right|V\left|\bar{D}^0K^0\right\rangle - 2\left\langle \bar{D}^0K^0\right|V\left|D^-K^+\right\rangle + \left\langle D^-K^+\right|V\left|D^-K^+\right\rangle\Big] = \frac{1}{2}\left[V_{\bar{D}^0K^0\to\bar{D}^0K^0} - 2V_{\bar{D}^0K^0\to D^-K^+} + V_{D^-K^+\to D^-K^+}\right],$$
$$V^{I=1}_{\bar{D}K\to\bar{D}K} = \langle \bar{D}K;1,1|\,V\,|\bar{D}K;1,1\rangle = \left\langle \bar{D}^0K^+\right|V\left|\bar{D}^0K^+\right\rangle = V_{\bar{D}^0K^+\to\bar{D}^0K^+}. \tag{A.6}$$

To end this appendix, we find it useful to summarize all the results:

$$\begin{aligned}
V^{I=1}_{DK\to DK} &= \frac{1}{2}\left[V_{D^+K^0\to D^+K0} - 2V_{D^+K^0\to D^0K^+} + V_{D^0K^+\to D^0K^+}\right],\\
V^{I=1}_{DK\to D_s\pi} &= \frac{1}{\sqrt{2}}\left[V_{D^+K^0\to D_s^+\pi^0} - V_{K^+D^0\to D_s^+\pi^0}\right],\\
V^{I=1}_{D_s\pi\to D_s\pi} &= V_{D_S^+\pi^0\to D_S^+\pi^0},\\
V^{I=1}_{\bar{D}K\to\bar{D}K} &= V_{\bar{D}^0K^+\to\bar{D}^0K^+},\\
V^{I=0}_{\bar{D}K\to\bar{D}K} &= \frac{1}{2}\left[V_{\bar{D}^0K\to\bar{D}^0K^0} - 2V_{\bar{D}^0K^0\to D^-K^+} + V_{D^-K^+\to D^-K^+}\right],\\
V^{I=0}_{DK\to DK} &= \frac{1}{2}\left[V_{D^+K^0\to D^+K^0} + 2V_{D^+K^0\to D^0K^+} + V_{D^0K^+\to D^0K^+}\right],\\
V^{I=0}_{DK\to D_s\eta} &= \frac{1}{\sqrt{2}}\left[V_{D^+K^0\to D_s^+\eta} + V_{D^0K^+\to D_s^+\eta}\right],\\
V^{I=0}_{D_s\eta\to D_s\eta} &= V_{D_s^+\eta\to D_s^+\eta}.
\end{aligned} \tag{A.7}$$

Appendix **B**

Amplitudes V within the $SU(4)$ Lagrangian

In this appendix, we provide the results found for the kernel V used in the resolution of the Bethe-Salpeter equation when considering the $SU(4)$ model of Refs. [**?**, 65]. In terms of the Mandelstam variables, we get

$$
\begin{aligned}
V_{K^+D^0\to K^+D^0} &= -\frac{1}{6f^2}\left\{(s-u)+\gamma(t-s)+m_K^2+M_D^2\right\},\\
V_{K^+D^0\to K^0D^+} &= -\frac{1}{6f^2}\left\{(s-u)+\gamma(t-u)+M_D^2+m_K^2\right\},\\
V_{D^0K^+\to \pi^0D_s^+} &= -\frac{1}{6\sqrt{2}f^2}\left\{(u-s)+\gamma(t-s)+M_D^2+m_K^2\right\},\\
V_{K^+D^0\to \eta D_s^+} &= -\frac{1}{6\sqrt{6}f^2}\left\{3(u-s)+\gamma(2u-t-s)+2m_\pi^2-3m_K^2-M_D^2\right\},\\
V_{K^0D^+\to K^0D^+} &= -\frac{1}{6f^2}\left\{(s-u)+2\gamma(t-u)+m_K+M_D^2\right\},\\
V_{K^0D^+\to \pi^0D_s^+} &= \frac{1}{6\sqrt{2}f^2}\left\{(u-s)+\gamma(t-s)+M_D^2+m_K^2\right\},\\
V_{K^0D^+\to \eta D_s^+} &= -\frac{1}{6\sqrt{6}f^2}\left\{3(u-s)+\gamma(2u-s-t)+2m_\pi^2-3m_K^2-M_D^2\right\},\\
V_{\pi^0D_s^+\to \pi^0D_s^+} &= 0,\\
V_{\pi^0D_s^+\to \eta D_s^+} &= 0,
\end{aligned}
$$

$$V_{\bar{D}^0K^+\to\bar{D}^0K^+} = -\frac{1}{6f^2}\left\{(u-s)+\gamma(t-s)+m_K^2+M_D^2\right\},$$
$$V_{D^-K^+\to D^-K^+} = 0,$$
$$V_{\bar{D}^0K^0\to\bar{D}^-K^+} = -\frac{1}{6f^2}\left\{(u-s)+\gamma(t-s)\right\},$$
$$V_{\bar{D}^0K^0\to\bar{D}^0K^0} = 0.$$

The corresponding s-wave projected amplitudes are

$$V_{K^0D^+\to K^0D^+} = V_{K^+D^0\to K^0D^+} = V_{K^+D^0\to K^+D^0} = -\frac{1}{6f^2}\left\{-\frac{(M_D^2-m_K^2)^2}{s}\left(\gamma+\frac{1}{2}\right)+\frac{3s}{2}\right\},$$
$$-V_{K^0D^+\to\pi^0D_s^+} = V_{K^+D^0\to\pi^0D_s^+} = -\frac{1}{6\sqrt{2}f^2}\left\{-\frac{3s}{2}(\gamma+1)+(M_D^2-m_K^2)(m_\pi^2-M_D^2)\frac{(\gamma-1)}{2s}\right.$$
$$\left.+M_D^2(\gamma+2)+m_\pi^2\left(\frac{\gamma}{2}+\frac{1}{2}\right)+m_K^2\left(\frac{\gamma}{2}+\frac{3}{2}\right)\right\},$$
$$V_{K^0D^+\to\eta D_s^+} = V_{K^+D^0\to\eta D_s^+} = -\frac{1}{6\sqrt{6}f^2}\left\{-\frac{3s}{2}(\gamma+3)+M_D^2(\gamma+2)+m_K^2\left(\frac{\gamma}{2}-\frac{3}{2}\right)\right.$$
$$\left.+m_\eta^2\left(\frac{\gamma}{2}+\frac{3}{2}\right)+2m_\pi^2-\frac{3}{2s}(M_D^2-m_\eta^2)(M_D^2-m_K^2)(\gamma+1)\right\},$$
$$V_{\eta D_s^+\to\eta D_s^+} = -\frac{1}{9f^2}\left\{-\frac{3s}{2}\gamma-\frac{3\gamma}{2s}(M_D^2-m_\eta^2)^2+M_D^2(\gamma+2)+\gamma m_\eta^2+6m_K^2-4m_\pi^2\right\},$$
$$V_{\bar{D}^0K^+\to\bar{D}^0K^+} = -\frac{1}{6f^2}\left\{\frac{(M_D^2-m_K^2)^2}{2s}(1-\gamma)-\frac{3s}{2}(1+\gamma)+M_D^2(2+\gamma)+m_K^2(2+\gamma)\right\},$$
$$V_{\bar{D}^0K^0\to D^-K^+} = -\frac{1}{6f^2}\left\{(M_D^2+m_K^2)(1+\gamma)-\frac{3s}{2}(1+\gamma)+\frac{(M_D^2-m_k^2)^2}{2s}(1-\gamma)\right\},$$
$$V_{D^-K^+\to D^-K^+} = 0, \qquad V_{\bar{D}^0K^0\to\bar{D}^0K^0} = 0.$$

Using the results shown in the Appendix A, we can write the above amplitudes in the isospin base as

$$
\begin{aligned}
V^{I=0}_{DK\to DK} &= -\frac{1}{3f^2}\left\{\frac{3s}{2}-\frac{(M_D^2-m_K^2)^2}{s}(\gamma+1/2)\right\},\\
V^{I=0}_{DK\to D_s\eta} &= -\frac{1}{3\sqrt{3}f^2}\left\{-\frac{3s}{2}(\gamma+3)+M_D^2(\gamma+2)+\frac{m_K^2}{2}(\gamma-3)+\frac{m_\eta^2}{2}(\gamma+3)\right.\\
&\qquad \left.+2m_\pi^2+\frac{3}{2s}(M_D^2-m_\eta^2)(M_D^2-m_K^2)(\gamma+1)\right\},\\
V^{I=1}_{DK\to DK} &= 0,\\
V^{I=1}_{DK\to D_s\pi} &= -\frac{1}{3\sqrt{12}f^2}\left\{-\frac{3s}{2}(\gamma+1)+(M_D^2-m_K^2)(m_\pi^2-M_D^2)\frac{(\gamma-1)}{2s}\right.\\
&\qquad \left.+M_D^2(\gamma+2)+M_D^2(\gamma+2)+\frac{m_\pi^2}{2}(\gamma+1)+\frac{m_K^2}{2}(\gamma+3)\right\},
\end{aligned}
$$

$$
\begin{aligned}
V^{I=1}_{\bar{D}K\to\bar{D}K} &= -\frac{1}{6f^2}\left\{\frac{(M_D^2-m_K^2)^2}{2s}(1-\gamma)-\frac{3s}{2}(1+\gamma)+M_D^2(2+\gamma)+m_K^2(2+\gamma)\right\},\\
V^{I=0}_{\bar{D}K\to\bar{D}K} &= \frac{1}{6f^2}\left\{(M_D^2+m_K^2)(1+\gamma)-\frac{3s}{2}(1+\gamma)+\frac{(M_D^2-m_K^2)^2}{2s}(1-\gamma)\right\}.
\end{aligned}
$$

Appendix C

Determination of the a^i_j coefficients

In this appendix we give the details of the calculation of the a^i_j coefficients appearing in Eqs. (5.20), (5.32), (5.33), which are related to the Lorentz decomposition of Eq. (5.22), and to determine Eq. (5.37). By contracting I^1_α, $I^2_{\mu\alpha}$ and $I^3_{\mu\nu\alpha}$ with the corresponding Lorentz structures, we can get a set of coupled equations whose solution, in each case, allow us to write the a^i_j coefficients in terms of scalar integrals. We obtain (the expression for the a^1_1 coefficient can be found in Eq. (5.25) but, for convenience, we write it here again)

$$
\begin{aligned}
a^1_1 &= \frac{k^2(\mathbb{PI}^1)-(k\cdot P)(\mathbb{KI}^1)}{k^2P^2-(k\cdot P)^2},\\
a^2_1 &= \frac{\left[(P\cdot k)^2-k^2P^2\right]\mathbb{GI}^2+k^2\mathbb{PPI}^2+P^2\mathbb{KKI}^2-2(P\cdot k)\mathbb{KPI}^2}{2[(P\cdot k)^2-k^2P^2]},\\
a^2_3 &= \frac{1}{2[(P\cdot k)^2-k^2P^2]^2}\left[P\cdot k\left(k^2P^2-(P\cdot k)^2\right)\mathbb{GI}^2-3k^2(P\cdot k)\mathbb{PPI}^2\right.\\
&\quad \left.+2\left(k^2P^2+2(P\cdot k)^2\right)\mathbb{KPI}^2-3P^2(P\cdot k)\mathbb{KKI}^2\right],\\
a^3_1 &= \frac{1}{2\left[(P\cdot k)^2-k^2P^2\right]^2}\left[k^2\left(k^2P^2-(P\cdot k)^2\right)\mathbb{GPI}^3-P\cdot k\left(k^2P^2-(P\cdot k)^2\right)\mathbb{GKI}^3\right.\\
&\quad \left.-k^4\mathbb{PPPI}^3+3k^2(P\cdot k)\mathbb{PPKI}^3+P^2(P\cdot k)\mathbb{KKKI}^3-\left(k^2P^2+2(P\cdot k)^2\right)\mathbb{KKPI}^3\right],\\
a^3_2 &= \frac{1}{2\left[(P\cdot k)^2-k^2P^2\right]^2}\left[-P\cdot k\left(k^2P^2-(P\cdot k)^2\right)\mathbb{GPI}^3+P^2\left(k^2P^2-(P\cdot k)^2\right)\mathbb{GKI}^3\right.\\
&\quad \left.+k^2(P\cdot k)\mathbb{PPPI}^3-\left(k^2P^2+2(P\cdot k)^2\right)\mathbb{PPKI}^3-P^4\mathbb{KKKI}^3+3P^2(P\cdot k)\mathbb{KKPI}^3\right], \quad \text{(C.1)}
\end{aligned}
$$

$$
\begin{aligned}
a_4^3 = &-\frac{1}{2\left[(P\cdot k)^2-k^2P^2\right]^3}\left[3k^2(P\cdot k)\left(k^2P^2-(P\cdot k)^2\right)\mathbb{GPI}^3-\left(k^2P^2-(P\cdot k)^2\right)\right.\\
&\times\left(k^2P^2+2(P\cdot k)^2\right)\mathbb{GKI}^3-5k^4(P\cdot k)\mathbb{PPPI}^3+3k^2\left(k^2P^2+4(P\cdot k)^2\right)\mathbb{PPKI}^3\\
&\left.+P^2\left(k^2P^2+4(P\cdot k)^2\right)\mathbb{KKKI}^3-3(P\cdot k)\left(3k^2P^2+2(P\cdot k)^2\right)\mathbb{KKPI}^3\right],\\
a_6^3 = &-\frac{1}{2\left[(P\cdot k)^2-k^2P^2\right]^3}\left[\left((P\cdot k)^2-k^2P^2\right)\left(2(P\cdot k)^2+k^2P^2\right)\mathbb{GPI}^3\right.\\
&-3P^2(P\cdot k)\left((P\cdot k)^2-k^2P^2\right)\mathbb{GKI}^3+k^2\left(4(P\cdot k)^2+k^2P^2\right)\mathbb{PPPI}^3\\
&-3(P\cdot k)\left(2(P\cdot k)^2+3k^2P^2\right)\mathbb{PPKI}^3-5P^4(P\cdot k)\mathbb{KKKI}^3\\
&\left.+3P^2\left(4(P\cdot k)^2+k^2P^2\right)\mathbb{KKPI}^3\right].
\end{aligned}
$$

where,

$$
\begin{aligned}
&\mathbb{PI}^1 = P^\mu I^1_\mu, \quad \mathbb{KI}^1 = k^\mu I^1_\mu,\\
&\mathbb{GI}^2 \equiv g^{\mu\alpha}I^2_{\mu\alpha}, \quad \mathbb{PPI}^2 \equiv P^\mu P^\alpha I^2_{\mu\alpha}, \quad \mathbb{KPI}^2 \equiv k^\mu P^\alpha I^2_{\mu\alpha}, \quad \mathbb{KKI}^2 \equiv k^\mu k^\alpha I^2_{\mu\alpha},\\
&\mathbb{GPI}^3 \equiv g^{\mu\nu}P^\alpha I^3_{\mu\nu\alpha}, \quad \mathbb{GKI}^3 \equiv g^{\mu\nu}k^\alpha I^3_{\mu\nu\alpha}, \quad \mathbb{PPPI}^3 \equiv P^\mu P^\nu P^\alpha I^3_{\mu\nu\alpha},\\
&\mathbb{PPKI}^3 \equiv P^\mu P^\nu k^\alpha I^3_{\mu\nu\alpha}, \quad \mathbb{KKKI}^3 \equiv k^\mu k^\nu k^\alpha I^3_{\mu\nu\alpha}, \quad \mathbb{KKPI}^3 \equiv k^\mu k^\nu P^\alpha I^3_{\mu\nu\alpha}.
\end{aligned}
\tag{C.2}
$$

Note that the a_j^i coefficients in Eq. (C.1) and the scalars in Eq. (C.2) depend on the masses m_1, m_2 and m_3 of the particles involved in the triangular loop as well as on the mass of the K_R^* state and the masses of the particles to which it can decay, which we represent by m_a and m_b (see Fig. 5.6).

Using Eq. (5.21), and working in the rest frame of the decaying particle, we can write

$$
\begin{aligned}
&\mathbb{PI}^1 = \int\frac{dq^0}{(2\pi)}\int\frac{d^3q}{(2\pi)^3}\frac{P^0q^0}{F(q^0,\vec{q})}, \quad \mathbb{KI}^1 = \int\frac{dq^0}{(2\pi)}\int\frac{d^3q}{(2\pi)^3}\frac{k^0q^0-\vec{k}\cdot\vec{q}}{F(q^0,\vec{q})},\\
&\mathbb{GI}^2 = \int\frac{dq^0}{(2\pi)}\int\frac{d^3q}{(2\pi)^3}\frac{q^{0\,2}-\vec{q}^{\,2}}{F(q^0,\vec{q})}, \quad \mathbb{PPI}^2 = \int\frac{dq^0}{(2\pi)}\int\frac{d^3q}{(2\pi)^3}\frac{(P^0q^0)^2}{F(q^0,\vec{q})},\\
&\mathbb{KPI}^2 = \int\frac{dq^0}{(2\pi)}\int\frac{d^3q}{(2\pi)^3}\frac{(k^0q^0-\vec{k}\cdot\vec{q})P^0q^0}{F(q^0,\vec{q})}, \quad \mathbb{KKI}^2 = \int\frac{dq^0}{(2\pi)}\int\frac{d^3q}{(2\pi)^3}\frac{(k^0q^0-\vec{k}\cdot\vec{q})^2}{F(q^0,\vec{q})}.
\end{aligned}
\tag{C.3}
$$

where

$$
F(q^0,\vec{q}) = [q^{0\,2}-\omega_1^2+i\varepsilon][(k^0-q^0)^2-\omega_2^2+i\varepsilon][(P^0-q^0)^2-\omega_3^2+i\varepsilon], \tag{C.4}
$$

with $\omega_1 = \sqrt{\vec{q}^{\,2}+m_1^2}$, $\omega_2 = \sqrt{(\vec{k}-\vec{q})^2+m_2^2}$ and $\omega_3 = \sqrt{\vec{q}^{\,2}+m_3^2}$. The integrals in Eq. (C.3) are particular cases of the most general integral $I(a,b,b',c,d,e)$ defined as

$$
I(a,b,b',c,d,e) = \int\frac{dq^0}{(2\pi)}\int\frac{d^3q}{(2\pi)^3}\frac{a\,q^{0\,2}+(b+b'\cos^2\theta)\,\vec{q}^{\,2}+c\,q^0|\vec{q}|\cos\theta+d\,q^0+e\,|\vec{q}|\cos\theta}{[q^{0\,2}-\omega_1^2+i\varepsilon][(k^0-q^0)^2-\omega_2^2+i\varepsilon][(P^0-q^0)^2-\omega_3^2+i\varepsilon]}. \tag{C.5}
$$

Indeed, we can write the integrals in Eq. (C.3) as

$$\begin{aligned}
&\mathbb{PI}^1 = I(0,0,0,0,P^0,0), \quad \mathbb{KI}^1 = I(0,0,0,0,k^0,-|\vec{k}|), \quad \mathbb{GI}^2 = I(1,-1,0,0,0,0)\\
&\mathbb{PPI}^2 = I(P^{0^2},0,0,0,0,0), \quad \mathbb{KPI}^2 = I(k^0P^0,0,0,-|\vec{k}|P^0,0,0),\\
&\mathbb{KKI}^2 = I(k^{0^2},0,|\vec{k}|^2,-2k^0|\vec{k}|,0,0),
\end{aligned} \tag{C.6}$$

where $P^0 = m_{K^*_R}$ and

$$k^0 = \frac{P^{0^2} - m_a^2 + m_b^2}{2P^0}, \quad |\vec{k}| = \frac{\lambda^{1/2}(P^{0^2}, m_a^2, m_b^2)}{2P^0}. \tag{C.7}$$

The q^0 integration in Eq. (C.5) can be performed analytically by using Cauchy's theorem. After that, the resulting integration in d^3q is regularized. This is done by means of a cut-off $\Lambda \sim 700$ MeV, in agreement with the cut-off used in the study of the $KD\bar{D}^*$ system, in which the K^*_R state was predicted [29]. In this way, we get

$$I(a,b,b',c,d,e) = -\frac{i}{(2\pi)^2}\int_0^\Lambda dq q^2 \int_{-1}^{1} d\cos\theta\, \frac{N(q,\theta;a,b,b',c,d,e)}{D(q,\theta)}, \tag{C.8}$$

with $q = |\vec{q}|$ and

$$\begin{aligned}
N(q,\theta;a,b,b',c,d,e) &= a\,\omega_1\Big[k^{0^2}\{\omega_3(\omega_1+\omega_3)(\omega_1+\omega_2+\omega_3) - P^{0^2}(\omega_2+\omega_3)\}\\
&+ 2k^0P^0\omega_1\omega_2\omega_3 - \omega_2(\omega_1+\omega_2)\{\omega_3(\omega_1+\omega_3)(\omega_2+\omega_3) - P^{0^2}(\omega_1+\omega_2+\omega_3)\}\Big]\\
&+ q(\tilde{b}q+\tilde{e})\Big[-k^{0^2}\omega_2(\omega_1+\omega_3) + 2k^0P^0\omega_2\omega_3 + (\omega_1+\omega_2)\{(\omega_1+\omega_3)(\omega_2+\omega_3)\\
&\times(\omega_1+\omega_2+\omega_3) - P^{0^2}\omega_3\}\Big] + (\tilde{c}q+d)\omega_1\Big[-k^{0^2}P^0\omega_2 + k^0\omega_3\{(\omega_1+\omega_3)\\
&\times(\omega_1+2\omega_2+\omega_3) - P^{0^2}\} + P^0\omega_2(\omega_1+\omega_2)(\omega_1+\omega_2+2\omega_3)\Big],\\
D(q,\theta) &= 2\omega_1\omega_2\omega_3(k^0-\omega_1-\omega_2+i\varepsilon)(k^0+\omega_1+\omega_2)(P^0-\omega_1-\omega_3+i\varepsilon)\\
&\times(P^0+\omega_1+\omega_3)(P^0-k^0-\omega_2-\omega_3+i\varepsilon)(k^0-P^0-\omega_2-\omega_3+i\varepsilon),
\end{aligned} \tag{C.9}$$

where we have introduced $\tilde{b} \equiv b + b'\cos^2\theta$, $\tilde{c} = c\cos\theta$ and $\tilde{e} = e\cos\theta$.

Similarly,

$$\begin{aligned}
\mathbb{GPI}^3 &= \int \frac{dq^0}{(2\pi)} \int \frac{d^3q}{(2\pi)^3} \frac{(q^{0^2} - |\vec{q}|^2)(P^0 q^0)}{F(q^0, \vec{q})}, \\
\mathbb{GKI}^3 &= \int \frac{dq^0}{(2\pi)} \int \frac{d^3q}{(2\pi)^3} \frac{(q^{0^2} - |\vec{q}|^2)(k^0 q^0 - |\vec{k}||\vec{q}|\cos\theta)}{F(q^0, \vec{q})}, \\
\mathbb{PPPI}^3 &= \int \frac{dq^0}{(2\pi)} \int \frac{d^3q}{(2\pi)^3} \frac{(P^0 q^0)^3}{F(q^0, \vec{q})}, \\
\mathbb{PPKI}^3 &= \int \frac{dq^0}{(2\pi)} \int \frac{d^3q}{(2\pi)^3} \frac{(P^0 q^0)^2 (k^0 q^0 - |\vec{k}||\vec{q}|\cos\theta)}{F(q^0, \vec{q})}, \\
\mathbb{KKKI}^3 &= \int \frac{dq^0}{(2\pi)} \int \frac{d^3q}{(2\pi)^3} \frac{(k^0 q^0 - |\vec{k}||\vec{q}|\cos\theta)^3}{F(q^0, \vec{q})}, \\
\mathbb{KKPI}^3 &= \int \frac{dq^0}{(2\pi)} \int \frac{d^3q}{(2\pi)^3} \frac{(k^0 q^0 - |\vec{k}||\vec{q}|\cos\theta)^2 P^0 q^0}{F(q^0, \vec{q})}.
\end{aligned} \tag{C.10}$$

The integrals in Eq. (C.10) are particular cases of the most general integral $\mathscr{I}(a,b,c,d,e,e',f,f',f'')$ defined as

$$\begin{aligned}
&\mathscr{I}(a,b,c,d,e,e',f,f',f'') \\
&\quad = \int \frac{dq^0}{(2\pi)} \int \frac{d^3q}{(2\pi)^3} \frac{a q^{0^4} + \tilde{b} q^{0^3} |\vec{q}| + c q^{0^3} + \tilde{d} q^{0^2} |\vec{q}| + \tilde{e} q^0 |\vec{q}|^2 + \tilde{f} |\vec{q}|^3}{[q^{0^2} - \omega_1^2 + i\varepsilon][(k^0 - q^0)^2 - \omega_2^2 + i\varepsilon][(P^0 - q^0)^2 - \omega_3^2 + i\varepsilon]},
\end{aligned} \tag{C.11}$$

with $\tilde{b} \equiv b\cos\theta$, $\tilde{d} \equiv d\cos\theta$, $\tilde{e} \equiv (e + e'\cos^2\theta)$, $\tilde{f} \equiv (f + f'\cos\theta + f''\cos^3\theta)$. Particularly, we can write

$$\begin{aligned}
&\mathbb{GPI}^3 = \mathscr{I}(0,0,P^0,0,-P^0,0,0,0,0), \quad \mathbb{GKI}^3 = \mathscr{I}(0,0,k^0,-|\vec{k}|,-k^0,0,0,|\vec{k}|,0), \\
&\mathbb{PPI}^3 = \mathscr{I}(0,0,P^{0^3},0,0,0,0,0,0,0), \quad \mathbb{PPKI}^3 = \mathscr{I}(0,0,P^{0^2}k^0,-P^{0^2}|\vec{k}|,0,0,0,0,0), \\
&\mathbb{KKKI}^3 = \mathscr{I}(0,0,k^{0^3},-3k^{0^2}|\vec{k}|,0,3k^0|\vec{k}|^2,0,0,-|\vec{k}|^3), \\
&\mathbb{KKPI}^3 = \mathscr{I}(0,0,k^{0^2}P^0,-2k^0|\vec{k}|P^0,0,|\vec{k}|^2P^0,0,0,0).
\end{aligned} \tag{C.12}$$

The integral on the q^0 variable of Eq. (C.11) can be obtained using Cauchy's theorem and the remaining integration in d^3q is regularized using a cut-off $\Lambda \sim 700$ MeV. In this way,

$$\mathscr{I}(a,b,c,d,e,e',f,f',f'') = -\frac{i}{(2\pi)^2} \int_0^\Lambda dq q^2 \int_{-1}^{1} d\cos\theta \, \frac{\mathscr{N}(q,\theta;a,b,c,d,e,e',f,f',f'')}{D(q,\theta)}, \tag{C.13}$$

where

$$\begin{aligned}
\mathscr{N}(q,\theta;a,b,c,d,e,e',f,f',f'') &= a\,\omega_1\Big[k^{0^4}\omega_3\{(\omega_1+\omega_3)^2-P^{0^2}\} \\
&-k^{0^2}\omega_2\Big\{P^{0^4}-2P^{0^2}\omega_3(2\omega_1+\omega_2+\omega_3)+\omega_3(\omega_1+\omega_3)(\omega_1^2+2\omega_1\omega_2+3\omega_1\omega_3 \\
&+2\omega_2\omega_3+\omega_3^2)\Big\}+2k^0P^0\omega_1^3\omega_2\omega_3+\omega_2(\omega_1+\omega_2)\Big\{P^{0^4}(\omega_1+\omega_2) \\
&-P^{0^2}\omega_3\Big(\omega_1^2+2\omega_3(\omega_1+\omega_2)+3\omega_1\omega_2+\omega_2^2\Big)+\omega_3(\omega_1+\omega_3)(\omega_2+\omega_3) \\
&\times\Big(\omega_1(\omega_2+\omega_3)+\omega_2\omega_3\Big)\Big\}\Big]+q\Big[\tilde{b}\,\omega_1\Big\{k^{0^3}\omega_3\Big((\omega_1+\omega_3)^2-P^{0^2}\Big) \\
&+k^{0^2}P^0\omega_2\Big(\omega_3(2\omega_1+\omega_3)-P^{0^2}\Big)-k^0\omega_2\omega_3\Big((\omega_1+\omega_3)\{\omega_1(\omega_2+2\omega_3) \\
&+\omega_2\omega_3\}-P^{0^2}(2\omega_1+\omega_2)\Big)+P^0\omega_2(\omega_1+\omega_2)\Big(P^{0^2}(\omega_1+\omega_2) \\
&-\omega_3\{\omega_3(\omega_1+\omega_2)+2\omega_1\omega_2\}\Big)\Big\}+\tilde{d}\,\omega_1\Big\{k^{0^2}\Big(\omega_3(\omega_1+\omega_3)(\omega_1+\omega_2+\omega_3) \\
&-P^{0^2}(\omega_2+\omega_3)\Big)+2k^0P^0\omega_1\omega_2\omega_3-\omega_2(\omega_1+\omega_2)\Big(\omega_3(\omega_1+\omega_3)(\omega_2+\omega_3) \\
&-P^{0^2}(\omega_1+\omega_2+\omega_3)\Big)\Big\}+q\Big\{\tilde{e}\,\omega_1\Big(-k^{0^2}P^0\omega_2+k^0\omega_3\{(\omega_1+\omega_3)(\omega_1+2\omega_2+\omega_3) \\
&-P^{0^2}\}+P^0\omega_2(\omega_1+\omega_2)(\omega_1+\omega_2+2\omega_3)\Big)+\tilde{f}q\Big(-k^{0^2}\omega_2(\omega_1+\omega_3)+2k^0P^0\omega_2\omega_3 \\
&+(\omega_1+\omega_2)\{(\omega_1+\omega_3)(\omega_2+\omega_3)(\omega_1+\omega_2+\omega_3)-P^{0^2}\omega_3\}\Big)\Big\}\Big] \\
&-c\,\omega_1\Big[k^{0^3}\omega_3(P^0-\omega_1-\omega_3)(P^0+\omega_1+\omega_3)+k^{0^2}P^0\omega_2\{P^{0^2}-\omega_3(2\omega_1+\omega_3)\} \\
&+k^0\omega_2\omega_3\{(\omega_1+\omega_3)(\omega_1\omega_2+2\omega_1\omega_3+\omega_2\omega_3)-P^{0^2}(2\omega_1+\omega_2)\} \\
&+P^0\omega_2(\omega_1+\omega_2)\{\omega_3(\omega_3(\omega_1+\omega_2)+2\omega_1\omega_2)-P^{0^2}(\omega_1+\omega_2)\}\Big]. \qquad \text{(C.14)}
\end{aligned}$$

Next, we determine the I^0 and $\vec{I}^{\,1}$ integrals of Eq. (5.36). By means of the Cauchy's theorem we can integrate on the q^0 variable and get the following integration in d^3q, which is regularized by using a cut-off $\Lambda \sim 700$ MeV,

$$\begin{aligned}
I^0 &= -\frac{i}{(2\pi)^2}\int_0^\Lambda dq q^2 \int_{-1}^{1} d\cos\theta \frac{\mathbb{N}(q,\theta)}{D(q,\theta)}, \\
\vec{I}^{\,1} &= -\frac{i}{(2\pi)^2|\vec{k}|^2}\vec{k}\int_0^\Lambda dq q^2 \int_{-1}^{1} d\cos\theta \frac{\mathbb{N}(q,\theta)}{D(q,\theta)}\vec{k}\cdot\vec{q}, \qquad \text{(C.15)}
\end{aligned}$$

where

$$\begin{aligned}
\mathbb{N}(q,\theta) &= -k^{0^2}\omega_2(\omega_1+\omega_3)+2k^0P^0\omega_2\omega_3+(\omega_2+\omega_3) \\
&\times\Big[(\omega_2+\omega_3)(\omega_1+\omega_3)(\omega_1+\omega_2+\omega_3)-P^{0^2}\omega_3\Big]. \qquad \text{(C.16)}
\end{aligned}$$

Bibliography

[1] Robert L. Jaffe. Multi-Quark Hadrons. 1. The Phenomenology of (2 Quark 2 anti-Quark) Mesons. *Phys. Rev.*, D15:267, 1977.

[2] John D. Weinstein and Nathan Isgur. Do Multi-Quark Hadrons Exist? *Phys. Rev. Lett.*, 48:659, 1982.

[3] E. van Beveren, T. A. Rijken, K. Metzger, C. Dullemond, G. Rupp, and J. E. Ribeiro. A Low Lying Scalar Meson Nonet in a Unitarized Meson Model. *Z. Phys.*, C30:615–620, 1986.

[4] Nils A. Tornqvist. Understanding the scalar meson $q\bar{q}$ nonet. *Z. Phys.*, C68:647–660, 1995.

[5] J. A. Oller, E. Oset, and J. R. Pelaez. Nonperturbative approach to effective chiral Lagrangians and meson interactions. *Phys. Rev. Lett.*, 80:3452–3455, 1998.

[6] J. A. Oller, E. Oset, and J. R. Pelaez. Meson meson interaction in a nonperturbative chiral approach. *Phys. Rev.*, D59:074001, 1999. [Erratum: Phys. Rev.D75,099903(2007)].

[7] R. H. Dalitz and S. F. Tuan. A possible resonant state in pion-hyperon scattering. *Phys. Rev. Lett.*, 2:425–428, 1959.

[8] R. H. Dalitz and S. F. Tuan. The phenomenological description of KN reaction processes. *Annals Phys.*, 10:307–351, 1960.

[9] Norbert Kaiser, P. B. Siegel, and W. Weise. Chiral dynamics and the low-energy KN interaction. *Nucl. Phys.*, A594:325–345, 1995.

[10] E. Oset and A. Ramos. Nonperturbative chiral approach to s wave $\bar{K}N$ interactions. *Nucl. Phys.*, A635:99–120, 1998.

[11] Ulf-G. Meißner and J. A. Oller. Chiral unitary meson baryon dynamics in the presence of resonances: Elastic pion nucleon scattering. *Nucl. Phys.*, A673:311–334, 2000.

[12] Eberhard Klempt and Alexander Zaitsev. Glueballs, Hybrids, Multiquarks. Experimental facts versus QCD inspired concepts. *Phys. Rept.*, 454:1–202, 2007.

[13] N. Brambilla et al. Heavy quarkonium: progress, puzzles, and opportunities. *Eur. Phys. J.*, C71:1534, 2011.

[14] Atsushi Hosaka, Toru Iijima, Kenkichi Miyabayashi, Yoshihide Sakai, and Shigehiro Yasui. Exotic hadrons with heavy flavors: X, Y, Z, and related states. *PTEP*, 2016(6):062C01, 2016.

[15] Eulogio Oset et al. Weak decays of heavy hadrons into dynamically generated resonances. *Int. J. Mod. Phys.*, E25:1630001, 2016.

[16] Richard F. Lebed, Ryan E. Mitchell, and Eric S. Swanson. Heavy-Quark QCD Exotica. *Prog. Part. Nucl. Phys.*, 93:143–194, 2017.

[17] Hua-Xing Chen, Wei Chen, Xiang Liu, and Shi-Lin Zhu. The hidden-charm pentaquark and tetraquark states. *Phys. Rept.*, 639:1–121, 2016.

[18] Stephen Lars Olsen, Tomasz Skwarnicki, and Daria Zieminska. Nonstandard heavy mesons and baryons: Experimental evidence. *Rev. Mod. Phys.*, 90(1):015003, 2018.

[19] Feng-Kun Guo, Christoph Hanhart, Ulf-G. Meißner, Qian Wang, Qiang Zhao, and Bing-Song Zou. Hadronic molecules. *Rev. Mod. Phys.*, 90(1):015004, 2018.

[20] Yan-Rui Liu, Hua-Xing Chen, Wei Chen, Xiang Liu, and Shi-Lin Zhu. Pentaquark and Tetraquark states. *Prog. Part. Nucl. Phys.*, 107:237–320, 2019.

[21] M. Tanabashi et al. Review of Particle Physics. *Phys. Rev.*, D98(3):030001, 2018.

[22] T. Armstrong et al. A Partial Wave Analysis of the $K^-\phi$ System Produced in the Reaction $K^- p \to K^+ K^- K^- p$ at 18.5-GeV/c. *Nucl. Phys.*, B221:1–15, 1983.

[23] Roel Aaij et al. Observation of $J/\psi\phi$ structures consistent with exotic states from amplitude analysis of $B^+ \to J/\psi\phi K^+$ decays. *Phys. Rev. Lett.*, 118(2):022003, 2017.

[24] P. Estabrooks, R. K. Carnegie, Alan D. Martin, W. M. Dunwoodie, T. A. Lasinski, and David W. G. S. Leith. Study of K pi Scattering Using the Reactions $K^{\pm}p \to K^{\pm}\pi^{+}n$ and $K^{\pm}p \to K^{\pm}\pi^{-}\Delta^{++}$ at 13-GeV/c. *Nucl. Phys.*, B133:490–524, 1978.

[25] A. Etkin et al. Measurement and partial wave analysis of the reaction $K^{-}p \to K^{0}_{s}\pi^{+}\pi^{-}N$ at 6-GeV/c. *Phys. Rev.*, D22:42–60, 1980.

[26] D. Aston et al. The Strange Meson Resonances Observed in the Reaction $K^{-}p \to \bar{K}0\pi^{+}\pi^{-}n$ at 11-GeV/c. *Nucl. Phys.*, B292:693, 1987.

[27] D. Aston et al. A Study of K- pi+ Scattering in the Reaction $K^{-}p \to K^{-}\pi^{+}n$ at 11-GeV/c. *Nucl. Phys.*, B296:493–526, 1988.

[28] Li Ma, Qian Wang, and Ulf-G. Meißner. Tri-meson bound state BBB^{*} via delocalized π Bond. 2018.

[29] Xiu-Lei Ren, Brenda B. Malabarba, Li-Sheng Geng, K. P. Khemchandani, and A. Martínez Torres. K^{*} mesons with hidden charm arising from $KX(3872)$ and $KZ_{c}(3900)$ dynamics. *Phys. Lett.*, B785:112–117, 2018.

[30] S. S. Kamalov, E. Oset, and A. Ramos. Chiral unitary approach to the K^{-} deuteron scattering length. *Nucl. Phys.*, A690:494–508, 2001.

[31] Ju-Jun Xie, A. Martinez Torres, and E. Oset. Faddeev fixed center approximation to the $N\bar{K}K$ system and the signature of a $N^{*}(1920)(1/2^{+})$ state. *Phys. Rev.*, C83:065207, 2011.

[32] L. Roca and E. Oset. A description of the $f_2(1270)$, $\rho_3(1690)$, $f_4(2050)$, $\rho_5(2350)$ and $f_6(2510)$ resonances as multi-$\rho(770)$ states. *Phys. Rev.*, D82:054013, 2010.

[33] A. Martinez Torres, E. J. Garzon, E. Oset, and L. R. Dai. Limits to the Fixed Center Approximation to Faddeev equations: the case of the $\phi(2170)$. *Phys. Rev.*, D83:116002, 2011.

[34] M. Bayar, J. Yamagata-Sekihara, and E. Oset. The $\bar{K}NN$ system with chiral dynamics. *Phys. Rev.*, C84:015209, 2011.

[35] M. Bayar, Xiu-Lei Ren, and E. Oset. States of $\rho D^{*}\bar{D}^{*}$ with $J = 3$ within the fixed center approximation to the Faddeev equations. *Eur. Phys. J.*, A51(5):61, 2015.

[36] V. R. Debastiani, J. M. Dias, and E. Oset. Study of the DKK and $DK\bar{K}$ systems. *Phys. Rev.*, D96(1):016014, 2017.

[37] Xiu-Lei Ren and Zhi-Feng Sun. Possible bound states with hidden bottom from $\bar{K}^{(*)}B^{(*)}\bar{B}^{(*)}$ systems. *Phys. Rev.*, D99(9):094041, 2019.

[38] J. Gasser and H. Leutwyler. Chiral Perturbation Theory to One Loop. *Annals Phys.*, 158:142, 1984.

[39] J. Gasser and H. Leutwyler. Chiral Perturbation Theory: Expansions in the Mass of the Strange Quark. *Nucl. Phys.*, B250:465–516, 1985.

[40] M. B. Voloshin. On Dynamics of Heavy Quarks in Nonperturbative QCD Vacuum. *Nucl. Phys.*, B154:365–380, 1979.

[41] Nathan Isgur and Mark B. Wise. Weak Decays of Heavy Mesons in the Static Quark Approximation. *Phys. Lett.*, B232:113–117, 1989.

[42] Gustavo Burdman and John F. Donoghue. Union of chiral and heavy quark symmetries. *Phys. Lett.*, B280:287–291, 1992.

[43] D. Gamermann, E. Oset, D. Strottman, and M. J. Vicente Vacas. Dynamically generated open and hidden charm meson systems. *Phys. Rev.*, D76:074016, 2007.

[44] Feng-Kun Guo, Peng-Nian Shen, Huan-Ching Chiang, Rong-Gang Ping, and Bing-Song Zou. Dynamically generated 0^+ heavy mesons in a heavy chiral unitary approach. *Phys. Lett.*, B641:278–285, 2006.

[45] J. Nieves and M. Pavon Valderrama. The Heavy Quark Spin Symmetry Partners of the $X(3872)$. *Phys. Rev.*, D86:056004, 2012.

[46] F. Aceti, M. Bayar, E. Oset, A. Martinez Torres, K. P. Khemchandani, Jorgivan Morais Dias, F. S. Navarra, and M. Nielsen. Prediction of an $I = 1$ $D\bar{D}^*$ state and relationship to the claimed $Z_c(3900)$, $Z_c(3885)$. *Phys. Rev.*, D90(1):016003, 2014.

[47] Xiu-Lei Ren, Brenda B. Malabarba, K. P. Khemchandani, and A. Martinez Torres. On the two-body decay processes of the predicted three-body K*(4307) resonance. *JHEP*, 05:103, 2019.

[48] David Griffiths. *Introduction to Elementary Particles*. Wiley-VCH, 2004.

[49] Mark Thomson. *Modern Particle Physics*. Cambridge University Press, 2014.

[50] David J. Gross and Frank Wilczek. Ultraviolet Behavior of Nonabelian Gauge Theories. *Phys. Rev. Lett.*, 30:1343–1346, 1973.

[51] H. David Politzer. Reliable Perturbative Results for Strong Interactions? *Phys. Rev. Lett.*, 30:1346–1349, 1973. [,274(1973)].

[52] Stefan Scherer and Matthias Schindler, R. *A Primer in Chiral Perturbation Theory*. Springer, 2001.

[53] Wolfram Weise and Anthony W. Thomas. *The Structure of the Nucleon*. Wiley-VCH, 2001.

[54] Yoichiro Nambu. Quasiparticles and Gauge Invariance in the Theory of Superconductivity. *Phys. Rev.*, 117:648–663, 1960. [,132(1960); ,132(1960)].

[55] J. Goldstone. Field Theories with Superconductor Solutions. *Nuovo Cim.*, 19:154–164, 1961.

[56] Jeffrey Goldstone, Abdus Salam, and Steven Weinberg. Broken Symmetries. *Phys. Rev.*, 127:965–970, 1962.

[57] Paolo Finelli. *Symmetry & Symmetry Breaking*. Nuclear Physics Course, University of Bologna, 2011.

[58] Mark B. Wise Aneesh V. Manohar. *Heavy Quark physics*. Cambridge monographs on particle physics, 2007.

[59] Thomas Mannel. *Effective Field Theories in Flavour Physics*. Springer, 2004.

[60] Steven Weinberg. Phenomenological lagrangians. *Physica*, A96(1-2):327–340, 1979.

[61] Steven Weinberg. Effective chiral Lagrangians for nucleon - pion interactions and nuclear forces. *Nucl. Phys.*, B363:3–18, 1991.

[62] Mark B. Wise. Chiral perturbation theory for hadrons containing a heavy quark. *Phys. Rev.*, D45(7):R2188, 1992.

[63] Nathan Isgur and Mark B. Wise. Spectroscopy with heavy-quark symmetry. *Phys. Rev. Lett.*, 66:1130–1133, Mar 1991.

[64] Masako Bando, Taichiro Kugo, and Koichi Yamawaki. Nonlinear Realization and Hidden Local Symmetries. *Phys. Rept.*, 164:217–314, 1988.

[65] D. Gamermann and E. Oset. Axial resonances in the open and hidden charm sectors. *Eur.Phys.J.A33:119-131, (2007)*, pages 119–131.

[66] John R. Taylor. *Classical Mechanics*. University Science, 2005.

[67] Charles J. Joachain. *Quantum Collision Theory*. North-Holland, 1975.

[68] John Butterworth. What goes inside a proton, www.theguardian.com/science/life-and-physics/2015/feb/21/what-goes-on-inside-a-proton, feb 2015.

[69] R.J. Eden, P.V. Landshoff, D.I. Olive, and J.C. Polkinghorne. *The analytic S-matrix*. Cambridge University Press, 1966.

[70] M Tanabashi and et al. Particla Data Group - reviews: Kenematics, cross secitions, formulae and plots. *Phys. Rev. D*, 030001(2018):218–243, 2018 update 2019.

[71] Chiral symmetry amplitudes in the s-wave isoscalar and isovector channels and the σ, $f_0(980)$, $a_0(980)$ scalar mesons. *Nuclear Physics A*, 620(4):438 – 456, 1997.

[72] E. Oset and A. Ramos. Non perturbative chiral approach to s-wave$\bar{K}n$ interactions. *Nuc. Phys. A635,99Nucl.Phys. A635 (1998) 99-120*, 1998.

[73] Ulf-G. Meibner J. A. Oller. Chiral dynamics in the presence of bound states: kaon-nucleon interactions revisited. *Phys.Lett.B500:263-272,(2001)*, 2001.

[74] J. A. Oller and E. Oset. n/d description of two meson amplitudes and chiral symmetry. *Phys. Rev. D*, 60:074023, Sep 1999.

[75] E. E. Salpeter and H. A. Bethe. A relativistic equation for bound-state problems. *Phys. Rev.*, 84:1232–1242, Dec 1951.

[76] Robert Mann. *An Introduction to Particle Physics and the Standard Model*. CRC Press, 2010.

[77] W.M Gibson and B. R. Pollard. *Symmetry Principles in Elementary Particle Physics*. Cambridge University Press, 1976.

[78] A. Martinez, Torres, E. Oset, and A. Ramos. An analysis of the lattice qcd spectra for $d^*_{s0}(2317)$ and $d^*_{s1}(2460)$. *Conference Proceedings, Hadron 2017, Salamanca, Spain, (2017)*, 09 2017.

[79] George Springer. *Introduction to Riemann Surfaces*. American Mathematical Society, 2002.

[80] Rami Shakarchi Elias M. Stein. *Complex Analysis*. Princeton University Press, 2010.

[81] L. D. Faddeev. Scattering theory for a three particle system. *Sov. Phys. JETP*, 12:1014–1019, 1961. [Zh. Eksp. Teor. Fiz.39,1459(1960)].

[82] Eric S. Swanson. Short range structure in the x(3872). *Phys.Lett.B588:189-195,(2004)[arXiv:hep-ph/0311229]*, 2004.

[83] Eric Braaten and Masaoki Kusunoki. Low-energy universality and the new charmonium resonance at 3870 mev. *Phys.Rev.D69:074005,(2004)[arXiv:hep-ph/0311147]*, 2004.

[84] J. Nieves and M. Pavón Valderrama. Heavy quark spin symmetry partners of the $x(3872)$. *Phys. Rev. D*, 86:056004, Sep 2012.

[85] D. Gamermann, J. Nieves, E. Oset, and E. Ruiz Arriola. Couplings in coupled channels versus wave functions: application to the $x(3872)$ resonance. *Phys. Rev.*, D81:014029, 2010.

[86] M. Ablikim et al. Observation of a Charged Charmoniumlike Structure in $e^+e^- \to \pi^+\pi^- J/\psi$ at $\sqrt{s}$ =4.26 GeV. *Phys. Rev. Lett.*, 110:252001, 2013.

[87] Z. Q. Liu et al. Study of $e^+e^- \to \pi^+\pi^- J/\psi$ and Observation of a Charged Charmoniumlike State at Belle. *Phys. Rev. Lett.*, 110:252002, 2013.

[88] T. Xiao, S. Dobbs, A. Tomaradze, and Kamal K. Seth. Observation of the Charged Hadron $Z_c^{\pm}(3900)$ and Evidence for the Neutral $Z_c^0(3900)$ in $e^+e^- \to \pi\pi J/\psi$ at $\sqrt{s} = 4170$ MeV. *Phys. Lett.*, B727:366–370, 2013.

[89] M. Ablikim et al. Observation of a charged $(D\bar{D}^*)^{\pm}$ mass peak in $e^+e^- \to \pi D\bar{D}^*$ at $\sqrt{s} =$ 4.26 GeV. *Phys. Rev. Lett.*, 112(2):022001, 2014.

[90] M. Ablikim et al. Confirmation of a charged charmoniumlike state $Z_c(3885)^{\mp}$ in $e^+e^- \to \pi^{\pm}(D\bar{D}^*)^{\mp}$ with double D tag. *Phys. Rev.*, D92(9):092006, 2015.

[91] Sasa Prelovsek and Luka Leskovec. Search for $Z_c^+(3900)$ in the 1^{+-} Channel on the Lattice. *Phys. Lett.*, B727:172–176, 2013.

[92] Sasa Prelovsek, C. B. Lang, Luka Leskovec, and Daniel Mohler. Study of the Z_c^+ channel using lattice QCD. *Phys. Rev.*, D91(1):014504, 2015.

[93] Ying Chen et al. Low-energy scattering of the $(D\bar{D}^*)^{\pm}$ system and the resonance-like structure $Z_c(3900)$. *Phys. Rev.*, D89(9):094506, 2014.

[94] Miguel Albaladejo, Pedro Fernandez-Soler, and Juan Nieves. $Z_c(3900)$: Confronting theory and lattice simulations. *Eur. Phys. J.*, C76(10):573, 2016.

[95] Victor Mukhamedovich Abazov et al. Evidence for $Z_c^{\pm}(3900)$ in semi-inclusive decays of b-flavored hadrons. *Phys. Rev.*, D98(5):052010, 2018.

[96] Chang-Zheng Yuan. The XYZ states revisited. *Int. J. Mod. Phys.*, A33(21):1830018, 2018.

[97] M Tanabashi and et al. Particla Data Group. *Phys. Rev. D*, 030001(2018):218–243, 2018 update 2019.

[98] F. Aceti, R. Molina, and E. Oset. The $X(3872) \to J/\psi\gamma$ decay in the $D\bar{D}^*$ molecular picture. *Phys. Rev.*, D86:113007, 2012.

[99] H. Nagahiro, J. Yamagata-Sekihara, E. Oset, S. Hirenzaki, and R. Molina. The gamma gamma decay of the $f_0(1370)$ and $f_2(1270)$ resonances in the hidden gauge formalism. *Phys. Rev.*, D79:114023, 2009.

[100] E. Oset and A. Ramos. Dynamically generated resonances from the vector octet-baryon octet interaction. *Eur. Phys. J.*, A44:445–454, 2010.

[101] Francesca Aceti, Melahat Bayar, Jorgivan Morais Dias, and Eulogio Oset. Prediction of a $Z_c(4000)$ $D^*\bar{D}^*$ state and relationship to the claimed $Z_c(4025)$. *Eur. Phys. J.*, A50:103, 2014.

[102] Ulf-G. Meißner. Low-Energy Hadron Physics from Effective Chiral Lagrangians with Vector Mesons. *Phys. Rept.*, 161:213, 1988.

[103] G. Passarino and M. J. G. Veltman. One Loop Corrections for e^+e^- Annihilation Into $\mu^+\mu^-$ in the Weinberg Model. *Nucl. Phys.*, B160:151–207, 1979.

[104] F. Aceti, J. M. Dias, and E. Oset. $f_1(1285)$ decays into $a_0(980)\pi^0$, $f_0(980)\pi^0$ and isospin breaking. *Eur. Phys. J.*, A51(4):48, 2015.

[105] J. Wess and B. Zumino. Consequences of anomalous Ward identities. *Phys. Lett.*, 37B:95–97, 1971.

[106] Edward Witten. Global Aspects of Current Algebra. *Nucl. Phys.*, B223:422–432, 1983.

[107] Yong-seok Oh, Taesoo Song, and Su Houng Lee. J/ψ absorption by π and ρ mesons in meson exchange model with anomalous parity interactions. *Phys. Rev.*, C63:034901, 2001.

[108] H. Nagahiro, L. Roca, and E. Oset. Meson loops in the $f_0(980)$ and $a_0(980)$ radiative decays into ρ, ω. *Eur. Phys. J.*, A36:73–84, 2008.

[109] H. Nagahiro, L. Roca, A. Hosaka, and E. Oset. Hidden gauge formalism for the radiative decays of axial-vector mesons. *Phys. Rev.*, D79:014015, 2009.

[110] S. Ozaki, H. Nagahiro, and A. Hosaka. Magnetic interaction induced by the anomaly in kaon-photoproductions. *Phys. Lett.*, B665:178–181, 2008.

[111] A. Martinez Torres, K. P. Khemchandani, F. S. Navarra, M. Nielsen, and Luciano M. Abreu. On $X(3872)$ production in high energy heavy ion collisions. *Phys. Rev.*, D90(11):114023, 2014. [Erratum: Phys. Rev.D93,no.5,059902(2016)].

[112] L. M. Abreu, K. P. Khemchandani, A. Martinez Torres, F. S. Navarra, and M. Nielsen. $X(3872)$ production and absorption in a hot hadron gas. *Phys. Lett.*, B761:303–309, 2016.

[113] A. Martinez Torres, K. P. Khemchandani, L. M. Abreu, F. S. Navarra, and M. Nielsen. Absorption and production cross sections of K and K^*. *Phys. Rev.*, D97(5):056001, 2018.

[114] L. M. Abreu, K. P. Khemchandani, A. Martínez Torres, F. S. Navarra, and M. Nielsen. Update on J/ψ regeneration in a hadron gas. *Phys. Rev.*, C97(4):044902, 2018.

[115] A. Bala et al. Observation of X(3872) in B→X(3872)Kπ decays. *Phys. Rev.*, D91(5):051101, 2015.

[116] R. Aaij et al. Observation of a narrow pentaquark state, $P_c(4312)^+$, and of the two-peak structure of the $P_c(4450)^+$. *Phys. Rev. Lett.*, 122:222001, Jun 2019.

[117] R. Aaij et al. Observation of $j/\psi\phi$ structures consistent with exotic states from amplitude analysis of $B^+ \to j/\psi\phi K^+$ decays. *Phys. Rev. Lett.*, 118:022003, Jan 2017.

[118] J. Hofmann and M. F. M. Lutz. Coupled-channel study of crypto-exotic baryons with charm. *Nucl. Phys.*, A763:90–139, 2005.

[119] T. Mizutani and A. Ramos. D mesons in nuclear matter: A DN coupled-channel equations approach. *Phys. Rev.*, C74:065201, 2006.